

ABSTRACT

Title:

**PERICELLULAR MATRIX
MECHANOSIGNALING EVENTS IN
DIFFERENTIATING HUMAN
MESENCHYMAL STEM CELLS:
MODULATING THE PERICELLULAR
MATRIX THROUGH SILENCING TYPE VI
COLLAGEN AND DECORIN**

Julianne Doreen Twomey, Ph.D., 2014

Directed By:

**Associate Professor Dr. Adam H. Hsieh,
Fischell Department of Bioengineering**

Stem cell therapies are currently being explored for their potential in the regeneration of load bearing tissues, such as cartilage. Current therapies lack the ability to intrinsically overcome a mechanically adverse environment at implantation. To advance the implementation of human mesenchymal stem cells (hMSCs) for cartilage repair, the mechanisms by which cells “feel” and interact with their micromechanical environment need to be understood. Chondrogenic hMSCs develop a thin pericellular matrix (PCM), consisting of type VI collagen (ColVI) and proteoglycans such as decorin (DCN). The PCM is believed to control mechanotransduction events, acting as both a biomechanical and biochemical buffer. This thesis studies the functional role of ColVI and DCN through targeted gene knockdown using shRNA lentiviral vectors complimentary to *col6a1* or *dcn*.

In the first part of the work, the biophysical role of the PCM was determined through comparisons of cellular deformability under uniaxial strain with or without ColVI and DCN knockdown. HMSCs were cultured in alginate scaffolds and were stimulated with transforming growth factor β for 1 to 2 weeks. We found that the PCM with ColVI knockdown lacked the ability to withstand applied compression and with DCN knockdown deformed in a strain-dependent manner. Next we analyzed the mechanosignaling initiation caused by a transient sinusoidal compressive load through studying cytoskeletal kinetics and gene expression. Altering the PCM through ColVI and DCN knockdown caused an increase in actin and vimentin cytoskeletal protein concentration that lacked a dynamic response to load. This led to a stronger fibroblast growth factor gene expression in ColVI knockdown. DCN also demonstrated direct control over cartilage oligomeric matrix protein gene expression, through a loss of TGF- β regulation. These results were further demonstrated during long term compressive culture. Unconfined sinusoidal compressive culture revealed the highest improvement in material properties in knockdown samples at day 14.

Through these studies, we demonstrated that ColVI and DCN are integral proteins in maintaining the structural microenvironment through protecting the cell from injurious deformation, maintaining cytoskeletal dynamics in response to load, and regulating the differentiation rate through TGF- β signaling. Finally, we demonstrated the ability to manipulate chondrogenic mechanotransduction events using genetic engineering.

PERICELLULAR MATRIX MECHANOSIGNALING EVENTS
IN DIFFERENTIATING HUMAN MESENCHYMAL STEM
CELLS: MODULATING THE PERICELLULAR MATRIX
THROUGH SILENCING TYPE VI COLLAGEN AND
DECORIN

By

Julianne Twomey

Dissertation submitted to the Faculty of the Graduate School of the
University of Maryland, College Park, in partial fulfillment
of the requirements for the degree of
Doctor of Philosophy
2014

Advisory Committee:

Associate Professor Dr. Adam H. Hsieh
Assistant Professor Dr. Steven M. Jay
Associate Professor Dr. Wenxia Song
Professor Dr. John P. Fisher
Professor Dr. William E. Bentley

© Copyright by
Julianne Doreen Twomey
2014

Dedication

I would like to dedicate this work to my family.

Acknowledgements

I would like to thank my advisor, Dr. Adam Hsieh for his support and guidance through this work. His mentorship helped shape the work and my growth as a graduate student. I would also like to thank the members of my committee for their suggestions and constructive recommendations on this project.

I would like to thank my undergraduate researchers for their contribution to this study and commitment to their work, specifically Emmarie Myers for her western blotting optimization, Dana Hartman for her whole cell and PCM deformation study, Kenny Rosenberg for his work on transient load effects on growth media samples, and Ben Bulka who designed and implemented the custom bioreactor used for my third aim. I would also like to acknowledge Pratiksha Thakore, who started the project with me.

I would like to thank the members of the Orthopaedic Mechanobiology Lab, past and present, for their help and guidance during my dissertation work. I'd especially like to thank Anshu Rastogi, who mentored me through RNA interference and who taught me to think as a microbiologist. I would like to thank the members of the Tissue Engineering and Biomaterials Lab who continued to be a sounding board for my constant and varying stem cell questions. I would like to thank my friends, for always lending an ear or a shoulder. I have unlimited gratitude for you always being there. And finally, I would like to thank my family, who always gave words of reassurance and support over the past six years. I would not have been able to successfully complete this work without help from all of you.

Table of Contents

Dedication	ii
Acknowledgements	iii
Table of Contents	iv
List of Tables	vii
List of Figures	viii
Chapter 1: Introduction	1
Chapter 2: Objectives and Specific Aims	3
Chapter 3: Background	5
3.1 Articular Cartilage.....	5
3.2 OA breakdown of ECM.....	6
3.3 Regenerative Therapies	7
3.4 hMSCs undergoing Chondrogenesis.....	10
3.5 PCM components	14
3.6 Type VI Collagen and Decorin	16
3.7 Mechanotransduction and signal transduction events.....	18
3.8 RNA interference and shRNA lentiviruses	20
3.9 Cellular Engineering	23
Chapter 4: Roles of type VI collagen and decorin in human mesenchymal stem cell biophysics during chondrogenic differentiation ¹	26
4.1 Introduction	26
4.2 Materials and Methods	28
4.2.1 Cell Culture.....	28
4.2.2 Lentivirus Preparation.....	29
4.2.3 shRNA Transduction	31
4.2.4 Determination of Viral Efficacy (Titering)	32
4.2.5 Cell Viability	32
4.2.6 Gene Expression	33
4.2.7 Western Blotting.....	35
4.2.8 Immunofluorescence	36
4.2.9 Cellular Deformation.....	37

6.2.1 Cell culture and viral transduction.....	93
6.2.2 Dynamic mechanical stimulation of cell-seeded alginate constructs	95
6.2.3 Gene expression	97
6.2.4 Material Properties.....	99
6.2.5 DNA quantitation.....	101
6.2.6 Statistical Analysis.....	101
6.3 Results.....	101
6.3.1 Targeted knockdown was unaffected by dynamic culture.....	101
6.3.2 Dynamic culture affected DNA quantity in non-infected samples	102
6.3.3 Dynamic culture affected material properties only after two weeks of culture	104
6.3.4 Dynamic stimulation does not enhance gene expression in conjunction with TGF- β culture	107
6.3.5 ColVI and DCN knockdown caused varying material changes to dynamic culture ...	109
6.3.6 Targeted PCM knockdown had a greater effect on gene expression than dynamic compressive culture	111
6.4 Discussion.....	114
6.5 Conclusions.....	120
Chapter 7: Conclusions and Future Work.....	121
Chapter 8: List of Abbreviations.....	129
Appendix A: PCR Amplification efficiencies of qRT-PCR primers created	132
Appendix B: Compiled Computer Aided Design of custom designed unconfined compression bioreactor	134
References.....	139

List of Tables

Table 4.1:	Sense and anti-sense hairpin sequences for shRNA constructs against <i>col6a1</i> or <i>dcn</i>	30
Table 4.2:	Sequences of primers used for qRT-PCR.....	34
Table 4.3:	Normalized AR values of each deformation and condition. ($p < 0.05$ and $p < 0.01$ with respect to increasing symbols. #: from Day 7 same strain, ‡: from D0 same strain. $N > 30$).....	49
Table 5.1:	Sense and anti-sense hairpin sequences for shColVI and shDcn.....	62
Table 5.2:	Sequences of Primers used for real time RT-PCR... ..	70
Table 6.1:	Sense and anti-sense hairpin sequences for shColVI and shDcn.....	94
Table 6.2:	Sequences of Primers used for Aim 3 qRT-PCR.....	99
Table A.1:	qRT-PCR amplification efficiencies determined through serial cDNA compared to relative threshold count.....	132

List of Figures

- Fig. 3.1:** OA degradation of cartilage seen in (A,B,C) is caused by a decrease in proteoglycan and collagen synthesis. Breakdown of cartilage causes fibrillation and focal defects (indicated by red arrow). Histological staining of cartilage shows a high concentration of proteoglycans (D) indicated by safranin-o staining (red, proteoglycans) which decreases in OA cartilage (E). (Adapted from Wilusz, R, 2013 (1))8
- Fig. 3.2:** Schematic of different methods of stem cell delivery into diseased osteoarthritic cartilage. MSCs can be directly injected into the defect site or seeded into specifically designed TEC scaffolds for implantation. TEC scaffolds improve matrix elaboration, differentiation, and mechanical properties to overcome the adverse environment at implantation (2). (As adapted from Noth, U, 2008 (2)).....10
- Fig 3.3:** (A) Genes expressed during chondrogenesis at different stages of differentiation. Various studies have broken chondrogenic differentiation into four stages during *in vitro* culture. (Peak expressions are indicated by bold type). (B) During chondrogenic differentiation, GAGs, proteoglycans and type II collagen accumulate around the cell. GAGs are stained with Safranin-O and aggrecan and type II collagen were stained with immunohistochemistry. (As adapted from Chen, W, 2009 (3) and Xu, J, 2008 (4)).....11
- Fig. 3.4:** Schematic of developing PCM around chondrogenic hMSCs. The PCM is composed of type VI collagen (ColVI), decorin (DCN), biglycan (BGN), aggrecan, and hyaluronan.....13
- Fig. 3.5:** Immunostaining for type VI collagen demonstrating the PCM during cartilage development at (A) 1 month and (B) 11 months of growth in wild-type mice. Arrows point to type VI collagen staining within the PCM of chondrons in the articular cartilage. Adapted from Alexopoulos, L, 2009 (5)).....15

Fig. 3.6:	ColVI microfibrils form a branched network. Red arrows indicate collagen bands and yellow arrows indicate decorin proteoglycans that “decorate” ColVI (Adapted from Keene, D, 1988 (6)).....16
Fig. 3.7:	OA progresses in type VI collagen knockout mice. Images shown are hematoxylin and eosin staining of femoral cartilage from 11 month old mice of (A) wild type, (B) heterozygous, and (C) knockout mice. Arrows point to fibrillation of articular cartilage within the knockout model. (Adapted from Alexopoulos, L, 2009 (5)).....17
Fig. 3.8:	Mechanotransduction can be analyzed through targeted disruption of pericellular matrix proteins using RNA interference. (Adapted from Hsieh, A, 2010 (7)).....20
Fig. 3.9:	shRNA initiated RNAi. shRNA sequences are inserted into the human genome using lentiviral vectors. mRNA folds on itself created a dsRNA initiating the endogenous RNAi mechanism that recognizes and degrades target mRNA (8).....22
Fig. 4.1:	Representative images of aspect ratio analysis under static applied strain. (A) The cell is stained with CMFDA (green), the PCM stained with 6ROX (red), and nuclei are stained with DAPI (blue). A yellow ellipse is shown around the cell and a blue ellipse is shown around the PCM to indicate how the major and minor diameters of the cell and the PCM+Cell were obtained. Scale bars indicate 20 μ m. (B) PCM+Cell of CM-hMSCs, shColVI- and shDcn- transduced cells at day 14 under static applied strain of 0%, 10% and 20%. Cells are stained as previously described. The white arrows indicate the direction of applied compression. Scale bars indicate 20 μ m.....38
Fig. 4.2:	Optimization of shColVI (A-E) and shDcn (A-F) to select the most efficient virus in knockdown target genes. (A) <i>Col6a1</i> and (B) <i>dcn relative</i> gene expression as assessed by qRT-PCR (n \geq 2). Data are shown as average values of the range of calculated fold differences ($2^{-\Delta\Delta Ct + SD}$ and $2^{-\Delta\Delta Ct - SD}$) \pm half of the range.....39
Fig.4.3:	Targeted knockdown of genes is improved with blasticidin selection in shRNA transduced cells at MOI (1). (A) <i>Col6a1</i> and (B) <i>dcn relative</i> gene expression as assessed by qRT-PCR relative to non-infected hMSCs cultured in parallel. Data

are shown as average values of the range of calculated fold differences ($2^{-\Delta\Delta Ct + SD}$ and $2^{-\Delta\Delta Ct - SD}$) \pm half the range (*p<0.05, **p<0.01, ***p<0.001; n \geq 2). Blasticidin selection caused a slight decrease in *col6a1* and *dcn* expression when non-transduced cells were removed.....40

Fig.4.4: Knockdown of target genes and protein in samples cultured in CM. (A) *Col6a1* and *dcn* relative gene expression as assessed by qRT-PCR (n \geq 3) (*p<0.05, **p<0.01 to non-infected and GFP-transduced hMSCs). Data are shown as average values of the range of calculated fold differences ($2^{-\Delta\Delta Ct + SD}$ and $2^{-\Delta\Delta Ct - SD}$) \pm half the range. (B) ColVI and DCN protein expression as analyzed by western blotting (D7, n=2; D14, n=2; D28, n=4) in GFP and shColVI groups relative to non-infected CM-hMSCs at corresponding time points. Relative protein expression was calculated as the ratio of the shRNA-transduced cells (target protein/ β -actin) to non-infected CM-hMSCs (target protein/ β -actin). Data are represented as mean \pm SEM. (C) Representative western blotting at day 14 for α 1(VI), DCN, and β -actin in non-infected CM-hMSCs, and GFP-, shColVI-, and shDcn-transduced cells. Positive controls (+) were run in parallel.....41

Fig. 4.5: Quantification of viability of alginate beads during chondrogenic culture using live-dead imaging and ImageJ particle analysis. Data shown is %live (green) cells of total cells counted \pm SEM (**p<0.05 from non-infected chondrogenic-hMSCS; +p<0.05 from the previous time point, n \geq 25).....43

Fig. 4.6. Chondrogenic gene expression in control and knockdown cells. (A) Gene expression for *acan* and (B) *sox9* in non-infected, and GFP-, shColVI- and shDcn- transduced hMSCs in alginate bead culture (n=3) .All data represent CM relative to their same infection condition cultured in GM at 7, 14, and 28 days (e.g $\Delta\Delta Ct_{acan,D7} = \Delta Ct_{acan,CM,D7} - \Delta Ct_{acan,GM,D7}$) (*p<0.05 CM culture relative to same condition same time point in GM; +p<0.05, relative to CM-hMSCs at same time point; #p<0.05, relative to CM-GFP hMSCs at same time point; n \geq 3). Data are shown as average values of the range of calculated fold differences ($2^{-\Delta\Delta Ct + SD}$ and $2^{-\Delta\Delta Ct - SD}$) \pm half the range.....44

Fig. 4.7: Confocal microscopy visualization of ColVI and DCN. (A) ColVI (green) immunofluorescence visualization within the PCM of non-infected, and GFP-, shColVI-, and shDcn-transduced hMSCs cultured in alginate beads in CM at 7, 14, and 28 days. Cell nuclei are stained with DAPI (blue). Red arrows point to punctate ColVI staining. All images were standardized to similar pixel intensity ranges for valid comparisons. Negative controls without primary or secondary labeling showed no ColVI staining (data not shown). Scale bar indicates 20µm. (B) Equivalent data for DCN (red) immunofluorescence visualization. Yellow arrows point to concentrated clusters of DCN around the cell membrane. Negative controls without primary or secondary labeling showed no DCN staining (data not shown). Scale bar indicates 20µm.....45

Fig. 4.8: Pericellular gene expression in control and knockdown cells. (A) Gene expression for *dcn*, (B) *bgn* and (C) *col6a1* in non-infected, and GFP-, shColVI- and shDcn- transduced hMSCs in alginate bead culture (n=3) in CM relative to the same infection condition cultured in GM at 7, 14, and 28 days (*p<0.05, **p<0.01, CM culture relative to same condition same time point in GM; +p<0.05, relative to CM-hMSCs at same time point; #p<0.05, relative to CM-GFP hMSCs at same time point; n≥3). Data are shown as average values of the range of calculated fold differences ($2^{-\Delta\Delta Ct + SD}$ and $2^{-\Delta\Delta Ct - SD}$) ± half the range..... 47

Fig. 4.9: Normalized aspect ratios (NAR) of cells cultured in GM or CM, and the PCM+Cell (CM-hMSCs). Each condition was subjected to 0%, 10% or 20% applied strain at 0, 7 and 14 days of culture in alginate beads. Graphs show normalized aspect ratios that are overlaid with progressively increasing strain increments (values are not cumulative). (p<0.05 and p<0.01 with respect to increasing symbols. *: from previous applied strain; +: from GM-hMSCs of same strain, same day; N>30). Data are shown as NAR ±SEM.....48

- Fig. 4.10:** Normalized aspect ratios of non-infected and GFP-, shColVI-, and shDcn-transduced hMSCs. Each condition was subjected to 0%, 10%, and 20% applied strain at (A) day 0, (B) day 7, and (C) day 14. Graphs show normalized aspect ratios that are overlaid with progressively increasing strain increments (values are not cumulative) (*p<0.05, **p<0.01 significant difference from GFP-transduced cells at same nominal strain; # p<0.05 significant deformation between 10% and 20% applied nominal strain). Data are shown as NAR ±SEM.....51
- Fig. 5.1:** (A) Aluminum molds with Ø6mm x 3mm well, (B) which are loaded with cell-seeded 2% (w/v) alginate solution, (C) compressed between two aluminum plates with Whatman and filter paper to allow CaCl₂ curing. (D) Once disks were cured, they were moved to a Ø60mm petri-dish containing a 1.5mm thick agarose mold with Ø8mm diameter wells punched out to maintain local position and unconfined conditions and equilibrated in warmed media for thirty minutes.....64
- Fig. 5.2:** Dynamic loading set-up. (A) Schematic of Ø60mm petri-dishes containing a 1.5mm thick agarose mold with Ø8mm diameter wells to maintain alginate disk position. Ø6mm x 3mm thick alginate disks were loaded in warmed media. (B) The Ø60 mm diameter petri dishes were fixed within a water bath maintained at 37°C. A Ø40mm polysulfone plunger was attached to a 200g load cell. Displacement controlled sinusoidal strain was applied using an LM-1, Bose/Electroforce materials testing machine. (C) Force and displacement feedback was collected over the hour of transient load. (D) Schematic of culture period, loading duration, and harvest times.....65

Fig. 5.3: Knockdown of target genes and protein in samples cultured in CM. Relative (A) *col6a1* and (B) *dcn* gene expression (fold difference) at day 7 and day 14, as assessed by qRT-PCR of GFP-, shColVI-, and shDcn-transduced cells relative to chondrogenic non-infected hMSCs (#: $p < 0.05$ to chondrogenic non-infected and GFP-transduced cells; $n \geq 3$). Data are shown as average values of the range of calculated fold differences ($2^{-\Delta\Delta Ct + SD}$ and $2^{-\Delta\Delta Ct - SD}$) \pm half of the range. Significant knockdown was achieved by shColVI samples at day 7 and 14 and shDcn achieved significant knockdown at day 14, which maintained significant knockdown during transient load. (C) Immunofluorescence visualization of ColVI and (D) DCN proteins surrounding chondrogenic cells. Non-infected and GFP-transduced cells cultured in chondrogenic media developed a type VI collagen PCM surrounding cells which was inhibited in shColVI cells. DCN staining showed DCN expression and accumulation during the two week chondrogenic phase, which shDcn inhibited.....73

Fig. 5.4: Confocal fluorescence visualization of AMFs at (A) day 7 and (B) 14 in non-infected GM and CM hMSCs and GFP-, shColVI-, and shDcn-transduced cells in free-swelling (FS) conditions and immediately following (0hr) and four hours post load (4hrs). Scale bars= 20 μ m. C) Corrected total cell fluorescence per cellular area intensities for all samples at day 7 and day 14. *: $p < 0.05$ from GM samples at each time point; #: $p < 0.05$ from CM & GFP at each time point; +: $p < 0.05$ from day 7 to day 14; A:B:C: $p < 0.05$ between loading harvests.....75

Fig. 5.5: Confocal fluorescence visualization of VIFs at (A) day 7 and (B) 14 in non-infected GM and CM hMSCs and GFP-, shColVI-, and shDcn-transduced cells in free-swelling (FS) conditions and immediately following (0hr) and four hours post load (4hrs). Scale bars= 20 μ m. C) Corrected total cell fluorescence per cellular area intensities for all samples at day 7 and day 14. *: $p < 0.05$ from GM samples at each time point; #: $p < 0.05$ from CM & GFP at each time point; +: $p < 0.05$ from day 7 to day 14; A:B:C: $p < 0.05$ between loading harvests.....77

Fig. 5.6: Confocal fluorescence visualization of MTs at (A) day 7 and (B) 14 in non-infected GM and CM hMSCs and GFP-, shColVI-, and shDcn-transduced cells in free-swelling (FS) conditions and immediately following (0hr) and four hours post load (4hrs). Scale bars= 20µm. C) Corrected total cell fluorescence per cellular area intensities for all samples at day 7 and day 14. *:p<0.05 from GM samples at each time point; #:p<0.05 from CM & GFP at each time point; +: p<0.05 from day 7 to day 14; A:B:C: p<0.05 between loading harvests.....78

Fig. 5.7: Confocal fluorescence visualization of vinculin at (A) day 7 and (B) 14 in non-infected GM and CM hMSCs and GFP-, shColVI-, and shDcn-transduced cells in free-swelling (FS) conditions and immediately following (0hr) and four hours post load (4hrs). Scale bars= 20µm. C) Corrected total cell fluorescence per cellular area intensities for all samples at day 7 and day 14. *:p<0.05 from GM samples at each time point; #:p<0.05 from CM & GFP at each time point; +: p<0.05 from day 7 to day 14; A:B:C: p<0.05 between loading harvests.....79

Fig. 5.8: Relative gene expression (fold difference) of day 7 (a) and day 14 (b) non-infected GM and CM cells and GFP-, shColVI-, and shDcn- transduced cells to free swelling GM-hMSCs at day 7. *:p<0.05 from GM samples at each time point; #:p<0.05 from CM & GFP at each time point; +: p<0.05 from day 7 to day 14; A:B:C: p<0.05 between loading harvests.....82

Fig. 5.9: Relative gene expression (fold difference) of day 7 (a) and day 14 (b) non-infected GM and CM cells and GFP-, shColVI-, and shDcn- transduced cells to free swelling GM-hMSCs at day 7. *:p<0.05 from GM samples at each time point; #:p<0.05 from CM & GFP at each time point; +: p<0.05 from day 7 to day 14; A:B:C: p<0.05 between loading harvests.....84

Fig. 6.1:	Custom designed polysulfone bioreactor designed to apply displacement controlled sinusoidal unconfined compression. (A) The bioreactor has four culture wells centrally located around the Zaber linear actuator. Each well contains one Ø60 mm petri dishes with 6 alginate disks (Ø6mm x 3mm in height) maintained in an agarose mold. (B) Once assembled, the polysulfone lid overlaps the base to ensure sterility while allowing free gas-exchange during loading while maintained in a temperature and gas controlled incubator. (D) The Ø50 loading platens are designed to concentrically locate above the individual wells to apply homogenous displacement controlled strain across all disks (E). Non-loaded (NL) static contact cultures incorporated an aluminum platen to maintain 0% strain for four hours per day (C,F) to mimic the nutrient diffusion limitations within the bioreactor.....96
Fig. 6.2:	Schematic of loading duration and harvest points.....97
Fig. 6.3:	Standard Linear Solid model was used to determine the mechanical properties of the stress-relaxation tests. (A) Representative spring-dashpot schematic of the standard linear solid model, where E_1 , E_2 , and η represent changing material properties under applied strain. $E_1 + E_2$ represents the instantaneous stiffness under an applied compression, E_1 represents the steady state stiffness of the construct, and η represents the viscosity of the changing disk under applied load. (B) Representative stress and strain curve vs. time for chondrogenic non-infected cells at day 14. (C) The standard linear solid model can determine the changing material properties from collected force and displacement data.....100
Fig. 6.4:	Relative <i>col6a1</i> and <i>dcn</i> gene expression (fold difference) of day 7 and day 14 non-infected GM and CM cells and GFP-, shColVI-, and shDcn- transduced cells in non-loaded and bioreactor culture to day 1 cultures. (#:p<0.05 from GM samples at each time point; *:p<0.05 from CM & GFP at each time point; +:p<0.05 between non-loaded and bioreactor cultured samples; @: p<0.05 between day 7 to day 14 culture; n≥ 3).....102

Fig. 6.5: Ratio of DNA content between bioreactor cultured and non-loaded disks in non-infected GM and CM and GFP-, shColVI-, and shDcn-transduced cells disks at 7 or 14 days. DNA was quantified using Quant-iT Picogreen and a lambda DNA standard curve Data shown is the average DNA concentration (ng/mL) of bioreactor culture / average DNA concentration in non-loaded samples (ng/mL) + standard deviation. (+:p<0.05 between non loaded and bioreactor cultured samples; n≥ 5).....103

Fig. 6.6: Mechanical properties of non-infected GM and CM, and GFP-transduced cell alginate disks in either non-loaded (NL) or bioreactor (BR) culture for 7 days. Viscosity (η), instantaneous (E_1+E_2) stiffness, and steady-state (E_1) stiffness was unaffected at day 7. All properties were determined using displacement controlled stress-relaxation tests with 10% strain applied at 0.05%/second, which was maintained for 1000 seconds. Stress and strain calculations were determined from the force and displacement data collected. Mechanical properties were determined from standard linear solid model: $\sigma = E_1 * \epsilon_0 * e^{-\frac{E_1 t}{\eta}} + E_2 * \epsilon_0$. (#:p<0.05 from GM samples at each time point; *:p<0.05 from CM & GFP at each time point; +:p<0.05 between non-loaded to bioreactor cultured samples; n≥5 disks per sample).....105

Fig. 6.7: Mechanical properties of non-infected GM, CM, and GFP-transduced cell alginate disks in either non-loaded (NL) or bioreactor (BR) culture for 14 days. Steady-state (E_1) stiffness significantly increased with dynamic culture. All properties were determined using displacement controlled stress-relaxation tests with 10% strain applied at 0.05%/second, which was maintained for 1000 seconds. Stress and strain calculations were determined from the force and displacement data collected. Mechanical properties were determined from standard linear solid model: $\sigma = E_1 * \epsilon_0 * e^{-\frac{E_1 t}{\eta}} + E_2 * \epsilon_0$. (#:p<0.05 from GM samples at each time point; *:p<0.05 from CM & GFP at each time point; +:p<0.05 between non-loaded to bioreactor cultured samples; n≥5 disks per sample).....106

Fig. 6.8: Relative *comp*, *acan*, *bgn*, *colla1*, *fgf2*, and *adamts4* gene expression (fold difference) of day 7 and day 14 non-infected GM and CM cells and GFP-transduced cells in non-loaded (yellow) and bioreactor (red) culture to day 1 cultures. (#:p<0.05 from GM samples at each time point; *:p<0.05 from CM & GFP at each time point; +:p<0.05 between non-loaded and bioreactor cultured samples; @: p<0.05 between day 7 to day 14 culture; n≥3).....108

Fig. 6.9: Mechanical properties of shColVI-, and shDcn- transduced cell alginate disks in either static (NL) or bioreactor (BR) culture for 7 or 14 days. Viscosity (η), instantaneous (E_1+E_2) stiffness, and steady-state (E_1) stiffness were affected in all shColVI samples at day 14. Viscosity was affected in shDcn samples at day 14. All properties were determined using displacement controlled stress-relaxation tests with 10% strain applied at 0.05%/second, which was maintained for 1000 seconds. Stress and strain calculations were determined from the force and displacement data collected. Mechanical properties were determined from standard linear solid model: $\sigma = E_1 * \epsilon_0 * e^{-\frac{E_1 t}{\eta}} + E_2 * \epsilon_0$. (#:p<0.05 from GM samples at each time point; *:p<0.05 from CM & GFP at each time point; +:p<0.05 between non-loaded to bioreactor cultured samples; n≥5 disks per sample).....110

Fig. 6.10: Relative *comp*, *acan*, *bgn*, *colla1*, *fgf2*, and *adamts4* gene expression (fold difference) of day 7 and day 14 shColVI- transduced cells in non-loaded (yellow) and bioreactor (red) culture to day 1 cultures. (#:p<0.05 from GM samples at each time point; *:p<0.05 from CM & GFP at each time point; +:p<0.05 between non-loaded to bioreactor cultured samples; @: p<0.05 between day 7 to day 14 culture; n≥3).....112

Fig. 6.11: Relative *comp*, *acan*, *bgn*, *colla1*, *fgf2*, and *adamts4* gene expression (fold difference) of day 7 and day 14 shDcn- transduced cells in non-loaded (yellow) and bioreactor (red) culture to day 1 cultures. (#:p<0.05 from GM samples at each time point; *:p<0.05 from CM & GFP at each time point; +:p<0.05 between non-loaded to bioreactor cultured samples; @: p<0.05 between day 7 to day 14 culture; n≥3).....113

Fig. 7.1:	Schematic outlining the overall goals of the three aims within this dissertation work. Aim 1 analyzed the biophysical contribution of ColVI and DCN, Aim 2 analyzed mechanosignaling gene expression and cytoskeletal kinetics following applied load, and Aim 3 analyzed mechanical property and gene expression differences between knockdown and control samples under long term sinusoidal unconfined compression.....	122
Fig. 7.2:	Schematic of shRNA modified stem cells for tissue engineering. ShColVI and shDcn knockdown can be used for increased hypertrophic differentiation and TGF- β exposure.(As adapted from Noth, U, 2008 (2)).....	127
Fig. 7.3:	Stratification strategy using shColVI and shDcn knockdown chondrocyte-like cells. Different composition and mechanical properties can be achieved through layering different knockdown populations within a TEC. (As adapted from Tat, SK, 2009 (9)).....	128
Fig. A-1:	Representative figure determining primer efficiency of <i>col6a1</i> . The log of the concentration is plotted against the threshold value achieved at each concentration.....	133
Fig. A-2:	(A) Lid and (B) base of custom designed unconfined compressive bioreactor. Individual petri dishes are placed within each culture well of the bioreactor. The base and lid are concentrically placed on top of each other (C), with the Zaber linear actuator attached through the middle of the bioreactor. The lid's position is maintained by posts (D) to maintain the concentric position of the plungers above each culture well. A side view of the plungers located above the culture wells are seen in (E).....	134
Fig. A-3:	Engineering drawing of bioreactor base. Drawings shown are the top, bottom, and side views. Dimensions are in millimeteres. All drawings were created using SolidWorks (created by Ben A. Bulka).....	135
Fig. A-4:	Engineering drawing of bioreactor base. Views shown are the top and cross-sectional as noted. Dimensions are in millimeteres. All drawings were created using SolidWorks (created by Ben A. Bulka).....	136

Fig. A-5: Engineering drawing of bioreactor lid. Views shown are top and cross-sectional cut as noted. Dimensions are in millimeters. All drawings were created using SolidWorks (created by Ben A. Bulka).....137

Fig. A-6: Engineering drawing of bioreactor lid. Views shown are bottom, top, and cross-sectional cut as noted. Dimensions are in millimeters. All drawings were created using SolidWorks (created by Ben A. Bulka).....137

Fig. A-7: Engineering drawing of bioreactor base bottom. Views shown are top and side. Dimensions are in millimeters. All drawings were created using SolidWorks (created by Ben A. Bulka).....138

Chapter 1: Introduction

Human mesenchymal stem cells (hMSCs) have demonstrated great potential in the development of regenerative therapies for load-bearing tissues, such as articular cartilage. This is due to their ability to maintain a basal phenotype and multipotentiality during expansion, reducing the need for autologous chondrocytes for defect repair (10). Differentiation can be induced through various methods, including biochemical stimulation from exogenous addition of growth factors (11) or biomechanical induction (12). hMSCs are dynamically sensitive, and differentiation lineage commitment will depend on the method of dynamic stimulation (13,14). Currently proposed approaches lack the capability of controlling stem cell response to the adverse environment in the mechanically compromised tissue at the site of implantation. One method to overcome this is genetically engineering the biological response to mechanical stresses using RNAi, but first, the mechanisms through which cells “feel” and interact with their micromechanical environment need to be explored. Mechanotransduction is the process through which cells react to a mechanical stimulus and elicit a chemical response. Mechanosignaling pathways are critical to understand how cells, particularly those in load bearing tissues, maintain their structural environment during physiologic activity. The mechanotransduction events of chondrocytes and chondrogenic stem cells are not fully understood and need to be explored for advancement of regenerative therapies.

Mechanical stimulation induces changes, such as increases in the cellular synthesis of a highly organized matrix to withstand physiologic stresses (15,16). hMSCs undergoing chondrogenesis create a thin layer of matrix that around the cell called the pericellular

matrix (PCM). The PCM consists of type VI collagen (ColVI), hyaluronan and proteoglycans such as decorin (DCN) (17-21). The PCM serves as both a biomechanical and biochemical buffer, and controls the amount of mechanical load that deforms the chondrocyte as well as the biological response. The accumulative level and composition of the PCM is important for regulating cellular deformation, with specific components modulating the assembly and aggregation of other proteins. The effect of targeted gene knockdown of structural proteins on the PCM's function will reveal their roles in chondrocyte mechanotransduction and biological responses to physiologic loading.

The goal of this thesis was to examine the role of type VI collagen and decorin in the biological response to mechanical stimulation using shRNA knockdown. This work demonstrated that ColVI and DCN are integral in cellular mechanotransduction. These studies demonstrated the ability to genetically engineer hMSCs, controlling matrix synthesis to examine the functional roles of PCM proteins using targeted knockdown.

Chapter 2: Objectives and Specific Aims

Specific Aims

The biochemical response to mechanical loading of chondrogenic hMSCs is believed to be controlled through the PCM due to its temporally specific and changing micromechanical environment. ColVI and DCN are believed to be important within the PCM due to their synthesis and accumulation during differentiation (20,22). RNA interference (RNAi) mediated knockdown of these proteins allows a stable continuous examination during chondrogenic differentiation in response to biochemical induction and biomechanical stimulation. An altered PCM will change the mechanotransduction mechanisms and therefore the biological response. The targeted knockdown of ColVI and DCN elucidated their roles in the complex regulation of cellular reactions to mechanical load.

Global Hypothesis: Structural proteins within the PCM of differentiating stem cells determine the biological response to mechanical stress

Aim1: *Determine roles of type VI collagen and decorin in human mesenchymal stem cell biophysics during chondrogenic differentiation*

The first aim was to determine whether chondrogenic differentiation can successively progress without type VI collagen and decorin within the PCM. Secondly, it was determined whether type VI collagen and decorin are essential in shielding the cells from deformation.

Aim 2: *Determine type VI collagen and decorin's role in the mechanosignaling initiation and cytoskeletal kinetics of differentiating hMSC*

The PCM is important in shielding the cell from harmful mechanical stresses. The second aim was to determine whether type VI collagen and decorin, while contributing to the micromechanical environment, also are essential in initiating mechanosignaling cascades in response to transient loading during PCM development.

Aim 3: *Determine type VI collagen and decorin's influence on cell-seeded alginate scaffold material properties and chondrogenic gene expression during long term dynamic compressive culture*

The final aim of this study was to determine the roles of type VI collagen and decorin in the biological response to dynamic culture, analyzing the changes in gene expression and micromechanical PCM properties following sinusoidal compressive culture.

Chapter 3: Background

3.1 Articular Cartilage

Articular cartilage (AC) covers the ends of articulating surfaces of bones to ensure normal, pain-free motion and act as a shock absorber. AC is composed of 60-80% water (21,23,24), with the remainder being collagens, proteoglycans (PGs), and noncollagenous proteins (25). Only 1-2% of the final volume of cartilage is composed of chondrocytes, the main cell type within AC. Cartilage is avascular, aneural, and alymphatic causing limited self-repair (24). Chondrocytes create a highly organized matrix, giving AC the ability to withstand pressurization, compression, tension, and shear without failure (15,16,25). The cartilage matrix dissipates these mechanical loads to the cells, preventing cellular injury while allowing mechanical stimulation.

Cartilage extracellular matrix (ECM) surrounding chondrocytes consists of structural proteins, with type II collagen in the highest quantity (21,25), that form an oriented meshwork providing tensile strength and resiliency to mechanical stress. PGs within the ECM are negatively charged, due to their attached glycosaminoglycan (GAG) side chains and aid in the hydration of the tissue providing the ability to pressurize and withstand impact loading (24). PGs are either large aggregating molecules (aggrecan) or small proteoglycans, such as biglycan, decorin, and fibromodulin (25). Aggrecan is the most abundant PG present in the ECM of articular chondrocytes (17). Decorin and fibromodulin bind to type II collagen, aiding in the fibrillogenesis and organization of the collagen network.

3.2 OA breakdown of ECM

Osteoarthritis (OA) is one of the most common forms of joint disease, resulting in tissue failure of articular cartilage (26). During OA, there is a biochemical and biomechanical breakdown of cartilage ECM. PGs are degraded (fig. 3.1), resulting in a loss of fixed charge (27) and stiffness (28) and collagen breakdown results in a mechanical loss of integrity (Fig. 3.1) (27). This ECM degradation creates fissures and focal defects along the articulating surface of cartilage, which are exasperated during physiologic loading (1). This may be due to the inability of the chondrocytes to respond to anabolic signals (29). OA symptoms include cellular hypertrophy and terminal differentiation (29) coupled with increasing expression of type X collagen, alkaline phosphatase and the transcription factor *runx2* (27). The breakdown of ECM during OA could be due to the imbalance of anabolic (pericellular matrix (PCM) proteins) and catabolic enzymes (metalloproteinase-2 (MMP-2) (30), tissue inhibitors of metalloproteinases-2 (TIMP-2) (30,31), MMP-7 (31), MMP-13, A Disintegrin And Metalloproteinase with Thrombospondin Motifs-4 (ADAMTS-4), interleukin 1- β (IL-1 β) (31,32) and tumor necrosis factor- α (TNF- α) (32)) produced by chondrocytes.

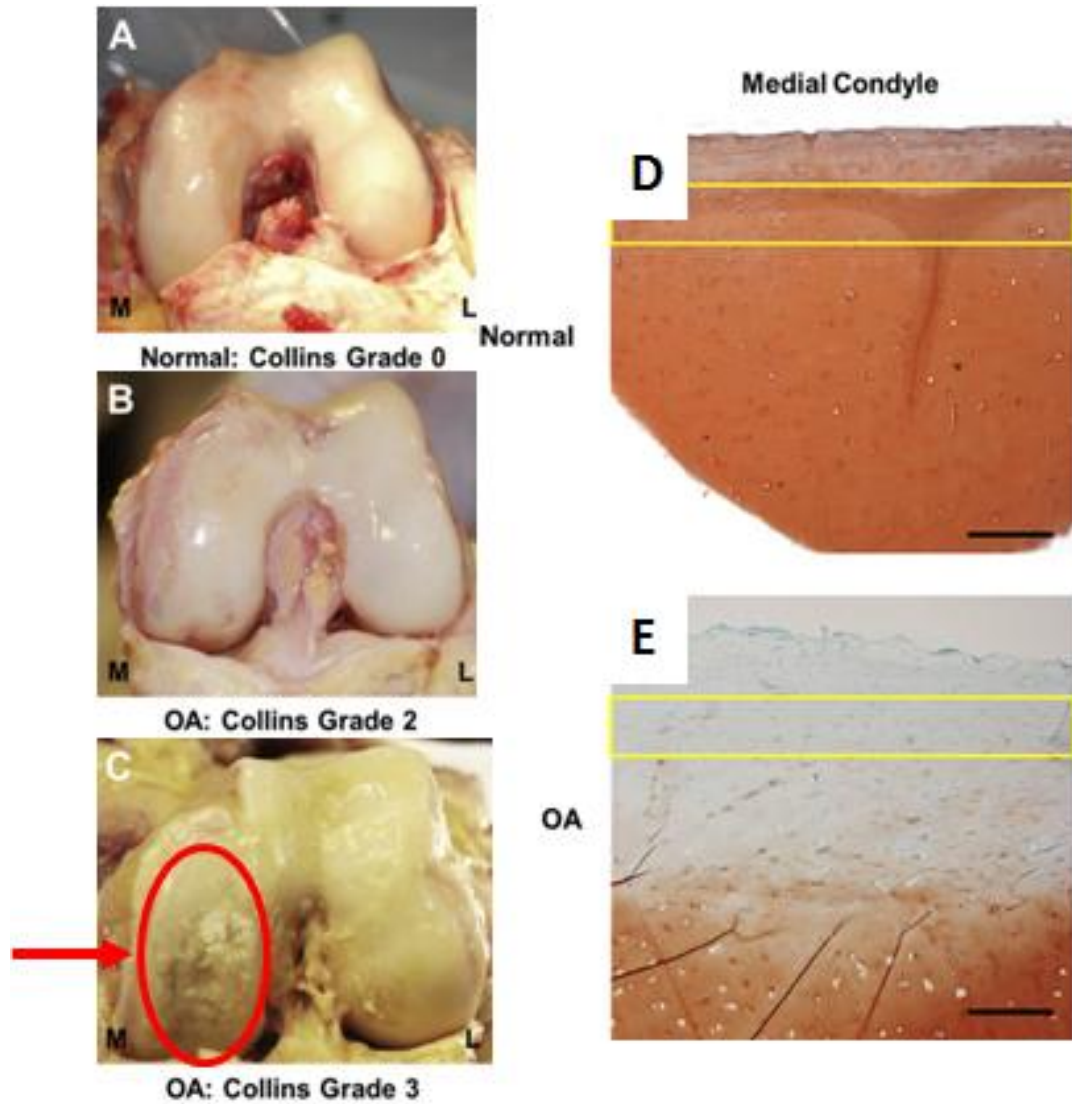


Fig. 3.1: OA degradation of cartilage seen in (A,B,C) is caused by a decrease in proteoglycan and collagen synthesis. Breakdown of cartilage causes fibrillation and focal defects (indicated by red arrow). Histological staining of cartilage shows a high concentration of proteoglycans (D) indicated by safranin-o staining (red, proteoglycans) which decreases in OA cartilage (E). (Adapted from Wilusz, R, 2013 (1)).

3.3 Regenerative Therapies

Current regenerative treatments for OA include debridement (33), drilling (34) and autologous chondrocyte implantation (ACI). These treatments mainly result in

physiologically weaker fibrocartilage. ACI, while showing better mechanical stability, still has limitations of minimal autologous chondrocytes retrieved, loss of phenotype during *in vitro* expansion, and donor site atrophy (10,35). Chondrocytes implanted into a defect within articular cartilage must overcome an adverse environment in which physiologically harmful mechanical stresses are present. Cell seeded biosynthetic matrices have been developed to protect the cells from excessive mechanical loading and aid the re-differentiation of chondrocytes expanded in monolayer (33,36,37).

Chondrocytes or progenitor cells have successful matrix synthesis (of type II collagen and PGs) when seeded in a three-dimensional matrix (38). To improve cartilage repair, growth factors, cytokines, and hormones have been incorporated in 3D scaffolds, such as transforming growth factor- β 3 (TGF- β 3), fibroblast growth factor (FGF), insulin growth factor (IGF), platelet derived growth factor (PDGF), and bone morphogenetic proteins (BMPs) (39). Hydrogel biosynthetic scaffolds for articular cartilage repair have had success with cell proliferation and cartilage ECM synthesis (40,41), but still lack the ability to fully maintain a chondrocyte-like phenotype within the scaffold and reach similar mechanical properties to native tissue. These scaffolds are composed of various forms of materials, focusing on alginate (18,40,42), agarose (17,43,44), hyaluronic acid (41,45,46), and collagen (47) hydrogel cultures. These scaffolds maintain round cell shape, allow for nutrient delivery, and can be modified to fit within the defect site of the articular cartilage. To further mimic physiologic conditions, these hydrogels can be modified to incorporate chondroitin sulfate and other ECM proteins (40).

Mechanical stimulation of these tissue engineered constructs (TECs) form a more functionally relevant construct for implantation. Chondrocytes are mechanically sensitive

and respond to different mechanical loadings with increases in synthesis of types I and II collagen, aggrecan, and versican under dynamic compression in culture (39). TECs are designed to control gene expression response to maintain chondrocyte phenotype as well as to control the application of mechanical stresses (48). This external control over the microenvironment is one way to control a cell's biological response to aid in tissue repair.

HMSCs collected from bone marrow aspirates can be expanded and then manipulated along the chondrogenic lineage (49,50) for repair of OA cartilage, but currently lack the ability to completely repair the tissue to its original physiologic function. HMSCs are implanted into TECs or directly into repair sites to repopulate the diseased location (fig. 3.2), but create a different PCM and ECM than autologous chondrocytes (20). This structurally different ECM (20) responds to mechanical loading in the joint differently (41).

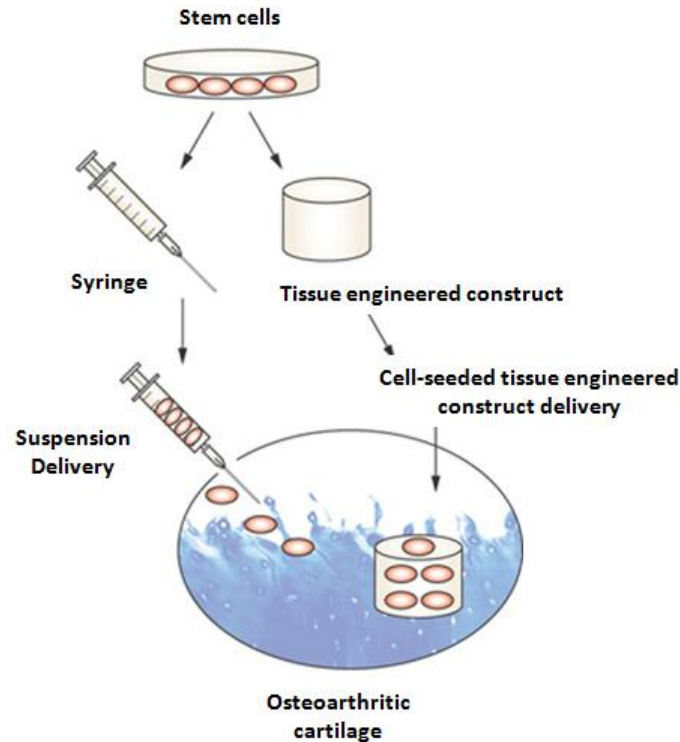


Fig. 3.2: Schematic of different methods of stem cell delivery into diseased osteoarthritic cartilage. MSCs can be directly injected into the defect site or seeded into specifically designed TEC scaffolds for implantation. TEC scaffolds improve matrix elaboration, differentiation, and mechanical properties to overcome the adverse environment at implantation (2). (As adapted from Noth, U, 2008 (2)).

3.4 hMSCs undergoing Chondrogenesis

HMSCs have the ability to commit to a lineage through both biomechanical (13,14,51,52) and biochemical induction (11). Varying methods of culture have been studied, including pellet (38,49) and hydrogel cultures (22,53). Gene expression during differentiation of hMSCs is temporally specific (fig. 3.3A). Initial upregulation of adhesion and signaling molecules such as integrins, fibronectin, TGF- β 1, TGF- β 2, TGF- β 3, BMP-4, BMP-5, SMAD4, EGF, VEGF, FGF-2, and Sox9 is seen (3). These

molecules can be analyzed to determine the effect of different mechanical and biochemical stimulations on chondrogenesis.

A)

Stage I (week 1)	Stage II (weeks 2-3)	Stage III (weeks 3-4)	Stage IV (weeks 5+)
MSC Proliferation	Chondroprogenitor differentiation	Chondrogenesis differentiation	Hypertrophic and terminal differentiation
<ul style="list-style-type: none"> •Aggrecan •BMP-2, -4, -5 •CD44 •COMP •EGF •FGF-2 •FGFR-2 •Fibronectin •Hyaluronan •Icam-1 •Integrin $\alpha 1, \alpha 2, \beta 1$ •sLRPs •SMAD-1, -4 •Sox4 •Sox9 •TGF-βR1 •TGF-$\beta 1, \beta 2, \beta 3$ •Type I collagen •Type II collagen •Type VI collagen •Type XI collagen •VEGF 	<ul style="list-style-type: none"> •Aggrecan •BMP-4, -5 •COMP •EGF •FGF-2 •FGFR-2 •Fibronectin •HAPLN1 •Icam-1 •Integrin $\alpha 1, \alpha 2, \beta 1$ •sLRPs •SMAD-1, -4 •Sox9 •TGF-βR1 •Type II collagen •Type X collagen •Type XI collagen •VEGF 	<ul style="list-style-type: none"> •Aggrecan •BMP-4, -5 •CHAD •COMP •FGF-2 •FGFR-2 •Indian Hedgehog •MATN3 •Runx2 •SMAD-1, -4 •Sox9 •Type II collagen •Type X collagen •Type XI collagen •VEGF 	<ul style="list-style-type: none"> •Aggrecan •Alkaline phosphatase •BMP-5 •COMP •Fibromodulin •Osteocalcin •Runx2 •Type I collagen •Type II collagen •Type IX collagen •Type X collagen •VEGF-A

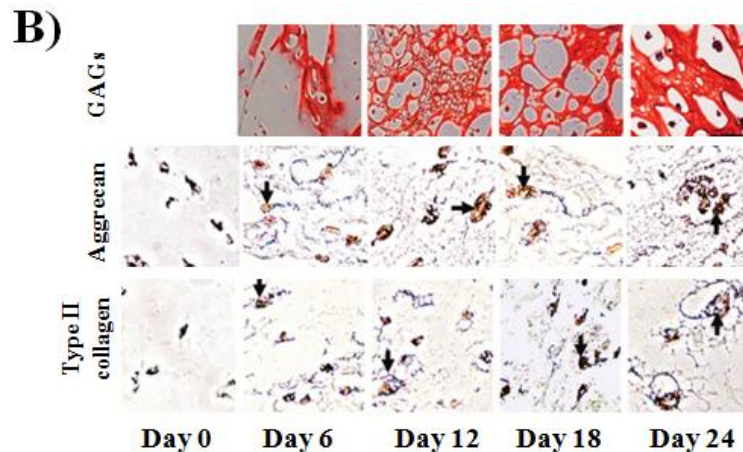


Fig 3.3: (A) Genes expressed during chondrogenesis at different stages of differentiation. Various studies have broken chondrogenic differentiation into four stages during *in vitro* culture. (Peak expressions are indicated by bold type). (B) During chondrogenic differentiation, GAGs, proteoglycans and type II collagen accumulate around the cell. GAGs are stained with Safranin-O and aggrecan and type II collagen were stained with immunohistochemistry. (As adapted from Chen, W, 2009 (3) and Xu, J, 2008 (4))

The form of mechanical loading applied to hMSCs will vary their lineage commitments. HMSCs dynamically pressurized for short term durations initiate chondrogenesis, in contrast to dynamic tension which initiates osteochondrogenesis (51,53). The degree, frequency, duration, and manner of mechanical loading can be sensed by hMSCs thereby affecting their gene expression. Intermittent unconfined dynamic compression or pressurization stimulates endogenous TGF- β cellular release causing upregulation of type II collagen and aggrecan (42,52). This improves chondrogenesis in short durations, but inhibits chondrogenesis long term with a decrease in GAG and collagen content, reaching terminal differentiation with expression of type X collagen when not supplemented with TGF- β 3 (54,55). To better achieve chondrocyte phenotype long-term, chemical stimulation using the TGF family is needed.

Chondrogenesis can be initiated with dexamethasone and members of the TGF family (11,17,49,52) when added to formulated culture medium *in vitro*. These upregulate *sox9* (22,38), type II collagen (*col2a1*) (22,49), and aggrecan (*acan*) gene expression as well as secretion of a type II collagen and proteoglycan rich pericellular matrix (fig. 3.4) (17,49). Melhorn hypothesizes that cells undergo genetic programming towards the chondrogenic lineage within three days of growth factor stimulation. PCM accumulation increases with growth factor treatment and shows dependence on concentration (11,42). When TGF- β is inhibited, chondrogenic markers are also inhibited, proving the integral role of growth factors (42). Chondrocyte phenotype is maintained with continued growth factor conditions and three dimensional culture conditions forming a type VI collagen rich PCM after 2 weeks (11,22). With increasing amounts of sGAGs and collagens secreted during

chondrogenic induction (fig. 3.3b), the mechanical properties of the scaffold will increase (55).

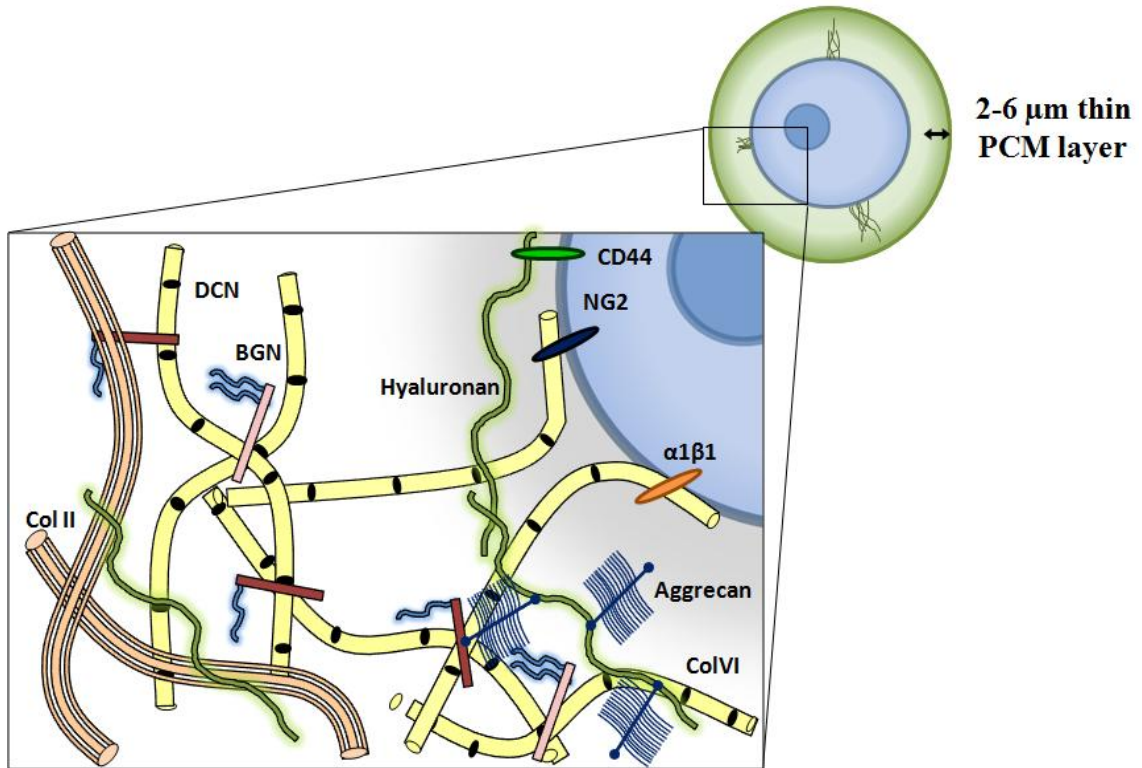


Fig. 3.4: Schematic of developing PCM around chondrogenic hMSCs. The PCM is composed of type VI collagen (ColVI), decorin (DCN), biglycan (BGN), aggrecan, and hyaluronan.

Mechanical and chemical signaling pathways interact complementarily when stimulated separately. Chondrogenesis is impaired when both stimulations are applied to hMSCs in long-term culture (54,55). Stimulation with TGF-β3 while undergoing intermittent long-term dynamic loading results in a lower amount of GAGs, collagen, and cell proliferation when compared to free swelling controls (54,55). Mechanical properties are also weakened (55). HMSCs treated with TGF-β3 for three weeks before long-term dynamic loading improved chondrogenesis and maintained chondrocyte phenotype over 6 weeks (55). The interplay between mechanical stress and *acan* and *sox9* expression is

complex and temporally dependent (54). Not only is the frequency and duration of loading important in regulating chondrocyte phenotype, but relaxation periods between loading also impacts chondrogenic gene expression. Constructs given longer relaxation times between cyclic loading showed improved synthesis of type II collagen and aggrecan (52). Mechanical stimulation improved matrix synthesis and homogeneity throughout agarose constructs while also increasing the equilibrium modulus (55). TEC mechanical properties improve with mechanical stimulation through uniform matrix synthesis (55).

Differentiation of hMSCs into physiologically functional chondrocytes need correct temporal applications of chemical and mechanical stimuli. The methods through which chondrogenesis is induced affects the new tissue being synthesized. Intrinsic control over the micromechanical environment of hMSCs undergoing chondrogenesis could have long-term effects on cellular protein synthesis and the mechanical properties of the tissue as a whole.

3.5 PCM components

The PCM is a thin layer surrounding chondrocytes and chondrogenic hMSCs, ranging between 2-6 microns thick (17,21,22). The PCM and chondrocyte together form a functional unit called a chondron, as seen in fig. 3.5 (19,21). The PCM is formed during cartilage formation, being found in young rats (fig. 3.5).

Acting as a biomechanical buffer, the PCM shields the cell from deformation which could be potentially detrimental while also enhancing small tissue strains for stimulation (16,19,22).

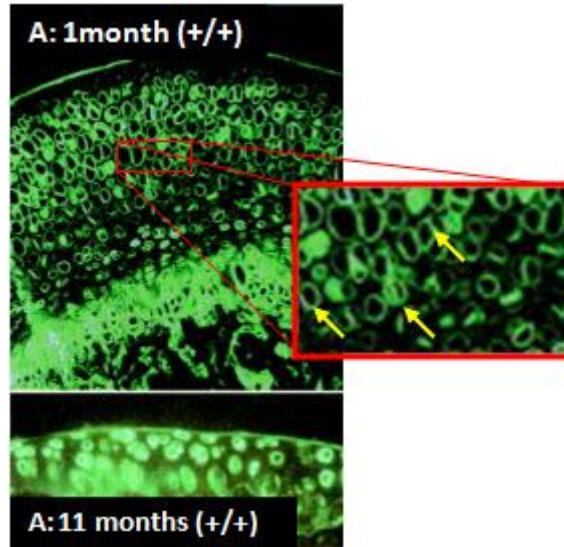


Fig. 3.5: Immunostaining for type VI collagen demonstrating the PCM during cartilage development at (A) 1 month and (B) 11 months of growth in wild-type mice. Arrows point to type VI collagen staining within the PCM of chondrons in the articular cartilage. Adapted from Alexopoulos, L, 2009 (5).

Cellular deformation decreases compared to applied bulk deformation of scaffolds with increasing amounts of PCM (22). The PCM's mechanical stability is frequency dependent (42), which may be due to fluid flow within the PCM or to its viscoelastic biphasic behavior (19). The increasing amounts of matrix accumulated during *in vitro* culture show an increase in strength and a decrease in viscoelastic properties associated with increased deposition of proteoglycans and collagen (42).

In addition to acting as a mechanical stabilizer, the PCM also aids maintenance of chondrocyte phenotype biochemically. The PCM sequesters TGF- β and latent TGF- β binding proteins in the fibrillar network (3,21). Sequestration of growth factors immediately surrounding the cell allows for ready availability when needed. Chondrocytes isolated with their PCM intact have a higher expression of type II collagen

and proteoglycans and lower expression of type I collagen than isolated chondrocytes (18). Growth factor availability and therefore stimulation is not only controlled through sequestration capabilities, but through the permeability of the PCM which is lower than the surrounding ECM (19). Precise control over the micromechanical environment's composition surrounding chondrocytes may aid in controlling mechanotransduction signaling events and the cellular response to mechanical stress.

3.6 Type VI Collagen and Decorin

Type VI collagen is a beaded filamentous heterotrimer fibril, about 125 nm in length consisting of three different α -chains (56) ($\alpha 1(VI)$, $\alpha 2(VI)$, and $\alpha 3(VI)$) that create a triple helical domain (57). These helical fibrils form dimers and tetramers intracellularly before being secreted into the PCM and assembling into the microfibrillar network (fig. 3.6) (58). PGs bind the PCM to the ECM through type II and VI collagen interactions (17,59).

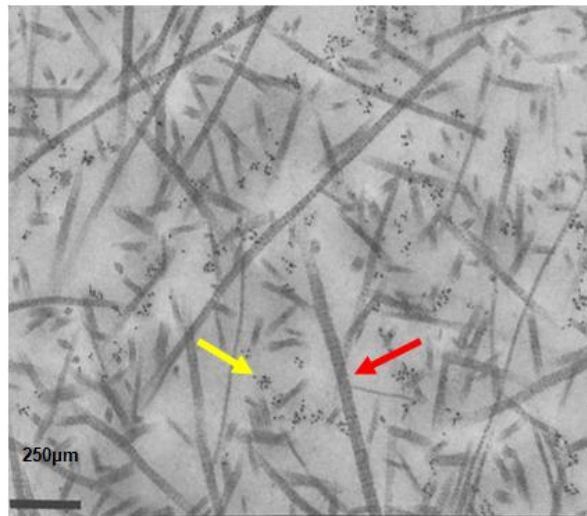


Fig. 3.6: ColVI microfibrils form a branched network. Red arrows indicate collagen bands and yellow arrows indicate decorin proteoglycans that “decorate” ColVI (Adapted from Keene, D, 1988 (6)).

The basketlike network of type VI collagen is bound to the cell membrane through integrin receptors, NG2 receptors (membrane bound chondroitin sulfate PGs) and hyaluronan (60). These cell membrane attachments may initiate a mechanosignaling cascade as a response to mechanical stimulation. Type VI collagen is exclusively found in the PCM of chondrocytes (20,57) and is maintained with low levels of transcription (20). Type VI collagen isn't necessary to maintain an "intact" PCM (5), but a PCM lacking type VI collagen decrease in stiffness, measuring a lower Young's modulus. Mice lacking type VI collagen also show a faster development of OA with increased fibrillation and focal defects along the surface of the articular cartilage (fig. 3.7) (5).

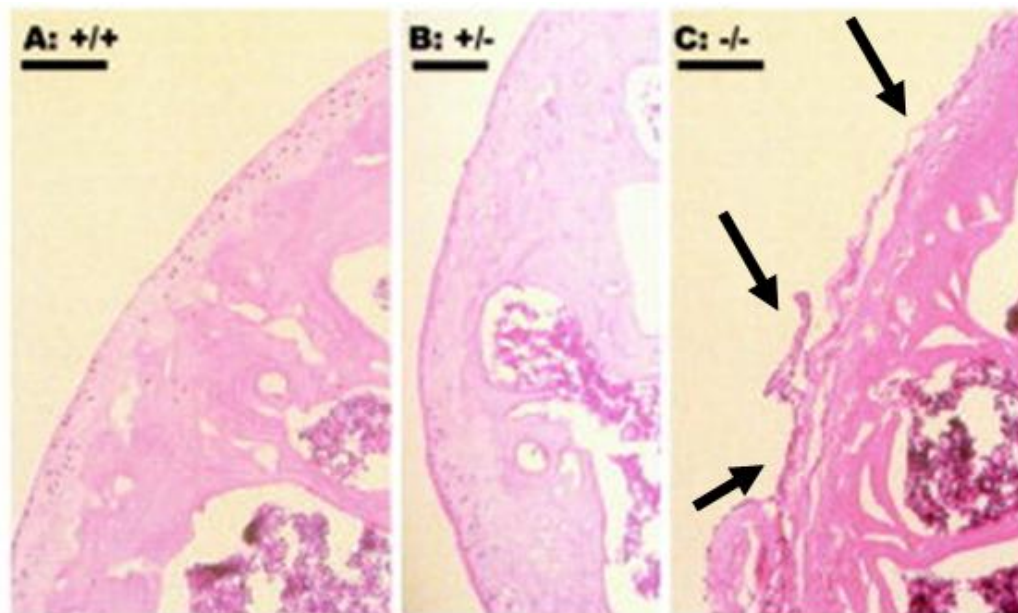


Fig. 3.7: OA progresses in type VI collagen knockout mice. Images shown are hematoxylin and eosin staining of femoral cartilage from 11 month old mice of (A) wild type, (B) heterozygous, and (C) knockout mice. Arrows point to fibrillation of articular cartilage surface within the knockout model. (Adapted from Alexopoulos, L, 2009 (5)).

Decorin is a ubiquitous small leucine rich proteoglycan (SLRP), consisting of a core protein with two dermatan sulfate chains attached (28,61). These GAGs aid in controlling

the collagen network spacing and fibril diameter (28). Decorin can bind to multiple collagens simultaneously (61), organizing the fibrillogenesis of collagen (fig. 3.6), as well as the structure of the collagen network. Knockout models of decorin result in an upregulation of biglycan (BGN), which is a PG similar to decorin but with three dermatan sulfate side chains. This shows a regulatory or a compensatory effect of decorin on other PCM PGs (28,61). Biglycan shares binding sites on collagen proteins with decorin, but has a lower affinity, causing a lower involvement in PCM and ECM organization (61). Decorin is involved in the sequestration of TGF- β 3, FGF-2, TNF- α , PDGF, and IGF-1 (61,62) and also has been associated with cell proliferation signaling (61), causing the cell to cease proliferation and enhance matrix synthesis.

3.7 Mechanotransduction and signal transduction events

Mechanical stimulations affect chondrocyte biological processes and are involved in tissue remodeling to maintain cartilage homeostasis. Various studies have examined the effects of substrate stiffness (48), 3D culture (55), and mechanical stimulations(63-65) on chondrocyte response. Determining the pathway through which cells feel their mechanical environment and create a chemical response will aid the development of TECs to better accommodate cell phenotype.

Isolated chondrocyte systems have been used to determine gene expression response to loading. The most frequently used are agarose or alginate constructs, because they regain chondrocyte roundness as well as providing a homogenous environment completely surrounding the cell (22,63,66) . Applying either unconfined or confined compression to the hydrogel constructs resembles physiologic loading to analyze gene

expression and matrix accumulation (53,55,67). Compression stimulates the activation of signaling pathways involving p38, mitogen-activated protein kinases (MAPK), cFos and cJun (63). ERK activated FGF2 and specific proteoglycans within the PCM have also been analyzed as potential mechanotransducers (68). The role of the PCM has been analyzed in mechanotransduction events through isolation of whole chondrons compared to singular chondrocytes (69).

Within cartilage, compression of the tissue causes a decrease in volume and surface area (16). A possible mechanism for initiating mechanosignaling is nuclear deformation during mechanical loading (70,71), which is seen to increase with culture time and PCM accumulation. Another mechanism would be cytoskeletal reorganization (42). Expression of RhoA and actin filament polymerization is associated with dedifferentiation and inhibits the activity of sox9 (72). Chondroprogenitor cell culture in alginate maintains low levels of actin polymerization and RhoA signaling, with the cell sensing the maintained round phenotype in culture (72). With matrices of increasing stiffness, chondrocytes lose their roundness, rearrange stress fibers in line with created focal adhesions (48), decrease synthesis of aggrecan and type II collagen, and increase proliferation, shifting towards a more hypertrophic and osteogenic phenotype (20). These systems, while establishing the relationship between varying forms of loading and chondrocyte response, do not elucidate the roles of individual components during the signaling cascade.

Targeted subtraction of varying proteins surrounding hMSCs undergoing chondrogenesis can help determine functional roles at varying points of chondrogenic mechanosignaling. Different approaches to analyzing chondrocyte mechanotransduction

can include disruption of the PCM, intracellular signaling cascade, and transmembrane disruption (fig. 3.8) (7). RNA interference (RNAi) is one method of specific protein knockdown which can be used to analyze the mechanotransduction pathway. Understanding the mechanism through which chondrocytes feel and respond to mechanical stress will improve design of tissue engineered constructs.

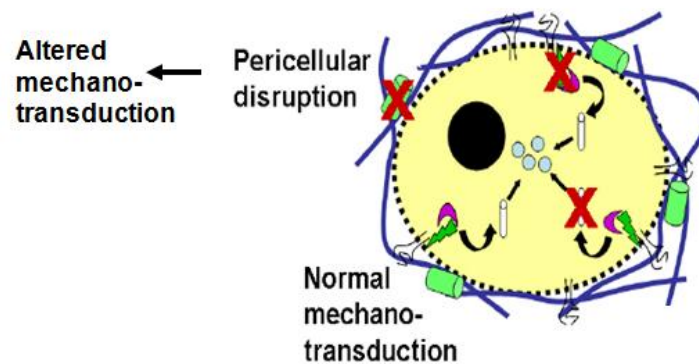


Fig. 3.8: Mechanotransduction can be analyzed through targeted disruption of pericellular matrix proteins using RNA interference. (Adapted from Hsieh, A, 2010 (7)).

3.8 RNA interference and shRNA lentiviruses

RNAi is an endogenous mechanism to protect against viral infection and insertable genetic elements as well as to regulate gene expression (73). This system is activated in mammalian cells when a long double stranded RNA (dsRNA) is detected within the cell (73). The RNase III-like enzyme Dicer cleaves the long dsRNA into 21-23 bp long short interfering RNAs (siRNAs) with 2- to 3- nucleotide long 3' overhangs (73-75). These siRNAs join with the RNA-induced silencing complex (RISC) where the sense and antisense strands of the siRNA are separated. The antisense of the siRNA guides the RISC to the target gene's transcript for homologous sequence-specific cleavage (73,75) silencing the gene.

RNAi can be initiated through chemically introduced siRNAs, which are able to suppress gene expression for up to a week (73,75) but are transient in nature, having short half-lives. The effectiveness of siRNAs are concentration dependent and is directly related to the amount of cell division occurring. SiRNAs also must be synthetically created, becoming a costly method of gene suppression (74). Lentiviral delivery of a small hairpin RNA (shRNA) construct into the host's genome allows a stable delivery of siRNAs to the cell for long-term activation of RNAi in a cost effective and rapid manner (73,75). The shRNA transcript activates the RNAi mechanism by first severing the loop sequence with Dicer before initiating the RISC sequence (fig.3.9) (74,75). The shRNA sequences are engineered for exact homology to the target gene.

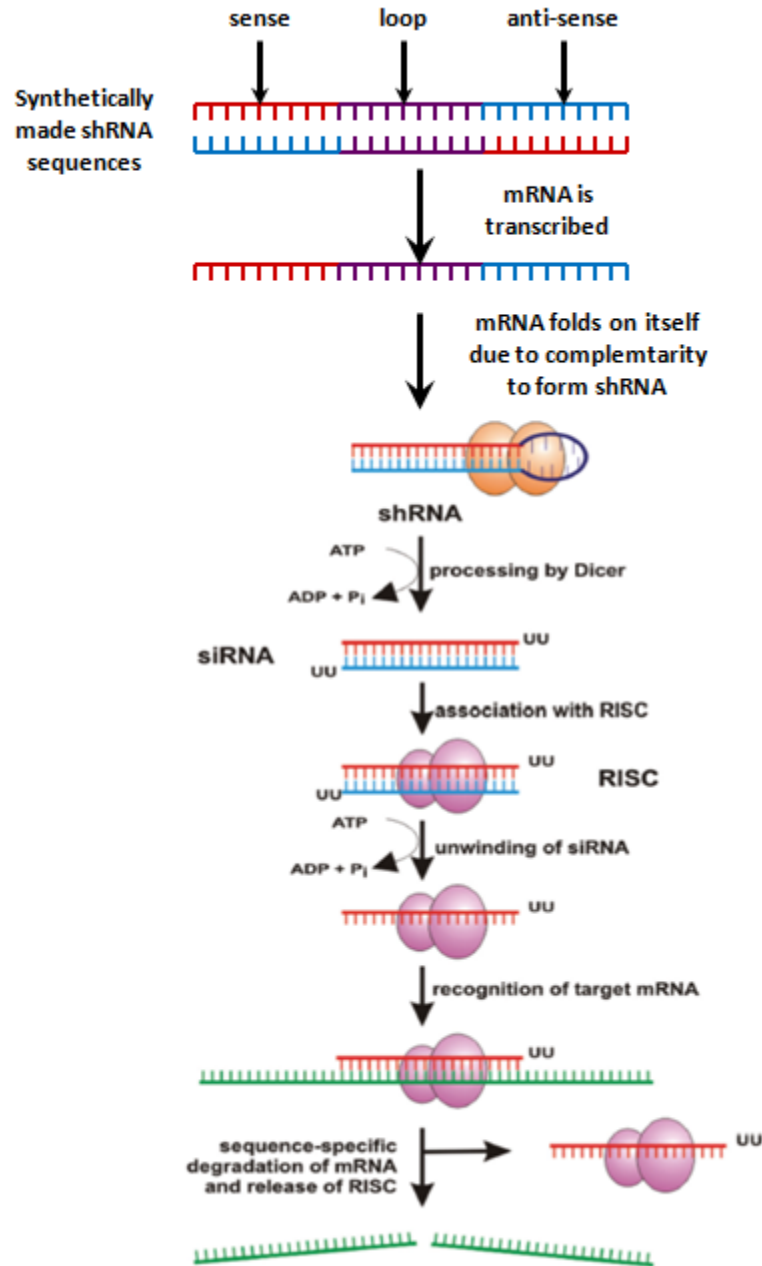


Fig. 3.9: shRNA initiated RNAi. shRNA sequences are inserted into the human genome using lentiviral vectors. mRNA folds on itself created a dsRNA initiating the endogenous RNAi mechanism that recognizes and degrades target mRNA (8).

The level of knockdown created by an shRNA lentiviral vector is dependent on the positional insertion of the viral DNA, the level of hairpin expression, the processing of the shRNA into siRNA (75) and the structure of the target mRNA (74). ShRNA

constructs must be homologous to the target gene (73). To ensure avoidance of off-target effects, BLAST searches of all used shRNA sequences using the NCBI website must be done (74). Selected regions should have non-repetitive sequences, no intronic sequences, no long base runs (in order to avoid slippage), and be around 50% GC content for stability. The un-translated regions of the gene should also be avoided and should be at least 50-100 nt downstream of the start codon (74). ShRNA sequences consist of two stem sequences that are complementary and each 19-29 nt long with a 4-23 nt loop sequence separating the stems (74). These sequences should be screened for effectiveness, since these guidelines do not ensure complete knockdown of target genes (74). Manipulating the expression of specific genes allows the examination of their functional roles and allows intrinsic control over mechanotransduction events, engineering the cell's sensitivity to mechanical stress.

RNAi can be utilized for reverse genetics to observe the function of specific genes or proteins through disruption (75). Due to incomplete silencing of transcribed genes, RNAi suppression is considered a “knockdown” as opposed to a “knockout” system. Long term effects of gene suppression for therapeutics have not yet been studied, with the possibility of causing oncogenesis. ShRNA lentiviral vectors remain useful *in vitro*, while further research needs to be conducted for *in vivo* implementation (15).

3.9 Cellular Engineering

Genetically engineering chondrocyte function has been attempted to enhance chondrogenesis, and to improve functional tissue repair. Genetic engineering of both autologous chondrocytes and hMSCs has been explored to determine if genetically

changing a cell to produce a specific microenvironment will improve tissue repair (28,76). The use of lentiviral delivery to suppress aggrecanases (77), or adenoviral delivery to suppress type I collagen and upregulate TGF- β 1 (78), has recovered the chondrocyte phenotype lost during expansion *in vitro* (76). Maintenance of the chondrocyte phenotype is important in cell based cartilage engineering and learning to manipulate the phenotype for long-term maintenance will overcome adverse environments for defect repair. Viral vectors have shown potential for tissue engineering purposes, both to improve defect repair and to control matrix synthesis of genetically modified cells.

The functional roles of specific proteins directly surrounding chondrocytes has been examined with lentiviral vectors as well. Chondrogenic mechanosignaling has also been examined through overexpression or silencing varying proteins (72,79). Over-expression of DCN and its mutated core protein in chondrocytes investigated its role in ECM organization and its mechanical contribution to cartilage properties (28). The cytoskeleton was found to be important in internal chondrogenic signaling, with silencing of vimentin or protein kinase A (77) and overexpression of RhoA (72) impeding chondrogenesis. Type VI collagen has been successfully knocked down in mammalian cells using transfected shRNA constructs to create a transgenic animal (80). The role of integrins in the dedifferentiation of chondrocytes has also been studied (67).

My research utilized this technology to examine the roles of proteins at varying points in mechanotransduction through targeted disruption. Changing a cell's response to mechanical loading intrinsically could help in overcoming adverse environments as well as improving a cell's adaptation to a tissue engineered construct for *in vivo* loading. This

is also a stable method to determine these proteins' roles in stimulating protein synthesis to mechanical loading before and after PCM aggregation.

Chapter 4: Roles of type VI collagen and decorin in human mesenchymal stem cell biophysics during chondrogenic differentiation¹

4.1 Introduction

The use of human mesenchymal stem cells (hMSCs) in regenerative medicine has the potential to repair damage in load bearing tissues such as articular cartilage (57,81), reducing the need for autologous chondrocytes. During chondrogenesis, hMSCs develop a pericellular matrix (PCM) that is rich in type VI collagen (ColVI) (21,60,82), fibronectin (17,82,83), hyaluronan (21,84), and proteoglycans (PGs) such as aggrecan, decorin (DCN), and biglycan (BGN) (17,82). This thin 2-6 micron layer of matrix acts as both a biomechanical buffer (42,84), controlling the amount of deformation applied to the cell (16,22,69), as well as a biochemical conductor, presenting the cell with growth factors and signaling molecules (3,21,22). The PCM is believed to modulate the mechanoresponsiveness of chondrocytes and chondrogenic hMSCs, but the exact roles of the individual PCM proteins have yet to be determined.

In articular cartilage, type VI collagen is found exclusively in the PCM surrounding chondrocytes (60,83) and is maintained through low levels of transcription, forming a microfibrillar network once secreted from the cell (22,58,60,82,83).

¹Accepted for publication: Twomey JD, Thakore PI, Hartman DA, Myers EGH, Hsieh AH. “Roles of type VI collagen and decorin in human mesenchymal stem cell biophysics during chondrogenic differentiation.” *European Cells and Materials*.

ColVI's interactions with the cell membrane at varying locations make it a primary candidate as a mechanotransducer (60,85,86). This complex network assembles and binds to the surrounding extracellular matrix (ECM) through interactions with type II collagen, aggrecan, and hyaluronan with aid from PGs such as DCN, BGN, as well as type IX collagen (6,17,58-60,82,87).

The PCM has shown direct control over cellular phenotype, as chondrocytes isolated without a PCM exhibit a phenotypic change characterized by greater *coll1a1* and lower *col2a1* expression than those isolated with a native PCM (18). The metabolic activity of hMSCs undergoing chondrogenic differentiation changes with PCM development and is also different from that of mature chondrocytes (17,83). Therefore it is believed that the PCM directly surrounding chondrogenic hMSCs is temporally changing and complex, with the microenvironment composition influencing chondrogenic potential and response (18,69,83).

Biomechanically, the developing PCM surrounding both mature chondrocytes and differentiating hMSCs has been found to reduce cell deformation in hydrogels under applied compression (22,42,84). Protein deposition and biosynthesis progressively alter PCM material properties, causing increases in stiffness and elastic-like response (42). The ability of the PCM to help articular chondrocytes resist deformation has been shown to depend on hyaluronan during initial PCM assembly, and speculated to depend on collagen and other matrix components at later time points (84). Native chondrocytes with their PCM, which have been termed chondrons, exhibit a unique viscoelastic response to compression due to mismatched stiffnesses among the chondrocyte, its PCM, and the cartilage ECM (88).

Toward an improved understanding of how individual components of the PCM biochemically and biophysically regulate hMSCs during chondrogenesis, our current study sought to elucidate the roles of ColVI and DCN in resisting cellular deformation as well as their relationships with other PCM gene expression. We determined the function of these specific proteins through targeted subtraction using shRNA-mediated RNA interference (RNAi) (75). Overall, we found that knockdown of ColVI and DCN differentially altered PCM accumulation, expression of other PCM components, and cell deformation in hydrogels. These results demonstrate that the microenvironment of chondrogenically differentiating hMSCs can be controlled using genetic engineering techniques to modulate PCM composition.

4.2 Materials and Methods

4.2.1 Cell Culture

Passage 2 hMSCs were obtained from Lonza (Lonza, Walkersville, MD) and were expanded in monolayer according to the manufacturer's protocols, subculturing with growth media (GM): high glucose DMEM (HG-DMEM) (Gibco/Invitrogen, Carlsbad, CA) supplemented with 10% fetal bovine serum (FBS) (Gibco), 100U/mL penicillin/streptomycin (Gibco), 1% MEM non-essential amino acids (Gibco), and 4mM L-Glutamine (Invitrogen). Cells were cultured in monolayer at 37°C with 5% CO₂, with media changes three times per week until passage 4 or 5, at which point they were used experimentally. Experimental and control groups were lifted from monolayer with 0.25% trypsin-EDTA (Gibco), centrifuged at 600xg for 5 minutes before being re-suspended in a 2% (w/v) alginate solution (Research Products International, Mount Prospect, IL) at a

concentration of 2.0×10^6 cells/mL. Cells were expelled drop-wise into a 102mM CaCl₂ solution using a 22 gauge needle and allowed to cure for 10 minutes. Alginate-hMSC beads were cultured in either GM or chondrogenic induction media (CM) containing HG-DMEM, ITS Universal Culture Supplement Premix (BD Biosciences, San Jose, CA), 10nM dexamethasone, 50µg/mL L-ascorbic acid (Sigma), 40 µg/mL L-Proline (Sigma), 100U/mL penicillin/streptomycin, 1mM sodium pyruvate, 0.584 g/mL L-glutamine, and 10ng/mL TGF-β3 (Lonza). Beads were cultured for 1, 2, or 4 weeks post seeding at 37°C with 5% CO₂.

4.2.2 Lentivirus Preparation

21-23 nt shRNA sequences were designed using RNAi Codex (web ref. 1) from either human *col6a1* [Gen Bank: NM_001848] or human *dcn* [GenBank: NM_001920] mRNA. Stem-loop-stem shRNA constructs were created, annealed to create complimentary oligos, and cloned into a lentiviral vector containing a blasticidin resistance gene with a U6 promoter and a Pol III termination sequence. The BLOCK-iT U6 RNAi Entry Vector Kit and the BLOCK-iT Lentiviral RNAi Expression System (Invitrogen, Carlsbad, CA) were used to generate shRNA constructs and packaged into a replication-deficient lentivirus (denoted shColVI A-E and shDcn A-F) using 293FT cells, Lipofectamine 2000 and a manufacturer-supplied packaging mix (Invitrogen). The chosen sequences are listed in Table 4.1. A lentiviral expression vector containing the gene for GFP was prepared in parallel using the Vivid Colors pLenti6.2-GW/EmGFP kit (Invitrogen) for a lentiviral control. Virus-containing supernatants were harvested 72 hours post transfection and stored at -80°C until used experimentally.

5'-"stem-loop-stem"-3' sense and 3'-"stem-loop-stem"-5' anti-sense sequences

shColVI	A	5'-CACCGCCTTTGGACTGAAAGGAGACGAATCTCCTTTCAGTCCAAAGG-3'
		3'-CGGAAACCTGACTTTCTCTGCTTAGAGGAAAGTCAGGTTTCCAAAA-5'
	B	5'-CACCGTGGGCATCAAAGACGTGTTTCGAAAAACACGTCTTTGATGCCAC-3'
		3'-CACCCGTAGTTTCTGCACAAAGCTTTTTGTGCAGAAACTACGGGTGAAAA-5'
	C	5'-CACCGCAAAGTCAAGTCCTTACCAACGAATTGGTGAAGGACTTGACTTTG-3'
		3'-CGTTTCAGTTCAGGAAGTGGTTGCTTAACCACTTCTGAACTGAAACAAAA-5'
	D	5'-CACCGCGGAGACGATAACAACGACATCGAAATGTCGTTGTTATCGTCTCCG-3'
		3'-CGCCTCTGCTATTGTTGCTGTAGCTTTACAGCAACAATAGCAGAGGCAAAA-5'
	E	5'-CACCGCTGTGTCTTACTAGAAACAACGAATTGTTTCTAGTAAGACACAGC-3'
		3'-CGACACAGAATGATCTTTGTTGCTTAACAAAGATCATTCTGTGTCGAAAA-5'
shDcn	A	5'-CACCGCTACTAGAGATATTCTTATCGAAATAAGAATATCTCTAGTAG-3'
		3'-CGATGATCTCTATAAGAATAGCTTTATTCTTATAGAGATCATCAAAA-5'
	B	5'-CACCGCAAATTTCCAGTTTAAGTACGAATACTTAAACTGGAAATTTG-3'
		3'-CGTTTAAAGGTCAAATTCATGCTTATGAATTTGACCTTTAAACAAAA-5'
	C	5'-CACCGCCAGGTTGTCTACCTTCATAACGAATTATGAAGGTAGACAACCTGG-3'
		3'-CGGTCCAACAGATGGAAGTATTGCTTAATACTTCCATCTGTTGGACCAAAA-5'
	D	5'-CACCGCGACTTTATCTGTCCAAGAATCGAAATCTTGGACAGATAAAGTCG-3'
		3'-CGCTGAAATAGACAGGTTCTTAGCTTTAAGAACCTGTCTATTTAAGCAAAA-5'
	E	5'-CACCGCCATTCAACTCGGAAACTATCGAAATAGTTTCCGAGTTGAATGGC-3'
		3'-CGGTAAGTTGAGCCTTTGATAGCTTTATCAAAGGCTCAACTTACCGAAAA-5'
F	5'-CACCGCCGTTTCAACAGAGAGGCTTACGAATAAGCCTCTCTGTTGAAACGG-3'	
	3'-CGGCAAAGTTGTCTCTCCGAATGCTTATTCGGAGAGACAACCTTGCCAAAA-5'	

Table 4.1: Sense and anti-sense hairpin sequences for shRNA constructs against *col6al* or *dcn*.

4.2.3 *shRNA Transduction*

For initial screening trials to identify optimal shRNA viral vectors, hMSCs were seeded at 60,000 cells/well in tissue culture treated polystyrene 6-well plates. Monolayers of hMSCs were infected with lentiviral particles in the presence of 6µg/mL Polybrene (Sigma) to aid in transduction efficiency. Each well was incubated with 100µL of either an shColVI (A-E) or an shDcn (A-F) vector for 24 hours. Cell monolayers were then washed and maintained in GM culture without selection for 1, 5, 8, or 14 days post infection, at which point gene expression was assessed.

In titering experiments, hMSCs were seeded at 60,000 cells/ well in in tissue culture treated polystyrene 6-well plates as previously described. hMSCs were infected with 100µL of either shColVI-D, shDcn-F(identified from our screen; hereafter labeled shColVI and shDcn, respectively), or the GFP control vector in the presence of 6µg/mL Polybrene (Sigma) to aid in transduction efficiency. The following day, virus was removed and cells were incubated for 24 hours in GM. To select for a pure population of transduced cells, monolayers were incubated with GM containing 12 µg/mL of blasticidin for 24 hours. We performed extensive preliminary sensitivity tests to identify this short-high intensity treatment for minimizing adverse effects of blasticidin culture. After transduced cell selection, cells were harvested from monolayer and flash frozen for DNA quantification using a Quant-iT PicoGreen dsDNA assay (Invitrogen, Carlsbad, CA).

In actual experiments, each well was incubated with either shColVI, shDcn, or the GFP control vector at a multiplicity of infection (MOI) of 1 for 24 hours. After virus

removal, cells were incubated with GM containing 12 $\mu\text{g}/\text{mL}$ of blasticidin for 24 hours. Blasticidin-free shRNA-infected control and non-infected control hMSCs were cultured in parallel. Some hMSCs were cultured for 1, 4, 7, or 14 days post-infection for gene expression studies. Some blasticidin-selected pure populations were trypsinized for alginate bead culture 24 hours post selection (day 0).

4.2.4 Determination of Viral Efficacy (Titering)

To determine the concentration of viral particles within the viral supernatant, a titering assay determines the number of cells transduced with the lentiviral vector. The titer of a virus determines the concentration of infecting viral particles, or titering units (TU), in suspension. Harvested cell samples underwent five freeze-thaw cycles for cell lysis, were combined with PicoGreen reagent, and fluorescence was read using a SpectraMax M5 plate reader (Molecular Devices, Sunnyvale, CA). Percentage of transduced cells was determined using a cell standard from PicoGreen assay to calculate the number of cells unaffected by the blasticidin resistance which indicates successful transduction. The titer (TU/mL) for each virus was calculated using the following equation: $T = (\% \text{ transduced cells} * \text{the number of seeded cells}) / \text{dilution of viral supernatant within media (mL/mL)}$.

4.2.5 Cell Viability

To determine the viability of cells in alginate beads, at each time point per sample two or three beads were centrally cut and transferred to a working solution of 5-chloromethylfluorescein diacetate (CMFDA) and ethidium homodimer-1 (EthD-1) (Invitrogen) and counterstained with 4',6-diamidino-2-phenylindole (DAPI) (Invitrogen).

From the cut face of the beads, ten confocal fluorescence image stacks of 30 μm depth were taken at 100x magnification with a Nipkow (spinning) disk-equipped Olympus IX81 microscope. Viability was assessed on sections using channel separation and threshold particle analysis using ImageJ (NIH). All results are expressed as a percentage of total cells that are viable (green only).

4.2.6 Gene Expression

Gene expression was quantitatively assessed as previously described (89). At each time point, cells (shColVI, shDcn, and GFP transduced, along with a non-infected hMSC control) were released with a 100 mM sodium citrate, 30 mM EDTA solution, spun down and re-suspended in a buffer solution containing β -Mercaptoethanol (Fisher Scientific, Pittsburgh, PA) before flash freezing. RNA was isolated (RNeasy Micro, Qiagen, CA) and total RNA was reverse transcribed. Gene expression was analyzed using qRT-PCR (MyiQ System, BioRad, CA) with primers designed for human genes (Table 4.2) using Primer3 software (web ref. 2).

Gene	Forward and Reverse sequences	GenBank accession no.
<i>col6a1</i>	5'-CTACACCGACTGCGCTATCA-3'	NM_001848
	5'-GCCACCGAGAAGACTTTGAC-3'	
<i>col6a2</i>	5'-ACCGAGATCAACCAGGACAC-3'	NM_001849
	5'-GGTCTCCCTGTCTTCCCTTC 3'	
<i>col6a3</i>	5'-GCCAACCATTGTCACACAAG-3'	NM_004369
	5'-TTCAGGCCTCACAGTGTCTG-3'	
<i>dcn</i>	5'-AATTGAAAATGGGGCTTTCC-3'	NM_001920
	5'-GCCATTGTCAACAGCAGAGA-3'	
<i>gapdh</i>	5'-GAGTCAACGGATTTGGTCGT-3'	NM_002046
	5'-TTGATTTTGGAGGGATCTCG-3'	
<i>acan</i>	5'-ACAGCTGGGGACATTAGTGG-3'	NM_001135
	5'-GTGGAATGCAGAGGTGGTTT-3'	
<i>sox9</i>	5'-AGTACCCGCACTTGCACAAC-3'	NM_000346
	5'-CGTTCTTCACCGACTTCCTC-3'	
<i>bgn</i>	5'-ACCTCCCTGAGACCCTGAAT-3'	NM_001711
	5'-CTGGAGGAGCTTGAGGTCTG-3'	
<i>col9a2</i>	5'-GCGGATTTCTGTGTCCAA-3'	NM_001852
	5'-CCGCATGCCCTTCACT-3'	

Table 4.2: Sequences of primers used for qRT-PCR.

All primer amplification efficiencies were determined using linear regression efficiency methods and were determined to be between 91.2% and 108.2% efficient ($R^2 > 0.99$) (90). Expression levels for *acan*, *sox9*, *bgn*, *col6a1*, *col6a2*, *col6a3*, *dcn*,

col9a2 and housekeeping gene *GAPDH* were analyzed using the $\Delta\Delta\text{Ct}$ method. Cycle threshold (Ct) values were averaged and ΔCt was calculated by subtracting the average Ct values of *GAPDH* from those of the gene of interest ($\Delta\text{Ct } col6a1 = \text{Ct } col6a1 - \text{Ct } GAPDH$). $\Delta\Delta\text{Ct}$ for each gene of interest was determined by subtracting the designated control ΔCt from the experimental ΔCt at each time point (i.e. $\Delta\Delta\text{Ct } col6a1_{D7} = (\Delta\text{Ct } col6a1_{shColVI, D7} - \Delta\text{Ct } col6a1_{GFP, D7})$). Relative gene expression levels (fold difference) were computed through the exponential relation $2^{-\Delta\Delta\text{Ct}}$ (91). Data are shown as average values of the range of calculated fold differences ($2^{-\Delta\Delta\text{Ct} + \text{SD}}$ and $2^{-\Delta\Delta\text{Ct} - \text{SD}}$) \pm range.

4.2.7 Western Blotting

To quantify protein translation, cells were released from alginate as described above. Samples were re-suspended in a lysis buffer (50 mM HEPES (Fisher), 150 mM sodium chloride (Fisher), 1% Triton X-100 (Ricca Chemical Compant, Arlington, TX), 1mM EDTA (Fisher), 10mM Na-pyrophosphate (Fisher), 10% glycerin (Fisher)) with a 1:100 concentration of protease inhibitor cocktail (Fisher Scientific) to precipitate out the proteins. A portion of the protein supernatant was separated for a modified Lowry assay to determine protein concentration using a Folin-Phenol color reaction detected by a ND-1000 Spectrophotometer (Nanodrop, Wilmington, DE). The remaining supernatant was mixed 1:1 with a loading buffer (13% (v/v) Tris-HCl, 20% (v/v) glycerol, 4.6% (w/v) SDS, 0.02% (w/v) bromophenol blue, 200mM dithiothreitol). SDS-PAGE was performed using pre-cast Criterion Tris-HCl gels (BioRad) using equal amounts of protein from each sample. Protein were detected with antibodies targeting β -actin (R-22; Santa Cruz Biotechnology, Inc., Dallas, TX), $\alpha 1(\text{VI})$ (H-200; Santa Cruz), and decorin (H80; Santa Cruz). For decorin detection, blots were incubated with 1 U/mL chondroitinase ABC

from proteus vulgaris to digest dermatan-sulfate GAG chains from the decorin core protein (C2905, Sigma-Aldrich) for three hours and washed with DPBS before blocking. Positive controls of CCD-1064Sk Cell Lysate (Santa Cruz) for β -actin and α 1(VI), and 293 Lysate (Santa Cruz) for DCN were run simultaneously to ensure valid detection. Semi-quantitative analysis was performed using ImageJ to determine band intensities. Protein expression levels are shown relative to non-infected cells \pm SEM.

4.2.8 Immunofluorescence

For immunofluorescence visualization, at each time point, alginate beads were sequentially fixed overnight in a 4% paraformaldehyde (PFA), .05M sodium cacodylate solution, equilibrated in 30% sucrose, embedded in Tissue-Tek O.C.T. compound (Sakura, Torrance, CA), and frozen and maintained at -80°C until use. Frozen sections (24 μm) were created using an HM550 series cryostat (Richard Allen Scientific, Kalamazoo, MI) and placed on gelatin-coated slides (Electron Microscopy Services, Hatfield, PA). For type VI collagen detection, sections were labeled with a rabbit IgG anti-human type VI collagen primary antibody (H-200; Santa Cruz). For decorin imaging, sections were incubated with 1 U/mL chondroitinase ABC for two hours and washed with DPBS before blocking. Sections were then labeled with a rabbit IgG anti-human decorin primary antibody (H80; Santa Cruz). Sections were visualized with biotinylated anti-rabbit IgG secondary antibodies and Texas red-labeled streptavidin (Labvision/Thermo Fisher Scientific, Kalamazoo, MI) and counterstained with DAPI. Fluorescence images were taken at 400x magnification with a Nipkow (spinning) disk-equipped Olympus IX81 microscope.

4.2.9 Cellular Deformation

For aspect ratio measurements under static compression, cells were isolated and re-embedded in new hydrogel constructs, to remove changing alginate bead properties, with their PCMs intact as previously described (22). After cells were released from alginate using sodium citrate and EDTA, they were incubated with CMFDA to stain cell cytoplasm, 6-Carboxy-X-Rhodamine (6-ROX; Invitrogen) to stain non-specifically for the PCM, and counterstained with DAPI. Stained cells were then resuspended in 2% (w/v) alginate and pipetted into a 6mm x 6mm x10mm mold with a 10 μ m porous membrane and Whatman thick blot paper (Biorad) paper attached to the top and bottom faces. The molds were immersed in 102mM CaCl₂ for two hours to cure (92). After curing, constructs were placed into a custom made micrometer-controlled deformation device (22) and imaged at 0%, 10%, and 20% uni-axial bulk strain. Fluorescence images were acquired at 400x magnification. Major and minor cell diameters (fig. 4.1) as well as the stained PCM (PCM+Cell) diameters were measured using Image J (NIH) and used to calculate aspect ratios ($AR = \text{minor cell diameter} / \text{major cell diameter}$). Normalized ARs (NAR) were calculated at each strain for each sample's population of average deformed AR compared to its un-deformed AR. Data are shown as $NAR \pm SEM$.

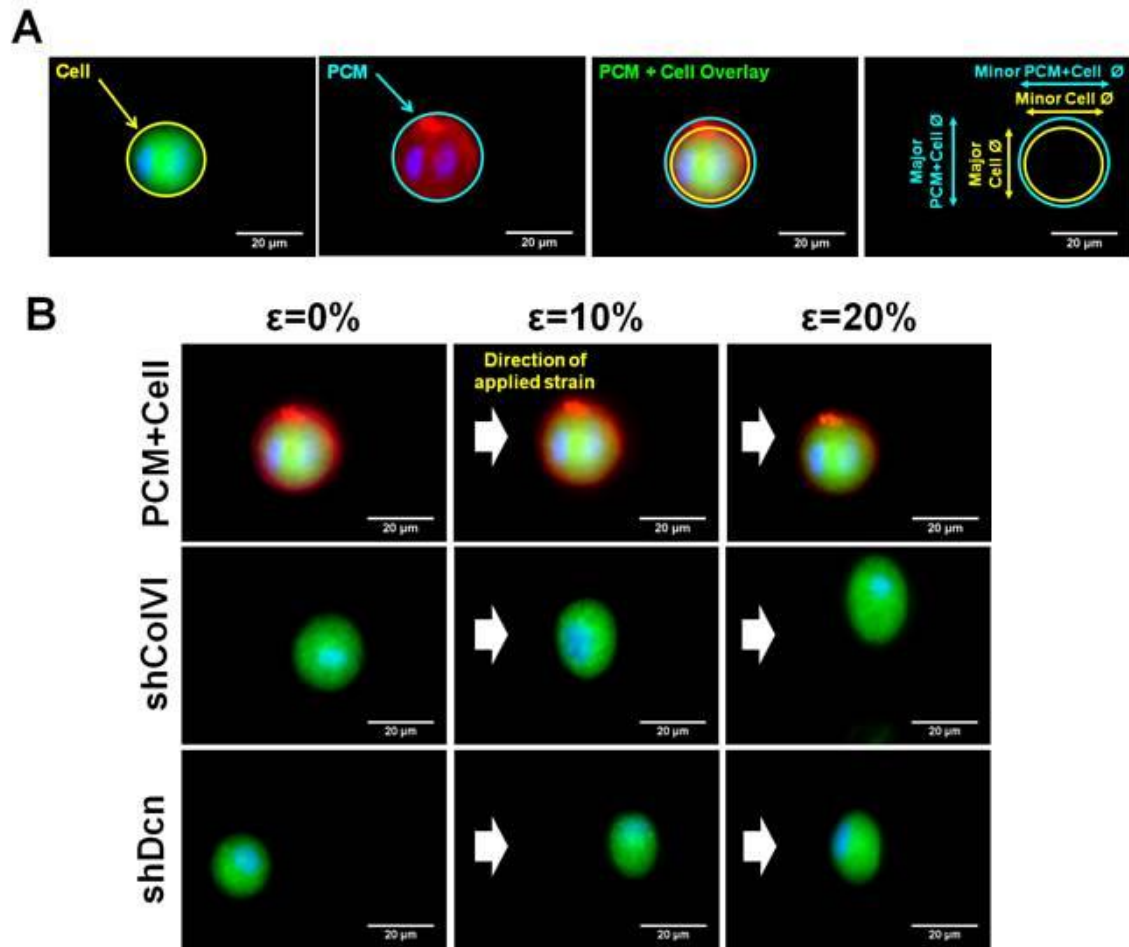


Fig. 4.1: Representative images of aspect ratio analysis under static applied strain. (A) The cell is stained with CMFDA (green), the PCM stained with 6ROX (red), and nuclei are stained with DAPI (blue). A yellow ellipse is shown around the cell and a blue ellipse is shown around the PCM to indicate how the major and minor diameters of the cell and the PCM+Cell were obtained. Scale bars indicate 20 μm . (B) PCM+Cell of CM-hMSCs, shCoIVI- and shDcn- transduced cells at day 14 under static applied strain of 0%, 10% and 20%. Cells are stained as previously described. The white arrows indicate the direction of applied compression. Scale bars indicate 20 μm .

4.2.10 Statistical Analysis

Statistical analyses for cell viability, gene expression, western blotting and aspect ratios were performed using one-way ANOVA. Tukey's HSD *post hoc* tests were performed for

pairwise comparisons. All computations were performed using JMP7 (Cary, NC) with statistical significance set to $\alpha < 0.05$ or $\alpha < 0.01$ as indicated in results.

4.3 Results

4.3.1 Lentiviral vectors can induce efficient shRNA-mediated RNAi in hMSCs

Initial screening was conducted on hMSC monolayers to identify optimal shRNA constructs to use for subsequent experiments. Because each shRNA sequence was designed to target different locations along the mRNA strand, variation in knockdown due to mRNA folding was expected. We found that the shColVI D construct (n=2) was most effective in knocking down *col6a1* transcript levels, resulting in decreases of up to 45% relative to non-infected hMSCs in monolayer over 14 days (fig. 4.2). The shDcn F construct induced the greatest knockdown of *dcn* expression, with up to 91% silencing over 14 days (n=2). Other constructs were less effective in inducing RNAi and were, therefore, excluded from subsequent experiments.

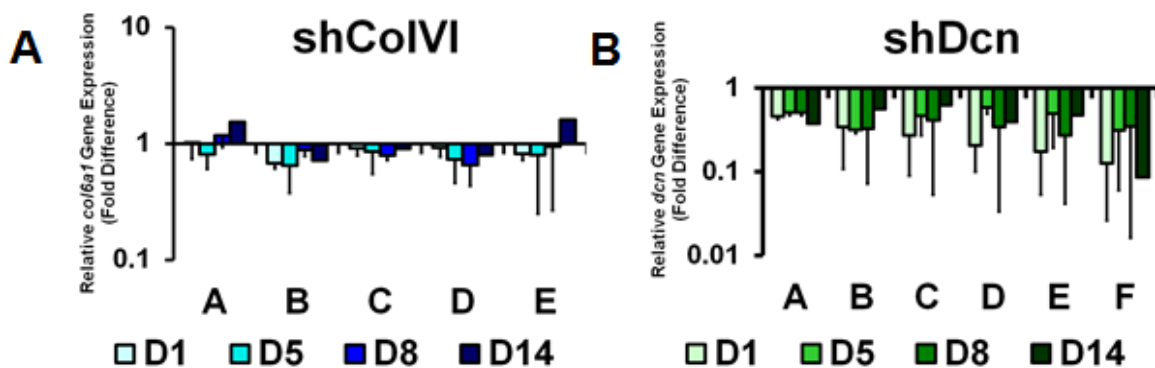


Fig. 4.2: Optimization of shColVI (A-E) and shDcn (A-F) to select the most efficient virus in knockdown target genes. (A) *Col6a1* and (B) *dcn* relative gene expression as assessed by qRT-PCR (n \geq 2). Data are shown as average values of the range of calculated fold differences ($2^{-\Delta\Delta C_t} \pm SD$ and $2^{-\Delta\Delta C_t - SD}$) \pm half of the range.

Based on the screen, we performed experiments using blasticidin selection, to eliminate any non-transduced cells, and assessed gene silencing in hMSCs with shColVI D and shDcn F constructs (hereafter labeled shColVI and shDcn, respectively). The pure population of shColVI-transduced cells exhibited *col6a1* expression that was significantly decreased by 67% at day 4 ($p < 0.01$, $n \geq 2$) and remained significantly depressed through 14 days ($p < 0.01$, $n \geq 2$) (fig. 4.3). Construct shDcn achieved a significant 89% knockdown of *dcn* expression at day 1 and maintained this diminished level over the entire 14 days ($p < 0.01$ for all time points, $n \geq 2$).

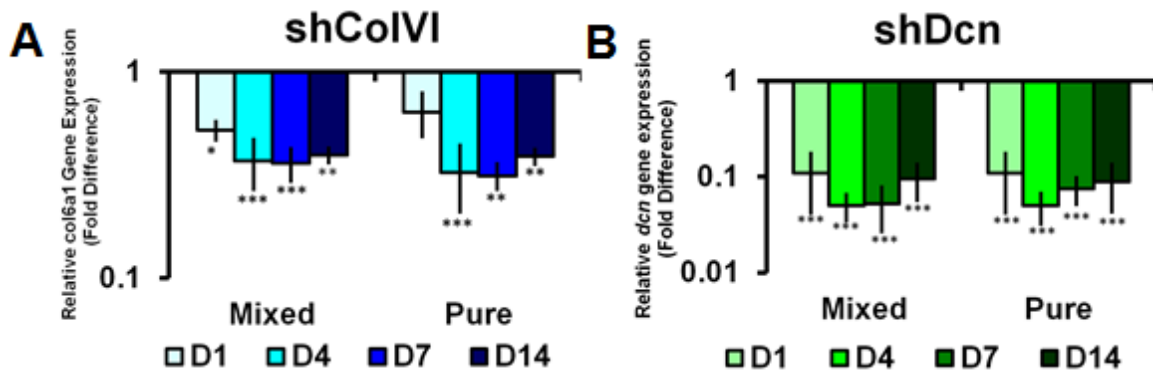


Fig.4.3: Targeted knockdown of genes is improved with blasticidin selection in shRNA transduced cells at MOI (1). (A) *Col6a1* and (B) *dcn* relative gene expression as assessed by qRT-PCR relative to non-infected hMSCs cultured in parallel. Data are shown as average values of the range of calculated fold differences ($2^{-\Delta\Delta Ct + SD}$ and $2^{-\Delta\Delta Ct - SD}$) \pm half the range (* $p < 0.05$, ** $p < 0.01$, *** $p < 0.001$; $n \geq 2$). Blasticidin selection caused a slight decrease in *col6a1* and *dcn* expression when non-transduced cells were removed.

4.3.2 Gene silencing of PCM proteins does not affect chondrogenic differentiation

As in our previous studies (22), we used alginate bead culture of hMSCs in TGF- β 3-supplemented chondrogenic induction media as a model system to study PCM formation during differentiation. To validate this approach for transduced cells, we verified

knockdown of the target genes, quantified cell viability, and confirmed chondrogenic gene expression.

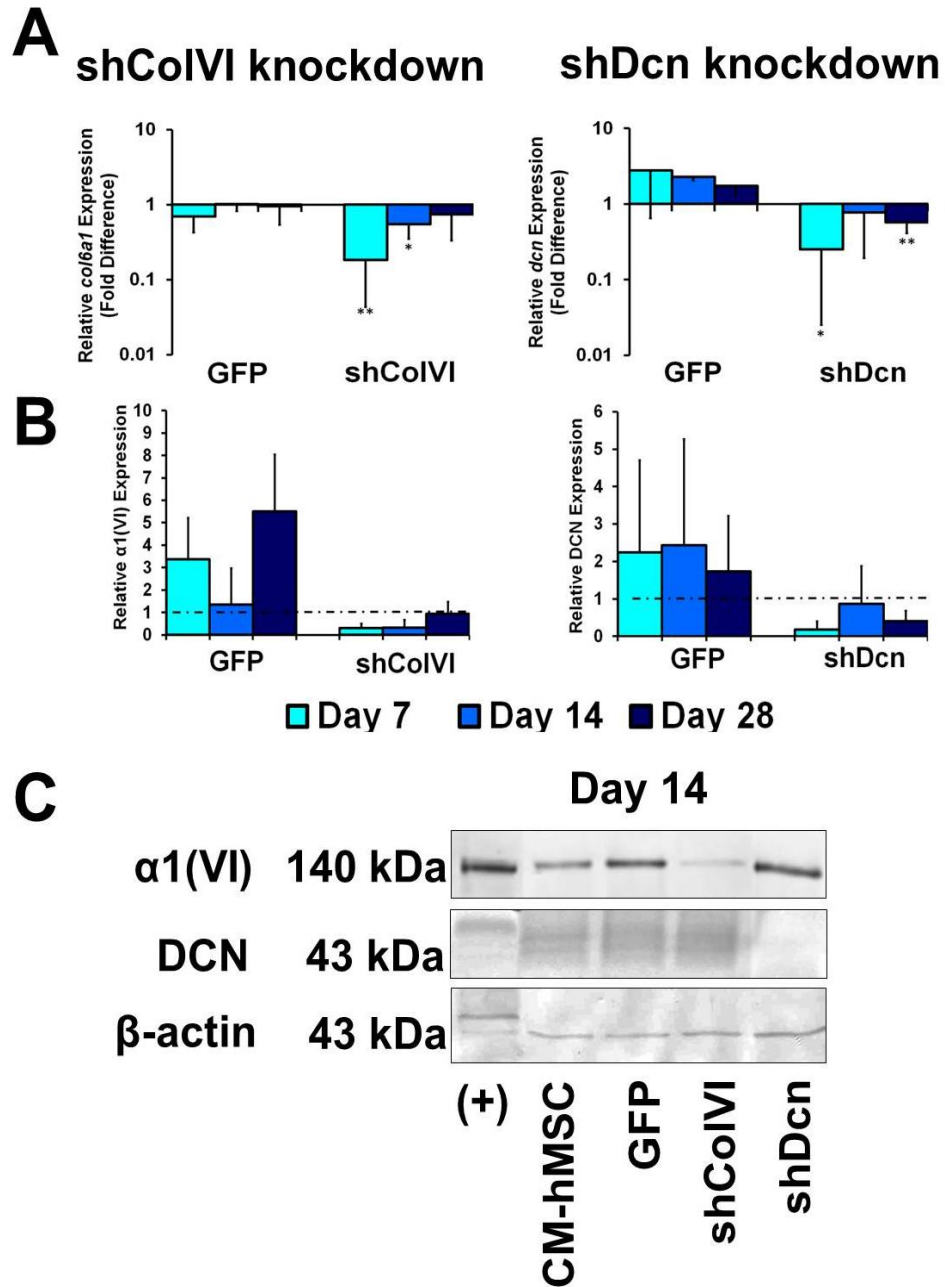


Fig.4.4: Knockdown of target genes and protein in samples cultured in CM. (A) *Col6a1* and *dcn* relative gene expression as assessed by qRT-PCR ($n \geq 3$) (* $p < 0.05$, ** $p < 0.01$ to non-infected and GFP-transduced hMSCs). Data are shown as average values of the range of calculated fold

differences ($2^{-\Delta\Delta Ct + SD}$ and $2^{-\Delta\Delta Ct - SD}$) \pm half the range. (B) ColVI and DCN protein expression as analyzed by western blotting (D7, n=2; D14, n=2; D28, n=4) in GFP and shColVI groups relative to non-infected CM-hMSCs at corresponding time points. Relative protein expression was calculated as the ratio of the shRNA-transduced cells (target protein/ β -actin) to non-infected CM-hMSCs (target protein/ β -actin). Data are represented as mean \pm SEM. (C) Representative western blotting at day 14 for α 1(VI), DCN, and β -actin in non-infected CM-hMSCs, and GFP-, shColVI-, and shDcn-transduced cells. Positive controls (+) were run in parallel.

Significant target gene knockdown was achieved for both shRNA constructs, as assessed by qRT-PCR, relative to controls of non-infected hMSCs and of a lentivirus transduced GFP expression cassette (Fig. 4.4A). For shColVI-transduced cells, *col61a1* knockdown remained statistically significant through 14 days but gradually diminished toward control levels by day 28 (Fig. 4.4A. day 7: 0.183 ± 0.140 , $p < 0.01$; day 14: 0.549 ± 0.200 , $p < 0.05$; day 28: 0.740 ± 0.406). For shDcn-transduced cells, *dcn* knockdown was statistically significant at 7 and 28 days (Fig. 4.4A. day 7: 0.253 ± 0.228 , $p < 0.05$; day 14: 0.769 ± 0.575 ; day 28: 0.574 ± 0.161 , $p < 0.01$) but not at 14 days. Western blots demonstrated that protein levels mirrored the temporal variations we observed for transcript levels (Fig. 4.4B and 4.4C). Cells transduced with their respective silencing constructs produced less α 1(VI) at day 7 and day 14, and less DCN at days 7 and 28.

To ensure viral treatment did not affect viability during the experiment, live-dead analysis was performed at 7, 14 and 28 days after hMSCs were embedded in alginate. Cells in all experimental groups maintained greater than 50% viability through the 28 days. There was no significant difference between non-infected and infected cells; therefore, the viral transduction did not affect cell viability (Fig. 4.5).

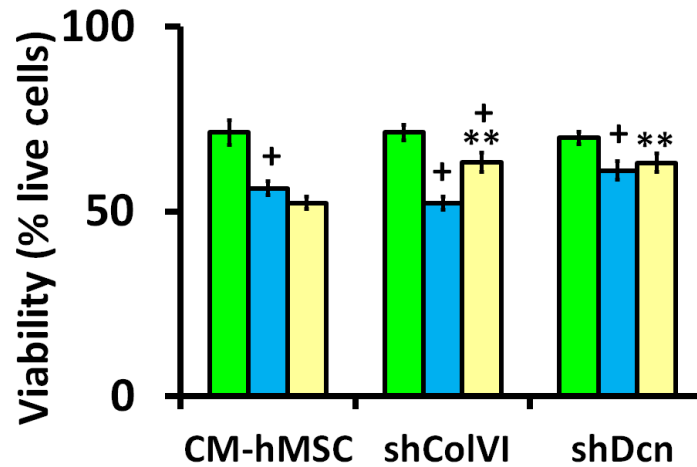


Fig. 4.5: Quantification of viability of alginate beads during chondrogenic culture using live-dead imaging and ImageJ particle analysis. Data shown is %live (green) cells of total cells counted \pm SEM (** $p < 0.05$ from non-infected chondrogenic-hMSCS; + $p < 0.05$ from the previous time point, $n \geq 25$).

To determine whether viral transduction or knockdown of *col6a1* and *dcn* might disrupt chondrogenesis, we analyzed *acan* and *sox9* expression in non-infected and GFP-, shColVI- or shDcn- transduced cells. Previous work has shown that hMSCs cultured in alginate hydrogels in GM exhibit some features of chondrogenesis, with pericellular deposition of type VI collagen during the first 7 days of culture, but only with TGF- β 3 supplementation did chondrogenesis progress fully (22). Higher transcript levels were measured for both chondrogenic markers across all groups when cultured in CM at all time points relative to corresponding transduced cells cultured in GM (Fig. 4.6A and 4.6B). Differences were statistically significant only at particular time points, likely due to fluctuating levels of gene expression during differentiation. There was no significant difference between non-infected controls and knockdown samples at any time point for

sox9 expression. These data indicate that transduction with the silencing cassette did not affect the ability of hMSCs to undergo chondrogenic differentiation.

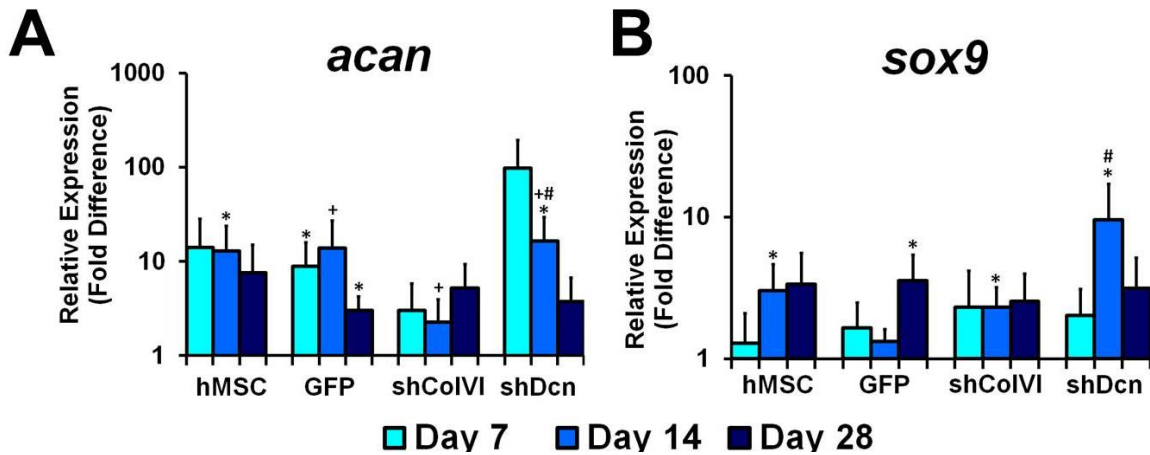


Fig. 4.6. Chondrogenic gene expression in control and knockdown cells. (A) Gene expression for *acan* and (B) *sox9* in non-infected, and GFP-, shColVI- and shDcn- transduced hMSCs in alginate bead culture (n=3). All data represent CM relative to their same infection condition cultured in GM at 7, 14, and 28 days (e.g. $\Delta\Delta Ct_{acan,D7} = \Delta Ct_{acan,CM,D7} - \Delta Ct_{acan,GM,D7}$) (*p<0.05 CM culture relative to same condition same time point in GM; +p<0.05, relative to CM-hMSCs at same time point; #p<0.05, relative to CM-GFP hMSCs at same time point; n≥3). Data are shown as average values of the range of calculated fold differences ($2^{-\Delta\Delta Ct + SD}$ and $2^{-\Delta\Delta Ct - SD}$) ± half the range.

4.3.3 Knockdown of *col6a1* and *dcn* alter PCM structure and gene regulation

The organization of the pericellular matrix is temporally dependent on its composition. DCN is a primary modulator of ColVI network assembly as well as a connector to type II collagen and aggrecan (59,82,87). Targeted subtraction of ColVI and DCN was expected to have direct impact on expression of pericellular proteins as well as PCM organization during chondrogenesis.

ColVI and DCN deposition during chondrogenesis fully enveloped the non-infected and GFP-transduced cells (Fig. 4.7A and 4.7B). In non- and GFP-infected cells, DCN was visualized in concentrated pockets directly surrounding the cell membrane, with diffuse staining extending away from the cell mainly at day 7 and becoming more tightly gathered by day 28 (Fig. 4.7B as denoted by yellow arrows). This is consistent with the notion that DCN binds proteins within the PCM to form a fully developed network, controlling protein spacing with its attached GAG chain.

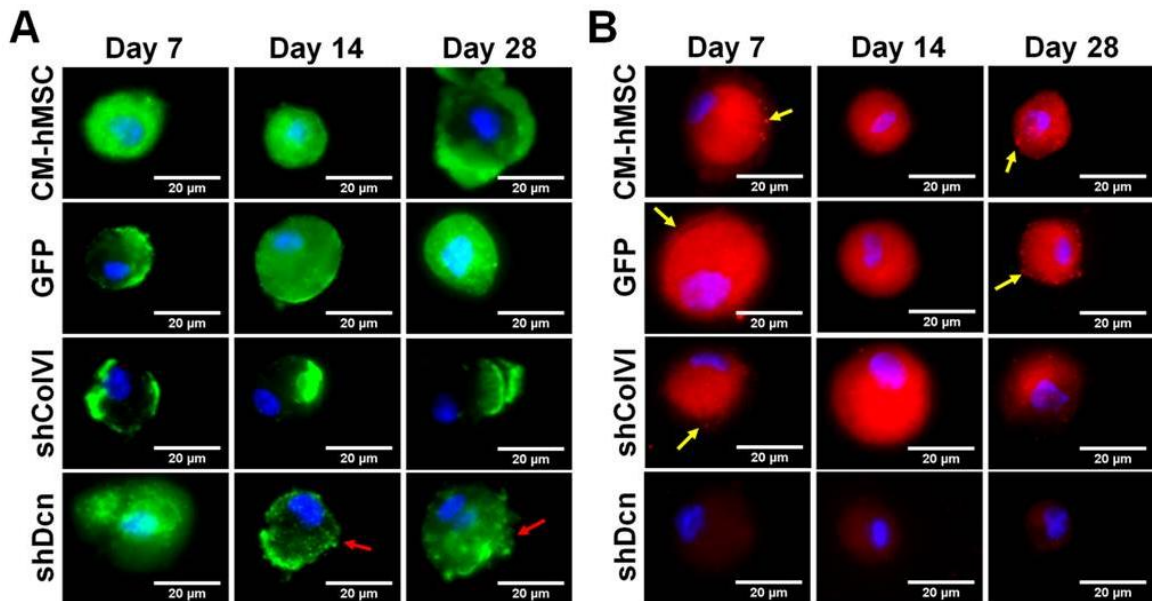


Fig. 4.7: Confocal microscopy visualization of ColVI and DCN. (A) ColVI (green) immunofluorescence visualization within the PCM of non-infected, and GFP-, shCoVI-, and shDcn-transduced hMSCs cultured in alginate beads in CM at 7, 14, and 28 days. Cell nuclei are stained with DAPI (blue). Red arrows point to punctate ColVI staining. All images were standardized to similar pixel intensity ranges for valid comparisons. Negative controls without primary or secondary labeling showed no ColVI staining (data not shown). Scale bar indicates 20μm. (B) Equivalent data for DCN (red) immunofluorescence visualization. Yellow arrows point to concentrated clusters of DCN around the cell membrane. Negative controls without primary or secondary labeling showed no DCN staining (data not shown). Scale bar indicates 20μm.

Knocking down ColVI resulted in lower *acan*, *bgn*, and *dcn* levels during the first 14 days of chondrogenesis relative to non-infected and GFP-transduced cells (Fig. 4.6A, 8A and 8B). This difference was diminished by 28 days. Visualization of DCN surrounding shColVI cells did not reflect the decreased transcription, showing similar fluorescence to control cells. Although ColVI knockdown affected *dcn* expression, DCN knockdown did not affect *col6a1* levels (Fig. 8C) but did alter its assembly. ColVI staining appeared to be membrane-bound and punctate, suggesting that DCN deficiency prevents ColVI from forming a continuous microfibrillar layer surrounding the cell (Fig. 7A as denoted by red arrows). This punctate staining was maintained over the course of the 28 day experiment. DCN knockdown also affected the expression of other PCM proteins, leading to increased levels of *acan*, *bgn*, and *sox9* during the first two weeks. These results indicate that PCM gene expression is cross-regulated, with the greatest effects being in the first two weeks of chondrogenesis.

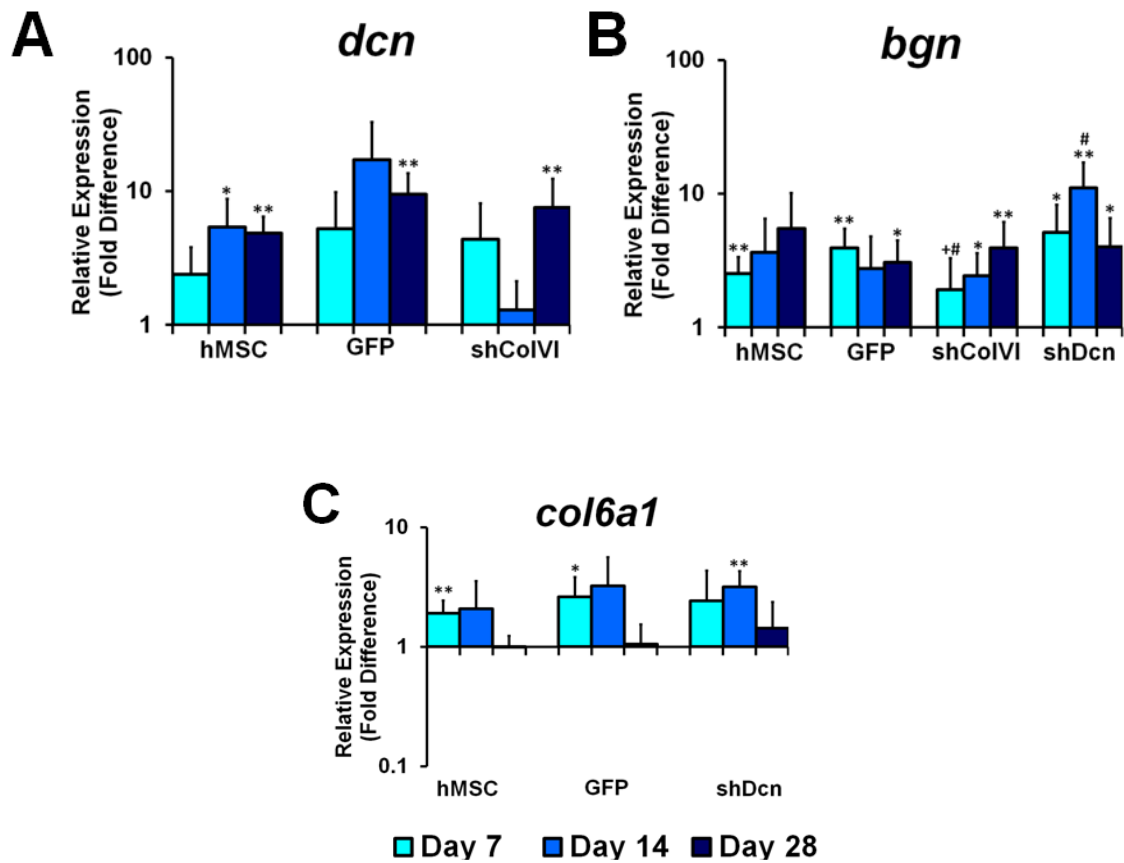


Fig. 4.8: Pericellular gene expression in control and knockdown cells. (A) Gene expression for *dcn*, (B) *bgn* and (C) *col6a1* in non-infected, and GFP-, shCoIVI- and shDcn- transduced hMSCs in alginate bead culture (n=3) in CM relative to the same infection condition cultured in GM at 7, 14, and 28 days (*p<0.05, **p<0.01, CM culture relative to same condition same time point in GM; +p<0.05, relative to CM-hMSCs at same time point; #p<0.05, relative to CM-GFP hMSCs at same time point; n≥3). Data are shown as average values of the range of calculated fold differences ($2^{-\Delta\Delta Ct + SD}$ and $2^{-\Delta\Delta Ct - SD}$) ± half the range.

4.3.4 Cellular and PCM stiffnesses evolve during chondrogenic differentiation

In an effort to understand the mechanical role of the developing PCM during chondrogenesis, we employed an approach to quantify both the deformation of the cell itself (CM-hMSC) and the aggregate deformation of the cell with its PCM (PCM+Cell) over time in chondrogenic media (Fig. 4.9). Day 0 baseline controls represent hMSCs

that had been embedded in alginate constructs directly from monolayer culture, and consequently had no exposure to chondrogenic media. At this time point, significant changes in normalized aspect ratios (NARs) were observed with applied strain. Note the nonlinear cell stiffness at day 0; cells deform greater from 0 to 10% applied strain than from 10 to 20%.

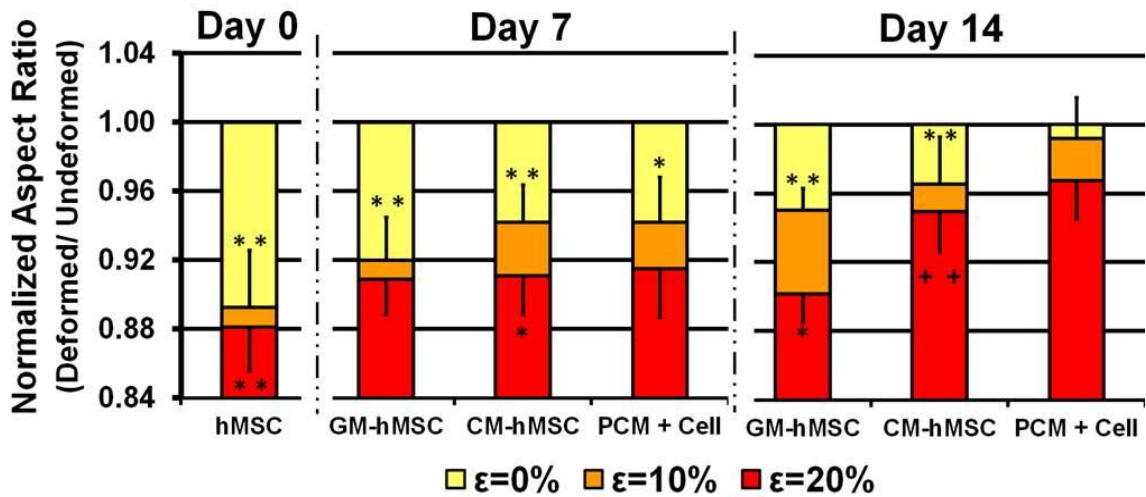


Fig. 4.9: Normalized aspect ratios (NAR) of cells cultured in GM or CM, and the PCM+Cell (CM-hMSCs). Each condition was subjected to 0%, 10% or 20% applied strain at 0, 7 and 14 days of culture in alginate beads. Graphs show normalized aspect ratios that are overlaid with progressively increasing strain increments (values are not cumulative). ($p < 0.05$ and $p < 0.01$ with respect to increasing symbols. *: from previous applied strain; +: from GM-hMSCs of same strain, same day; $N > 30$). Data are shown as $NAR \pm SEM$.

	$\epsilon=10\%$	$\epsilon=20\%$
Day 0	0.893 ± 0.032	0.881 ± 0.026
Day 7 GM	0.920 ± 0.025 (‡)	0.909 ± 0.021 (‡‡)
Day 14 GM	0.950 ± 0.013 (‡‡, #)	0.902 ± 0.017 (‡)
Day 7 CM	0.942 ± 0.022 (‡‡)	0.911 ± 0.022 (‡‡)
Day 14 CM	0.965 ± 0.028 (‡‡)	0.949 ± 0.024 (‡‡, ###)
Day 7 PCM+Cell	0.942 ± 0.026	0.915 ± 0.028
Day 14 PCM+Cell	0.992 ± 0.023 (###)	0.968 ± 0.023 (#)

Table 4.3: Normalized AR values of each deformation and condition. ($p < 0.05$ and $p < 0.01$ with respect to increasing symbols. #: from Day 7 same strain, ‡: from D0 same strain. $N > 30$).

At Day 7, GM cells (GM-hMSC) deformed less than Day 0 hMSCs, likely due to matrix production and assembly stimulated by 3D culture (22) which is relatively stable between day 7 and day 14. Because there was no discernible PCM around GM cells, deformations were measured for cells only. For the CM group, incomplete elaboration of the PCM resulted in similar deformations between the cell (CM-hMSC) and the PCM+Cell.

At Day 14, GM cells exhibited significantly less deformation than at Day 7, but only at 10% applied strain. For CM cells, the aggregate deformation of PCM+Cell was also correspondingly lower than at Day 7. The most striking change was in the PCM+Cell deformation, which was significantly lower at both 10 and 20% applied strain. Interestingly, under 10% strain, the change in NAR for CM cells was higher than that for the PCM+Cell, but these trends are reversed at 20% applied strain. This suggests that the

PCM is stiffer than the cell at 10% applied strain, but that the cell becomes relatively stiffer at 20%.

4.3.5 ColVI and DCN are essential for resisting cellular deformation during compression

Our results above are consistent with previous research findings that during chondrogenesis hMSCs develop a mechanically functional PCM (22,84), and that a change in its stiffness affects cell deformation (42). As a step toward elucidating the functional roles of specific PCM proteins, we examined cell deformations in genetically engineered CM-hMSCs. Again, for baseline measurements (Day 0), we seeded transduced and control cells into alginate disks, and immediately subjected them to compressive loading. Because of the universal lack of PCM, cells exhibited significant changes in normalized aspect ratios with each applied strain, with no significant differences between groups (Fig. 4.10A). Similar nonlinearity in cell stiffness as observed in the previous experiment (Fig. 4.9) was found across all groups.

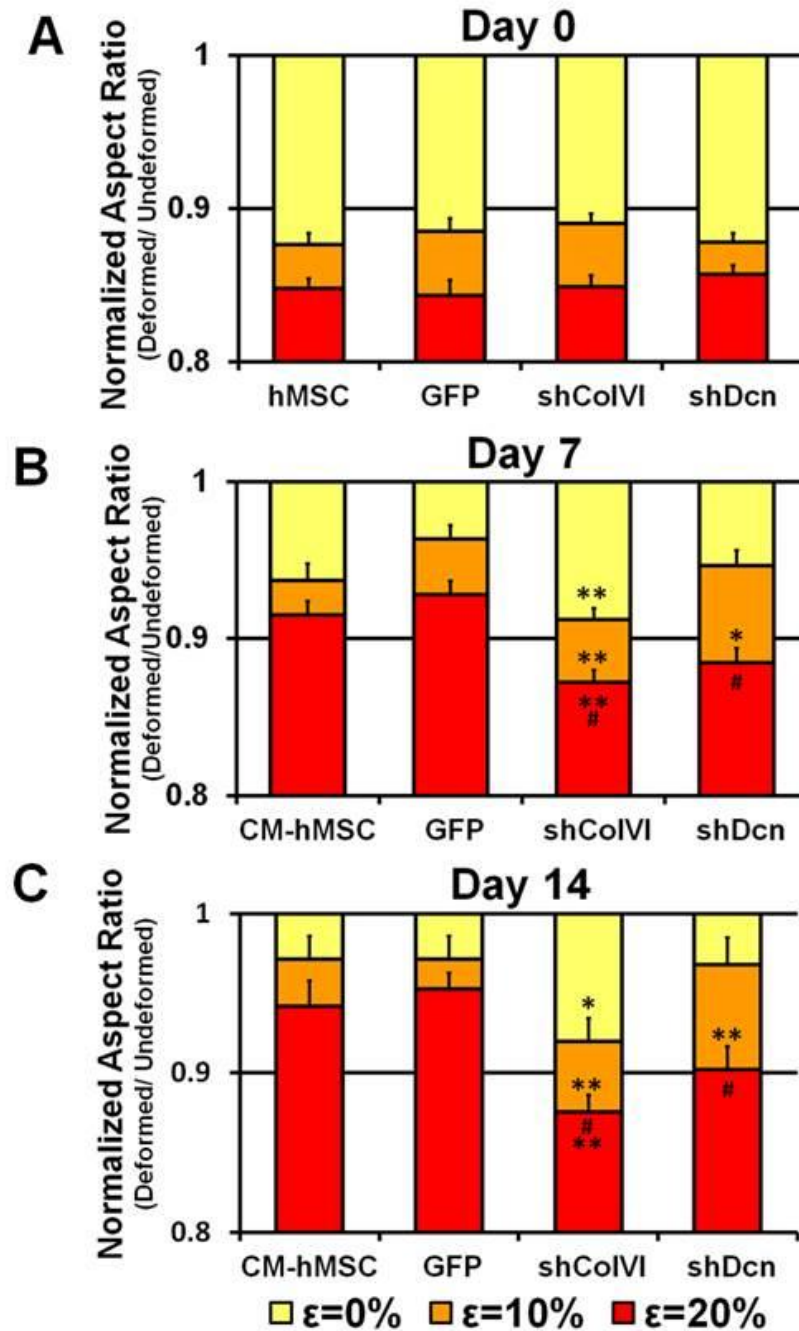


Fig. 4.10: Normalized aspect ratios of non-infected and GFP-, shColVI-, and shDcn-transduced hMSCs. Each condition was subjected to 0%, 10%, and 20% applied strain at (A) day 0, (B) day 7, and (C) day 14. Graphs show normalized aspect ratios that are overlaid with progressively increasing strain increments (values are not cumulative) (* $p < 0.05$, ** $p < 0.01$ significant difference from GFP-transduced cells at same nominal strain; # $p < 0.05$ significant deformation between 10% and 20% applied nominal strain). Data are shown as NAR \pm SEM.

With culture, all conditions showed a greater resistance to the applied compression. However, the extent to which cell deformations decreased was dependent on treatment. Both non-infected CM-hMSCs and GFP controls exhibited the greatest decreases in cell deformation at both Day 7 and Day 14. This was expected since the PCM was allowed to develop normally in both groups. In addition, their similarity to each other confirms that the lentiviral infection of hMSCs does not affect cell stiffness.

ColVI deficient cells showed the greatest deformations across all groups at both Day 7 and Day 14, and for both magnitudes of applied strain (Fig. 4.10B and 4.10C). Deformation was similar between Days 7 and 14, indicating that the cell's inability to put in place a mechanical barrier does not change with time. Although direct comparisons cannot be made, we measured greater shColVI cell deformations than GM-hMSCs in previous experiments (Fig. 4.9).

Knocking down DCN resulted in interesting strain-dependent trends in cell deformation that were similar between Days 7 and 14 (Fig. 4.10B and 4.10C). At low levels of applied strain, cells deformed comparably with non-infected CM-hMSC and GFP controls, suggesting that the PCM was mechanically robust enough to sustain similar loads. Other data in our lab indicates there is no apparent evidence of any intracellular mechanism that alters shDcn cell stiffness (data not shown). However, once applied strain reached 20%, cellular resistance to deformation collapsed. We attribute this behavior to the functional significance of decorin in mediating collagen-collagen interactions.

Overall, these results demonstrate control hMSCs that develop a full PCM are better able to maintain their cell-shape compared with cells with deficient PCMs. In particular, ColVI is required for resisting even low magnitude strains, while DCN is important in maintaining structural integrity at higher strains.

4.4 Discussion

Stem cell therapies are currently being explored for their potential in the regeneration of load bearing tissues, such as cartilage, due to both their pluripotency and their ability to maintain a basal phenotype during expansion *in vitro*. The PCM developed during chondrogenesis has been considered vital to the regulation of mechanotransduction events in differentiating hMSCs (57,81,93,94). Reconstruction of the PCM in isolated mature chondrocytes has been shown to be complex, temporally specific in composition, and highly dependent on protein-protein interactions within the PCM (95). Because chondrocyte function is closely tied to interactions with ECM proteins (96), altering the constituents of the PCM would likely induce cascading effects on cell-cell and cell-matrix interactions. PCM development in chondrogenic hMSCs is expected to be even more complex, due to the additional changes in gene regulation associated with differentiation. To elucidate the functional roles of individual components in the PCM, we investigated the consequences of knocking down *col6a1* and *dcn* mRNA expression using shRNA lentiviral vectors.

Type VI collagen is a 125 nm long heterotrimer that consists of three different α -chains ($\alpha 1(\text{VI})$, $\alpha 2(\text{VI})$, and $\alpha 3(\text{VI})$) and self-assembles into beaded filaments and larger fibrillar structures (56). ColVI trimer formation occurs intracellularly before being secreted into the PCM for microfibrillar networking via BGN or DCN (56,58,82,83) and

is maintained at low levels of transcription (22,83). DCN is a ubiquitous proteoglycan, consisting of a core protein with a single chondroitin sulfate (97) or dermatan sulfate (98) side chain. It interacts with multiple collagens to create functional bridges between the PCM and surrounding ECM, and is involved in controlling fibrillogenesis and growth factor bioavailability (3,21,28). This study shows that these two specific proteins, ColVI and DCN, have profound influence over PCM composition and biomechanical behavior surrounding hMSCs undergoing chondrogenesis.

One of our major findings was the significant contributions of ColVI and DCN in cellular resistance to deformation. A developing PCM has been implicated in acting as both a biomechanical buffer (22,84,99) as well as a biochemical bridge (57,93,94). Acting as a biomechanical buffer, the PCM shields the cell from deformation which could be potentially detrimental while also enhancing small tissue strains for stimulation (16,19,22). Previous studies analyzing deformation properties of chondrocytes in alginate hydrogels have shown that cells under compression form oblate spheroids with a decrease in cell diameter along the axis of loading and an increase in transverse cell diameters perpendicular to that axis (100). During initial matrix deposition, we found that the matrix and cell share similar deformations, due to the lack of full matrix envelopment. As the matrix stiffens to approach and then surpass cellular stiffness, the mechanical properties are contributed to more equally by both components (42). With a fully developed matrix, at higher strains the PCM+Cell would reorganize due to hydration changes and spatial consolidation of collagen. Studies examining the PCM surrounding mechanically isolated chondrons are consistent with an initial elastic response followed by a transiently changing flow-dependent creep response under applied stress (5,19). The

mechanical behavior is dependent on PCM structure, with the elastic response governed by matrix deposition (42) that is highly associated with sGAG and collagen accumulation (84), and the viscous response governed by the osmotic and porous properties of the PCM network (101).

By altering the presence of ColVI and DCN, we sought to determine their involvement in this composition dependent mechanical response. In mature articular chondrocytes, the PCM has a higher modulus than that of the cell (88). Previous studies in ColVI-null mice demonstrate that a PCM can be formed, but that ColVI-null chondrons have significantly reduced stiffness compared to wild-type chondrons (5). The lowered resistance to deformation we observed in ColVI knockdown cells during chondrogenic PCM development is consistent with this reduced stiffness. ColVI can therefore be considered the primary protein involved in buffering loads to differentiating hMSCs.

During PCM development, it has been seen that sGAGs are important in the initial stages of assembly, directly impacting cellular mechanical responses to load (84). PGs mediate the PCM to ECM interface through interactions with types II and VI collagen (3,17,59,82). Cells compensated for *dcn* knockdown by upregulating *bgn* expression, demonstrating a regulatory effect by DCN on other PCM small leucine rich PGs (sLRPs) (62). BGN core protein has significant sequence homology with that of DCN, but is structurally distinct and possesses two (instead of one) CS/DS chains (102-104). Similar compensatory effects have also been seen in DCN knockout models (3,28). BGN shares binding sites on collagen proteins with DCN, but has a lower affinity, causing a lower involvement in PCM and ECM organization (3) and the extra CS/DS- side chain on BGN

results in a looser collagen network (28,59,62,87,105). The looser collagen spacing possibly contributed to the significant increases in shDcn cellular deformation at higher strains. This network is bound to the cell membrane through HA core protein-CD44 interactions (98), NG2 receptors (membrane bound chondroitin sulfate PGs) or through direct binding to the $\alpha 1\beta 1$ integrin (85). From our confocal images, the altered ColVI assembly in shDcn knockdown cells appeared as punctate localizations completely surrounding the cells at these binding sites.

In addition to acting as a mechanical stabilizer, the PCM also aids maintenance of chondrocyte phenotype biochemically. Our data are in agreement with chondrogenic stage specific gene expression (4), with *col6a1* being significantly greater in the first seven days of chondrogenesis in non-infected and GFP-transduced cells, which decreases in expression by 28 days of culture. DCN is involved in the sequestration of TGF- $\beta 3$, FGF-2, TNF- α , PDGF, and IGF-1 (3,21,62) and has been associated with cell proliferation signaling (3), causing the cell to cease proliferation and enhance matrix synthesis. These growth factors cause PCM accumulation during chondrogenesis in a concentration dependent manner (11,42,97). Sequestration of growth factors immediately surrounding the cell allows for specifically stimulated responses, being released mechanically or enzymatically from their associated PG for presentation to the cell membrane. *Sox9*, *comp* and *HAPLN1* expression levels have shown to reach a peak by 12 days of culture associated with high levels of matrix assembly and metabolism (4). The large overexpression of *sox9* in shDcn cells at day 14 could be due to the lack of regulation and continuous bioavailability of TGF- $\beta 3$ to the cell.

Full PCM formation occurs within the first two weeks of TGF- β 3 stimulation *in vitro*, which parallels the upregulation of *acan* and *bgn* expression during the first 14 days, and then steadily matures as *acan* returns to control levels. PCM retention has been shown to be mediated through interactions between CD44 and hyaluronic acid, which lay a foundation for aggrecan accumulation and affects PCM volume and shape (19,98). Hyaluronan is critical for maintenance of the pericellular environment surrounding chondrocytes (96), interacting with type II collagen, aggrecan and link protein. The observed higher *acan* upregulation in shDcn cells could aid in matrix protein retention and reorganization, causing large changes in the mechanical composition of the PCM, affecting cellular metabolism. shColVI cells showed an opposite trend of *acan* and *bgn* expression, with lower expression levels during the first 14 days of culture than all other samples.

4.5 Conclusion

To our knowledge, this study is the first to elucidate the functional significance of DCN in the PCM. Furthermore, we extend our previous work (22) by demonstrating that ColVI is crucial for the biomechanical integrity of the PCM in chondrogenic hMSCs at all stages of differentiation. The use of shRNA expressing lentiviral vectors allows stable production of siRNAs by the cell (74). This approach has enabled us to characterize how specific PCM proteins govern the micromechanical environment of differentiating hMSCs over time. Although further studies are required to elucidate the downstream effects on mechanotransduction events, signaling cascades, and load-induced behaviors, our results provide some immediate insight into strategies that can be used to engineer specific microenvironments for eliciting desired cellular responses.

Chapter 5: Determining ColVI and DCN's role in differentiating hMSC mechanosignaling initiation and cytoskeletal kinetics²

5.1 Introduction

Mechanotransduction events during chondrogenesis determine how differentiating human mesenchymal stem cells (hMSCs) will develop into tissues. Understanding the molecular underpinnings of these events is necessary for providing the desired signaling to cells in tissue engineered constructs of compressive load-bearing tissues such as articular cartilage (48). Native cartilage tissue is composed of a complex network of interconnected collagens, proteoglycans, and non-collagenous proteins which are organized to withstand the applied compression, tension, and shear during physiologic loading (17-19,21). This highly organized matrix is maintained through a balance of anabolic and catabolic factors caused by mechanical stimulation (16,76,106,107). Under dynamic culture, chondrocytes increase synthesis of types I and II collagen, aggrecan and versican (16,39,108-111). It has been shown that the pericellular matrix (PCM) directly surrounding chondrocytes plays a central role in governing mechanobiology (13,94). Similarly, the developing PCM in chondrogenically differentiating hMSCs is likely to be involved in many of these cellular signaling events,

²I'd like to acknowledge the contribution of Kenny M. Rosenberg to this study.

and may regulate mechanoresponsiveness based on its evolving structure and function.

In native chondrons, the PCM has a distinct composition of type VI collagen (ColVI) (5,19,22,57,60), fibronectin and hyaluronan (21,84), and proteoglycans such as aggrecan, decorin (DCN), biglycan (17,20,82), and perlecan (68). We have previously shown that in chondrogenically differentiating hMSCs, ColVI and DCN are similarly expressed and completely envelop the cell over the course of two weeks (22). Activation of signaling molecules during this two week differentiation process is highly important, with expression peaks of members of the transforming growth factor β superfamily, fibroblast growth factor-2 (FGF-2) (68), cartilage oligomeric matrix protein (COMP) (107) and transcription factor Sox9 (112) as well as expression of various integrins at the cell surface (67). Since, the time dependent aggregation of matrix proteins surrounding the cell determines how the cell interacts with its microenvironment, it is possible that PCM growth is linked to the robustness of the cell's response to applied stimulation.

The PCM's control over mechanotransduction events occurs not only through its compositionally specific matrix, but also through its biomechanical properties (107). We've previously shown that by altering the cell's ability to form a fully developed PCM through shRNA lentiviral knockdown of ColVI and DCN, chondrogenic hMSCs show varying abilities to withstand applied static compression in hydrogels (113). The increase in deformation we witnessed could shift mechanosignaling through changing the cell's cytoskeletal response. Differentiating hMSCs have a highly dynamic cytoskeleton that is directly dependent on the evolving ECM (112,114) and is more pronounced in areas of intensive loading (112,115), having higher amounts of actin microfilaments (AMFs), vimentin intermediate filaments (VIFs), and microtubules (MTs). These proteins are

involved in maintaining the cell's structural integrity (114) during loading as well as transferring the loads to the nucleus to regulate gene expression (70,71,112,115,116) . Disruption of these components leads to drastic changes in chondrocyte phenotype through shifts in sGAG and collagen synthesis and transcription (72,117,118). The transmission of mechanical stimulation to the nucleus via the cytoskeleton is a physical pathway for mechanotransduction (71).

The intertwined relationship between matrix and cytoskeletal contributions to the mechanotransduction process is difficult to dissect. The goal of this study was to determine how knockdown of ColVI and DCN in chondrogenic hMSCs affects the dynamic response of the cytoskeleton following a short duration load and then further examine changes in gene expression. Understanding how extracellular proteins are involved in cellular homeostasis and metabolic response can further regenerative medicine by revealing one aspect to control these reactions. We found that ColVI and DCN knockdown affected AMF and VIF dynamics respectively and *bmp6*, *comp*, and *fgf2* were all sensitive to loading during chondrogenic PCM development. These results demonstrate how compositionally changing the PCM during differentiation using targeted knockdown can change the physicochemical response of chondrogenic hMSCs.

5.2 Materials and Methods

For this study we designed experiments to investigate how chondrogenic stem cell mechanobiology is affected by distinct PCM structure and composition. Five cell populations were examined:

- wild-type non-infected growth media controls (GM)
- wild-type non-infected chondrogenic hMSCs (CM)
- GFP lentivirus-transduced chondrogenic hMSCs (GFP)
- shColVI lentivirus-transduced chondrogenic hMSCs (shColVI)
- shDcn lentivirus-transduced chondrogenic hMSCs (shDcn)

To enable progressive accumulation of PCM, cells were pre-cultured in alginate beads for 7 or 14 days, at which point cells were recovered from alginate beads and re-embedded in newly formed alginate disk constructs. Disk constructs were then transiently subjected to one hour of cyclic dynamic loading, with free-swelling constructs as a reference group. Cell functional outcomes were assessed at various times (0hr, 1hr, and 4hr) after cessation of loading.

5.2.1 *shColVI and shDcn Lentiviral Prep*

Sequences for shRNA targeting either *col6a1* or *dcn* were designed using RNAi codex from either human *col6a1* (Gen Bank: NM_001848) or human *dcn* (GenBank: NM_001920) mRNA as previously described (Twomey, 2014). Briefly, shRNA lentiviral vectors were created using the BLOCK-iT U6 RNAi Entry Vector Kit and the BLOCK-iT Lentiviral RNAi Expression System (Invitrogen, Carlsbad, CA) consisting of 21 nt

shRNA sequences complimentary for *col6a1* or *dcn* (Table 5.1) and a blasticidin resistance gene with a U6 promoter and a Pol III termination sequence.

5'-'stem-loop-stem'-3' sense and 3'-'stem-loop-stem'-5' anti-sense sequences	
shColVI	5'-CACCGCGGAGACGATAACAACGACATCGAAATGTCGTTGTTATCGTCTCCG-3'
	3'-CGCCTCTGCTATTGTTGCTGTAGCTTTACAGCAACAATAGCAGAGGCAAAA-5'
shDcn	5'-CACCGCCGTTTCAACAGAGAGGCTTACGAATAAGCCTCTCTGTTGAAACGG-3'
	3'-CGGCAAAGTTGTCTCTCCGAATGCTTATTCGGAGAGACAACCTTGCCAAAA-5'

Table 5.1: Sense and anti-sense hairpin sequences for shColVI and shDcn.

Replication-deficient lentiviruses were created using 293FT cells, Lipofectamine 2000 and a manufacturer-supplied packaging mix (Invitrogen). A lentiviral expression vector containing the gene for GFP was prepared in parallel using the Vivid Colors pLenti6.2-GW/EmGFP kit (Invitrogen) to serve as a lentiviral control. Supernatant containing the viral vectors were stored at -80°C until used experimentally.

5.2.2 Cell culture and lentiviral transduction

hMSCs were purchased from Lonza and expanded in monolayer in a basal non-differentiation growth media (GM) consisting of high glucose DMEM (HG-DMEM) (Gibco/Invitrogen, Carlsbad, CA) supplemented with 10% fetal bovine serum (FBS) (Gibco), 100U/mL penicillin/streptomycin (Gibco), 1% MEM non-essential amino acids (Gibco), and 4mM L-Glutamine (Invitrogen). Cells were expanded in monolayer at 37°C with 5% CO₂ with media changes three times per week and used for experiments as passage 4 or 5.

Experimental hMSCs were infected in monolayer at a multiplicity of infection (MOI) of 1 with shColVI, shDcn, or GFP-expression (control) lentiviral vector in the presence of 6µg/mL Polybrene (Sigma) to aid in transduction efficiency for 24 hours. MOI was determined through a Quant-IT PicoGreen (Invitrogen) titer assay. After viral incubation, cells were cultured for 24 hours in GM, followed by 24 hours of GM containing 12 µg/mL of blasticidin to select for a pure population of transduced cells as previously described (113).

After selection, cells were lifted from monolayer using 0.25% trypsin-EDTA (Gibco), centrifuged at 600xg for 5 minutes before being re-suspended in a 2% (w/v) alginate solution (Research Products International, Mount Prospect, IL) at a concentration of 2.0×10^6 cells/mL. Alginate beads were formed by expelling alginate from a 22 gauge needle into a 102mM CaCl₂ bath. Beads were cured for 10 minutes, followed by a wash in PBS containing calcium and magnesium. Alginate-cell beads were cultured in chondrogenic induction media (CM) containing HG-DMEM, ITS Universal Culture Supplement Premix (BD Biosciences, San Jose, CA), 10nM dexamethasone, 50µg/mL L-ascorbic acid (Sigma), 40 µg/mL L-Proline (Sigma), 100U/mL penicillin/streptomycin, 1mM sodium pyruvate, 0.584 g/mL L-glutamine, and 10ng/mL TGF-β₃ (Lonza). Non-infected hMSC controls were cultured in alginate beads in either CM or GM in parallel. Differentiation of hMSCs and PCM accumulation occurred over 7 or 14 days of alginate bead culture at 37°C with 5% CO₂ with media changes three times per week. At these time points, a few beads per condition were collected for ColVI and DCN protein visualization. Other beads were used to recover cells with their PCMs intact from the alginate for dynamic loading experiments.

5.2.3 Application of Dynamic Loading

Cells were recovered from alginate at 7 or 14 days and re-embedded in new alginate hydrogel constructs in order to ensure the material properties of the alginate would be identical across 7 and 14 day pre-culture groups (22). To recover cells, beads were immersed in a 100mM sodium citrate, 30mM EDTA solution, centrifuged, and resuspended in 2% (w/v) alginate solution. The cell suspension was pipetted into cylindrical disk-shaped aluminum molds ($\text{\O}6\text{mm} \times 3\text{mm}$ in height) at a concentration of 10^6 cells/mL with a 5 μm porous membrane and Whatman filter paper attached to the top and bottom faces of the molds (Fig. 5.1) (92). Molds were immersed in a 102 mM CaCl_2 bath for 90 minutes to ensure complete alginate curing.

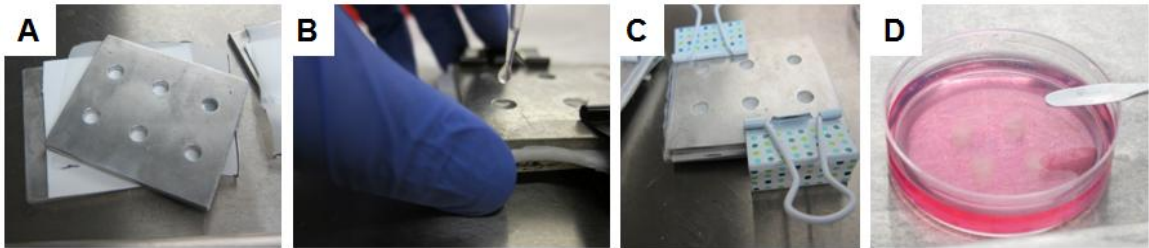


Fig. 5.1: (A) Aluminum molds with $\text{\O}6$ mm \times 3 mm well, (B) which are loaded with cell-seeded 2% (w/v) alginate solution, (C) compressed between two aluminum plates with Whatman and filter paper to allow CaCl_2 curing. (D) Once disks were cured, they were moved to a $\text{\O}60$ mm petri-dish containing a 1.5 mm thick agarose mold with $\text{\O}8$ mm diameter wells punched out to maintain local position and unconfined conditions and equilibrated in warmed media for thirty minutes.

Alginate constructs were then removed from the molds, washed twice with PBS containing magnesium and calcium, and then equilibrated at free-swelling conditions in their corresponding culture media for thirty minutes prior to applied dynamic loading. A schematic of the culture period and the loading is shown in Fig. 5.2D.

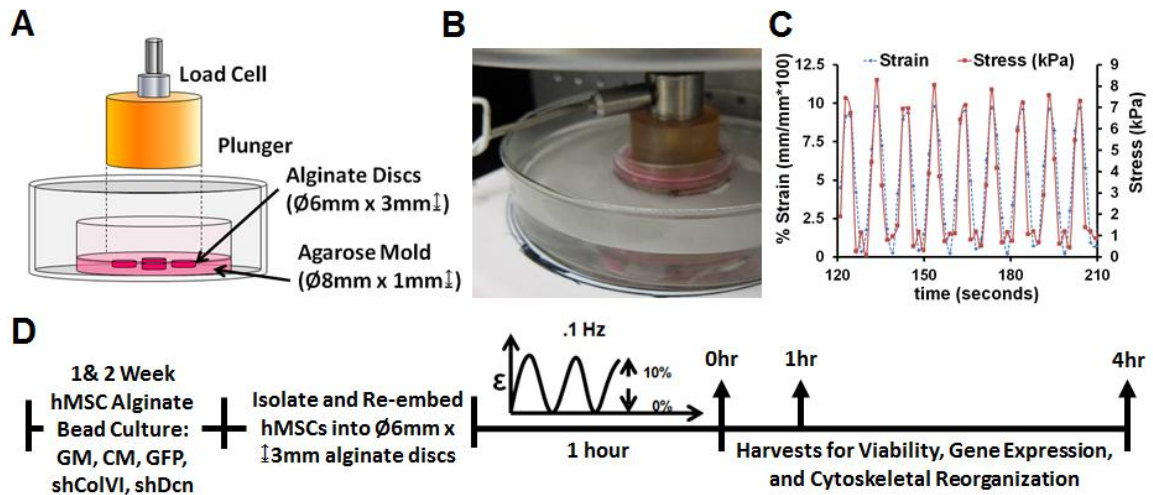


Fig. 5.2: Dynamic loading set-up. (A) Schematic of Ø60mm petri-dishes containing a 1.5mm thick agarose mold with Ø8mm diameter wells to maintain alginate disk position. Ø6mm x 3mm thick alginate disks were loaded in warmed media. (B) The Ø60 mm diameter petri dishes were fixed within a water bath maintained at 37°C. A Ø40mm polysulfone plunger was attached to a 200g load cell. Displacement controlled sinusoidal strain was applied using an LM-1, Bose/Electroforce materials testing machine. (C) Force and displacement feedback was collected over the hour of transient load. (D) Schematic of culture period, loading duration, and harvest times.

To maintain position and unconfined conditions during loading, Ø8 mm wells were punched out of a 1.5mm thick agarose gel cast in Ø60 mm petri dishes, and one alginate construct was placed into each well (fig. 5.2A). Petri-dishes were fixed within a water-bath maintained at 37°C. The compression fixture consisted of an impermeable polystyrene Ø40 mm compression plunger mounted to a materials testing system as shown in fig. 5.2A and 1B (LM-1, Bose/Electroforce, Eden Prairie, MN). Alginate constructs were immersed in serum-free media during loading. After an initial 2g tare load was applied to ensure alginate-platen contact, sinusoidal unconfined axial compressive loading was applied under displacement control at 0.1Hz from 0-10% strain. A representative plot of the loading configuration can be seen in fig. 5.2C. Dynamic

loading was applied for an hour, after which samples were removed from the fixture. Non-loaded free-swelling (FS) disks were maintained in similar agarose-petri dish conditions within 37°C, 5% CO₂ for the hour of loading. Following loading, disks were either harvested immediately, or returned to the incubator and maintained at 37°C and 5% CO₂ until harvests at one or four hours post loading for viability, gene expression, and immunofluorescence (fig. 5.2D).

5.2.4 Viability

We quantified cell viability following alginate re-embedding and loading. Disks were collected from free-swelling conditions or immediately following applied load (0 hr) and centrally cut to obtain and stained with 5-chloromethylfluorescein diacetate (CMFDA; Invitrogen) and ethidium homodimer-1 (EthD-1; Invitrogen) and counterstained with 4',6-diamidino-2-phenylindole (DAPI; Invitrogen). Ten confocal fluorescence image stacks were taken at 5 µm slices to total 30 µm of depth from the cut face of the bead were taken at 100x magnification with a Nipkow (spinning) disk-equipped Olympus IX81 microscope. Viability was assessed using channel separation and threshold particle analysis using ImageJ (NIH) to count the number of green and red only cells. All results are expressed as a percentage of total cells that are viable (green only).

5.2.5 Immunofluorescence visualization of ColVI, DCN, and cytoskeleton proteins

Alginate beads were collected at day 7 and 14 of culture and fixed in a 4% paraformaldehyde (PFA), 0.05M sodium cacodylate solution overnight. Beads were equilibrated in 30% sucrose, embedded in Tissue-Tek O.C.T. compound (Sakura,

Torrance, CA), and then frozen and maintained at -80°C until used for cryosectioning (HM550, Richard Allen Scientific, Kalamazoo, MI).

For ColVI and DCN immunofluorescence, 24 µm cryosections were placed on polysilane-coated slides (Electron Microscopy Services, Hatfield, PA), then blocked with normal goat serum (Vector Lab), prior to primary antibody labeling. For ColVI visualization, sections were labeled with a rabbit IgG anti-human type VI collagen primary antibody (H-200; Santa Cruz Biotechnology) as previously described (113). To visualize decorin, sections were incubated with 1 U/mL chondroitinase ABC for two hours and washed with DPBS before blocking. Sections were then labeled with a rabbit IgG anti-human decorin primary antibody (H80; Santa Cruz Biotechnology).

For visualization of cytoskeletal changes, 30 µm cryosections were treated with 0.1% Triton-X to permeabilize cell membranes prior to blocking and primary antibody incubation. Sections were labeled either with a rabbit polyclonal IgG anti-human actin primary antibody (H-300; Santa Cruz Biotechnology), a rabbit monoclonal IgG anti-human vimentin primary antibody (SP20; Thermo Scientific), a mouse monoclonal IgG₃ anti-human β-tubulin primary antibody (G-8; Santa Cruz Biotechnology), or a mouse monoclonal IgG₁ anti-human vinculin primary antibody (7F9; Santa Cruz Biotechnology).

All sections were visualized with biotinylated anti-rabbit or anti-mouse IgG secondary antibodies, Texas red-labeled streptavidin (Labvision/Thermo Fisher Scientific, Kalamazoo, MI), and DAPI. Confocal image stacks (1.25 µm slices) were taken at 400x magnification with a Nipkow (spinning) disk-equipped Olympus IX81

microscope. All proteins were imaged using identical exposure times for repeatability. Projection images were created from the image stacks for image analysis.

5.2.6 Fluorescence Intensity Measurements

Fluorescence intensity of the labeled proteins was quantified using ImageJ (119). Cells within each image were manually traced along their membrane perimeter and their corrected total cell fluorescence intensity measurements per cellular area were calculated using:

$$\text{CTCF (Corrected Total Cell Fluorescence) / Cellular Area} = (\text{Integrated Density} - (\text{Area of selected cell} \times \text{mean fluorescence of background reading})) / \text{Cellular Area (microns}^2\text{)}$$

All data are shown as the average CTCF/area \pm SEM ($N \geq 100$ cells per harvest and culture condition).

5.2.7 Gene Expression

To analyze the effect of type VI collagen and decorin knockdown on cell gene expression to transient mechanical loading, qRT-PCR was performed either immediately following, one hour after, or four hours after termination of cyclic loading. Free-swelling samples were harvested in parallel following one hour of free-swelling. At the appropriate time points, cells were released from their alginate scaffold as previously described using a 100mM sodium citrate, 30mM EDTA solution, spun down and re-suspended in a buffer solution containing β -Mercaptoethanol (Fisher Scientific, Pittsburgh, PA) before flash freezing. Total RNA was isolated (RNeasy Micro, Qiagen, CA) and reverse transcribed. Gene expression was analyzed using qRT-PCR (MyiQ

System, BioRad, CA) with primers designed for human genes (Table 5.2) using Primer3 software (web ref. 2). Gene expression levels for *18s*, *acan*, *bgn*, *bmp6*, *colla1*, *col6a1*, *comp*, *dcn*, *fgf2*, *rhoa1*, *runx2*, *sox9*, and *vim* were quantitatively assessed as previously described (89,113). All primer amplification efficiencies were determined using linear regression efficiency methods and were determined to be between 89.4% and 132.32% efficient ($R^2 > 0.99$) (90).

Gene	Forward and Reverse primers	GenBank accession no.
<i>18s</i>	5'-AAACGGCTACCACATCCAAG-3' 5'-CCTCCAATGGATCCTCGTTA-3'	NR_003286
<i>acan</i>	5'-ACAGCTGGGGACATTAGTGG-3' 5'-GTGGAATGCAGAGGTGGTTT-3'	NM_001135
<i>bgn</i>	5'-ACCTCCCTGAGACCCTGAAT-3' 5'-CTGGAGGAGCTTGAGGTCTG-3'	NM_001711
<i>bmp6</i>	5'-AAGAAGGCTGGCTGGAATTT-3' 5'-GAAGGGCTGCTTGTCGTAAG-3'	NM_001718
<i>colla1</i>	5'-GTGCTAAAGGTGCCAATGGT-3' 5'-CTCCTCGCTTTCCTTCCTCT-3'	NM_000088
<i>col6a1</i>	5'-CTACACCGACTGCGCTATCA-3' 5'-GCCACCGAGAAGACTTTGAC-3'	NM_001848
<i>comp</i>	5'-AGGACAACCTGCGTGACTGTG-3' 5'-GTTGTCCTTTTGGTCGTCGTT-3'	NM_000095
<i>dcn</i>	5'-AATTGAAAATGGGGCTTTC-3' 5'-GCCATTGTCAACAGCAGAGA-3'	NM_001920
<i>fgf2</i>	5'-TGCTGGTGATGGGAGTTGTA-3' 5'-CTGAGTATTCGGCAACAGCA-3'	NM_002006
<i>rhoa1</i>	5'-AAGGACCAGTCCCAGAGGT-3' 5'-TTCTGGGGTCCACTTTTCTG-3'	NM_001664
<i>runx2</i>	5'-TTTGCCTGGGTCATGTGTT-3' 5'-TGGCTGCATTGAAAAGACTG-3'	NM_001015051
<i>sox9</i>	5'-AGTACCCGCACTTGCACAAC-3' 5'-CGTTCTTCACCGACTTCCTC-3'	NM_000346
<i>vim</i>	5'-CACGAAGAGGAAATCCGGAGC-3' 5'-CAGGGCGTCATTGTTCCG-3'	NM_003380

Table 5.2: Sequences of Primers used for real time RT-PCR.

Expression levels were analyzed using the $\Delta\Delta C_t$ method. Cycle threshold (C_t) values were averaged and ΔC_t was calculated by subtracting the average C_t values of *GAPDH*

from those of the gene of interest ($\Delta Ct_{col6a1} = Ct_{col6a1} - Ct_{GAPDH}$) as previously described (Twomey, 2014). The $\Delta\Delta Ct$ for each gene of interest was determined by subtracting the ΔCt of the growth media free-swelling control at day 7 from the experimental ΔCt at each time point (i.e. $\Delta\Delta Ct_{col6a1,shColVI, D7@4hrs} = (\Delta Ct_{col6a1,shColVI, D7@4hrs} - \Delta Ct_{col6a1,GM, D7@FS})$). Free swelling growth media samples at day 7 were considered the experimental controls, with a minimal PCM developed during the initial 7 days of culture. Relative gene expression levels (fold difference) were computed through the exponential relation $2^{-\Delta\Delta Ct}$ (91). Data are shown as average values of the range of calculated fold differences ($2^{-\Delta\Delta Ct + SD}$ and $2^{-\Delta\Delta Ct - SD}$) \pm range.

5.2.8 Statistical Analysis

Statistical analyses for cell viability, gene expression, and CTCF/area measurements were performed using one-way ANOVA. Tukey's HSD *post hoc* tests were performed for pairwise comparisons. All computations were performed using JMP7 (Cary, NC) with statistical significance set to $\alpha < 0.05$ as indicated in results.

5.3 Results

5.3.1 ShColVI and shDcn lentiviral vectors caused significant targeted knockdown

Significant knockdown of *col6a1* and *dcn* was achieved by shColVI and shDcn successively over the 14 days of alginate culture (fig. 5.3). ShColVI maintained between 40-65% knockdown over the 14 days compared to non-infected chondrogenic hMSCs (fig 5.3A: *col6a1* gene expression: shColVI (D7: 0.345 ± 0.090 ; D14: 0.555 ± 0.143) versus GFP (D7: 0.815 ± 0.167 ; D14: 1.290 ± 0.270). ShDcn also maintained 63-73%

knockdown (fig 5.3B: *dcn* gene expression (shDcn (D7: 0.365 ± 0.346 ; D14: 0.267 ± 0.160) versus GFP (D7: 1.199 ± 0.609 ; D14: 2.310 ± 1.350)). Decreased accumulation of ColVI and DCN in the PCM was confirmed using immunofluorescence visualization (fig. 5.3C and 5.3D). Type VI collagen developed a full PCM completely enveloping the cell by day 14, with shColVI samples lacking ColVI labeling. DCN staining was robust within a well-developed PCM during the 14 days of chondrogenic culture, with shDcn inhibiting accumulation of DCN.

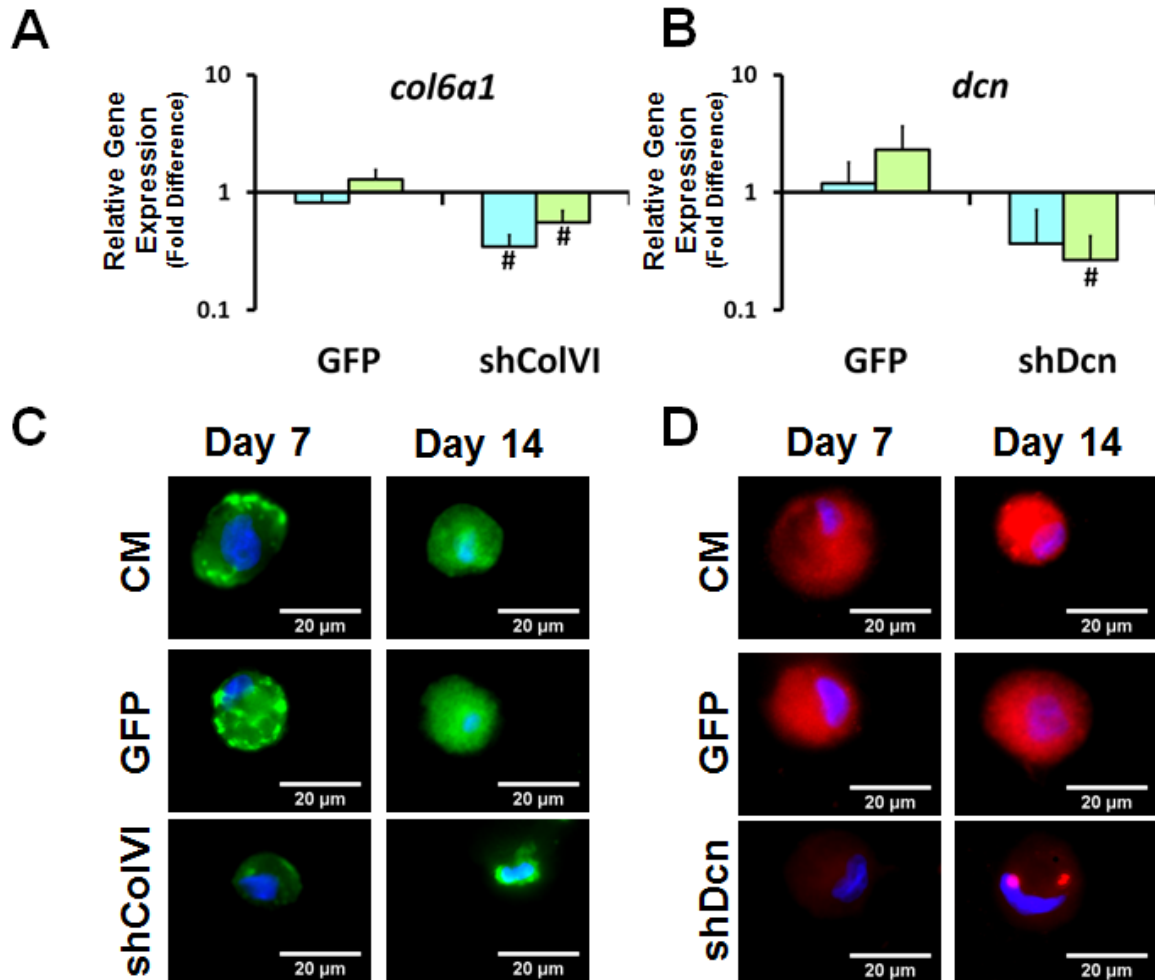


Fig. 5.3: Knockdown of target genes and protein in samples cultured in CM. Relative (A) *col6a1* and (B) *dcn* gene expression (fold difference) at day 7 and day 14, as assessed by qRT-PCR of GFP-, shColVI-, and shDcn-transduced cells relative to chondrogenic non-infected hMSCs (#: $p < 0.05$ to chondrogenic non-infected and GFP-transduced cells; $n \geq 3$). Data are shown as average values of the range of calculated fold differences ($2^{-\Delta\Delta Ct + SD}$ and $2^{-\Delta\Delta Ct - SD}$) \pm half of the range. Significant knockdown was achieved by shColVI samples at day 7 and 14 and shDcn achieved significant knockdown at day 14, which maintained significant knockdown during transient load. (C) Immunofluorescence visualization of ColVI and (D) DCN proteins surrounding chondrogenic cells. Non-infected and GFP-transduced cells cultured in chondrogenic media developed a type VI collagen PCM surrounding cells which was inhibited in shColVI cells. DCN staining showed DCN expression and accumulation during the two week chondrogenic phase, which shDcn inhibited.

5.3.2 Dynamic loading did not reduce viability

Cell viability was found to be unaffected by dynamic loading in any condition at both time points. Viability did significantly decrease in shColVI and shDcn samples at D14 compared to chondrogenic hMSCs, but were still 60% viable during dynamic loading.

5.3.3 ColVI and DCN differentially controlled cytoskeletal organization in response to load

The involvement of the cytoskeleton in mechanosignaling has been well established in both chondrocytes and chondrogenic hMSCs. For differentiating hMSCs, the dynamically changing PCM may alter the role of the cytoskeleton in cellular mechanobiology. To investigate the mechanoregulation of cytoskeletal elements in differentiating and engineered stem cell populations, we quantified relative changes in fluorescence intensity levels of g-actin (AMF), vimentin (VIF), β -tubulin (MT), and vinculin, at various time points after loading.

Actin microfilaments

Load-induced changes in AMF intensity levels differed between pre-culture durations, and across the five cell treatment groups (fig. 5.4C). At day 7, FS samples exhibited significantly lower values in GM cultures than the four FS chondrogenic cultures (fig. 5.4A and 5.4C). Cyclic compression of alginate constructs resulted in small, and in some instances statistically significant, changes in AMF intensity immediately after loading.

Day 14 AMF intensity data yielded more identifiable trends. For FS samples, again g-actin fluorescence was higher in chondrogenic groups compared with GM, similar to day 7. In fact, chondrogenic fluorescence was uniformly higher across loading groups, as well. Interestingly, cyclic loading resulted in transient increases in g-actin fluorescence immediately after loading for chondrogenic controls (non-infected and GFP) as well as shDcn. But this spike in AMF staining was absent in GM and shColVI cells (fig. 5.4C).

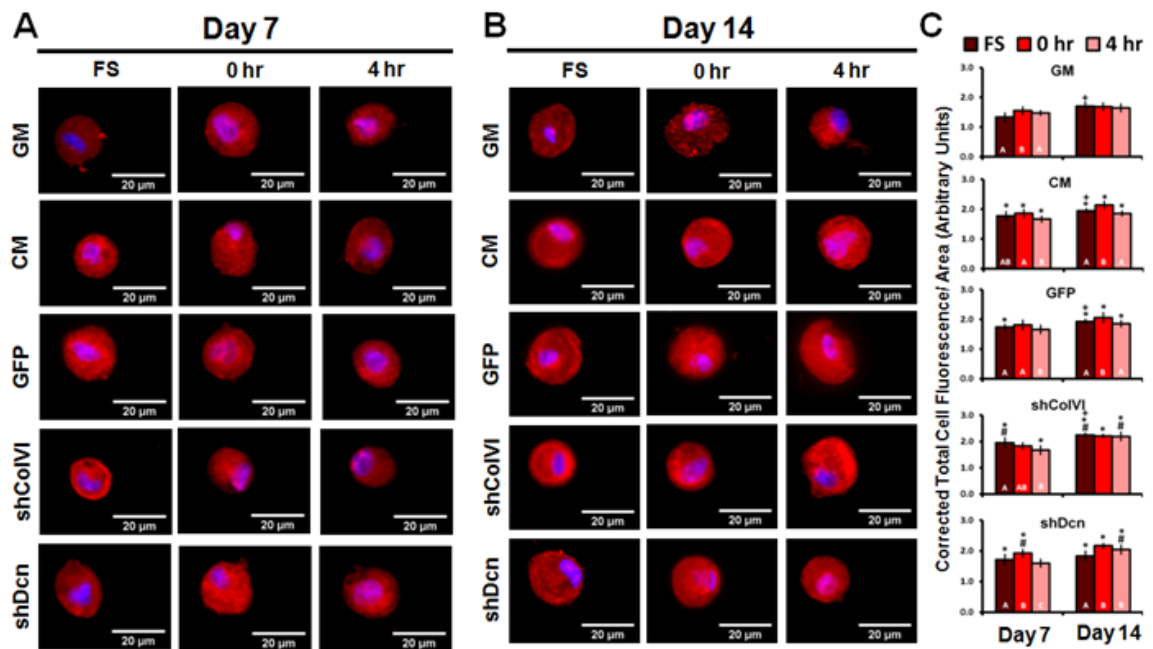


Fig. 5.4: Confocal fluorescence visualization of AMFs at (A) day 7 and (B) 14 in non-infected GM and CM hMSCs and GFP-, shColVI-, and shDcn-transduced cells in free-swelling (FS) conditions and immediately following (0 hr) and four hours post load (4 hrs). Scale bars = 20 μm. C) Corrected total cell fluorescence per cellular area intensities for all samples at day 7 and day 14. *;p<0.05 from GM samples at each time point; #;p<0.05 from CM & GFP at each time point; +; p<0.05 from day 7 to day 14; A:B:C: p<0.05 between loading harvests.

Vimentin intermediate filaments

The VIF network exhibited very different patterns from AMFs during culture and following load (fig. 5.5B). Vimentin staining was filamentous, with intense cortical and perinuclear staining, in agreement with current literature (116,117). Similar to actin, all chondrogenic groups possessed significantly higher intensities than GM corresponding to preculture and loading conditions. For GM, CM, and GFP cells, VIF intensities measured in FS samples were similar between Days 7 and 14 (fig. 5.5A and 5.5B). However, the response to loading strongly depended on pre-culture duration. Whereas cyclic compression induced no change or small decreases in VIF staining at Day 7, it resulted in progressively increasing intensities at Day 14.

For shColVI and shDcn groups, VIF intensities in both FS and loaded samples at Day 7 exhibited similar levels and trends as their non-infected and GFP chondrogenic controls. At Day 14, at which point the mechanical function of the PCM begins to differ significantly from wild-type (113), the baseline FS vimentin staining becomes significantly higher than all other FS groups. The VIF response to cyclic loading is correspondingly muted for shColVI and shDcn groups at Day 14, perhaps due to the already strong organization of the vimentin network.

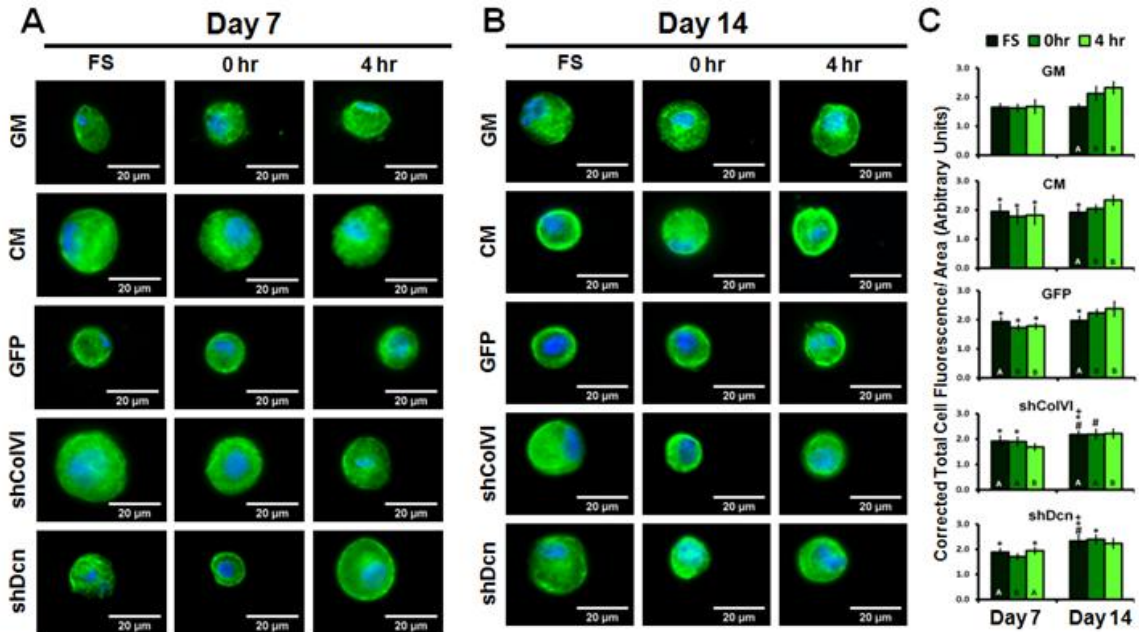


Fig. 5.5: Confocal fluorescence visualization of VIFs at (A) day 7 and (B) 14 in non-infected GM and CM hMSCs and GFP-, shColVI-, and shDcn-transduced cells in free-swelling (FS) conditions and immediately following (0 hr) and four hours post load (4 hrs). Scale bars = 20 μ m. (C) Corrected total cell fluorescence per cellular area intensities for all samples at day 7 and day 14. *:p<0.05 from GM samples at each time point; #:p<0.05 from CM & GFP at each time point; +: p<0.05 from day 7 to day 14; A:B:C: p<0.05 between loading harvests.

Microtubules

Microtubules were observed to exhibit similar features in dynamics as actin and vimentin. For FS conditions, chondrogenic groups generally possessed higher MT staining intensities than the GM groups. In response to cyclic compression, non-infected and GFP-transduced chondrogenic hMSCs had transient, but significant increases in staining immediately after loading, similar to what we observed in AMF staining (fig. 5.6C). Cyclic loading induced progressively increasing intensity levels in both Day 7 and Day 14 GM groups, similar to changes we observed in VIF (fig. 5.6A and 5.6B). This was also seen in shDcn at day 7. At day 14, shColVI and shDcn groups showed higher FS

intensity levels than all other FS groups and were initially unresponsive to load, but then decreased in intensity by four hours post load. MT staining was filamentous and localized cortically.

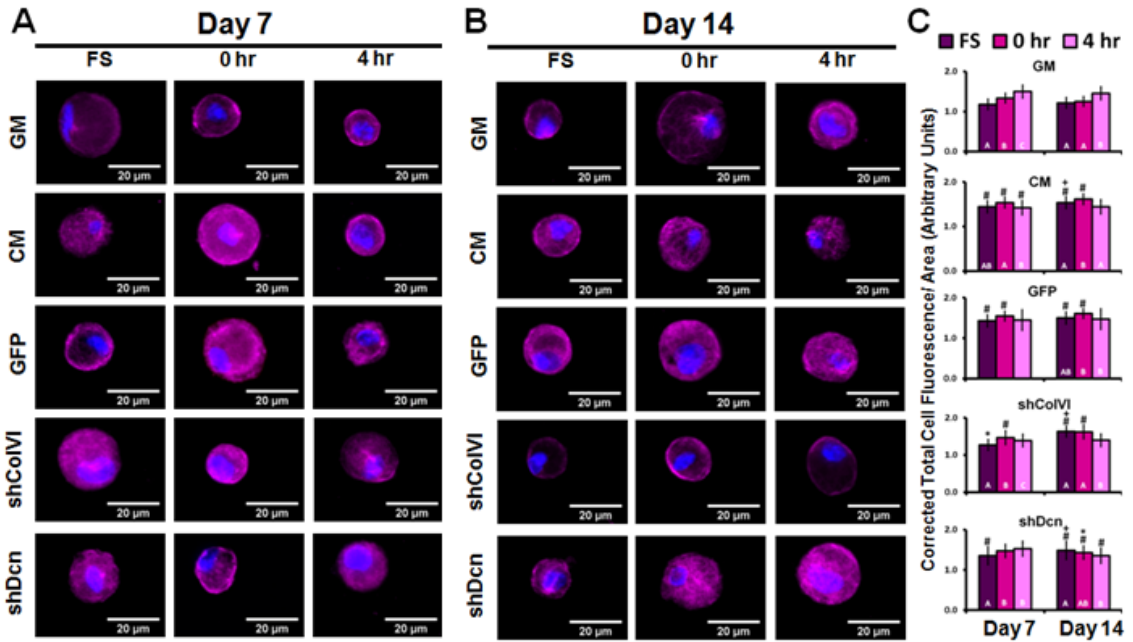


Fig. 5.6: Confocal fluorescence visualization of MTs at (A) day 7 and (B) 14 in non-infected GM and CM hMSCs and GFP-, shColVI-, and shDcn-transduced cells in free-swelling (FS) conditions and immediately following (0 hr) and four hours post load (4 hrs). Scale bars = 20µm. C) Corrected total cell fluorescence per cellular area intensities for all samples at day 7 and day 14. *:p<0.05 from GM samples at each time point; #:p<0.05 from CM & GFP at each time point; +: p<0.05 from day 7 to day 14; A:B:C: p<0.05 between loading harvests.

Vinculin

At Day 7, FS vinculin staining did not appear to depend on cell treatment in contrast to the other cytoskeletal elements, and all staining intensities generally increased with pre-culture duration from 7 to 14 days (fig. 5.7A, 5.7B, and 5.7C). The non-infected, GFP, and shColVI groups appeared to share similar features of vinculin staining. For

instance, the increased staining from 7 to 14 days was much higher in these three groups, and staining was more diffuse throughout the cell. In contrast, the GM and shDcn groups possessed more punctate staining under all conditions, but notably even after loading. Vinculin staining localized to the cell membrane in chondrogenic samples and continued to concentrate at the cell membrane four hours after load.

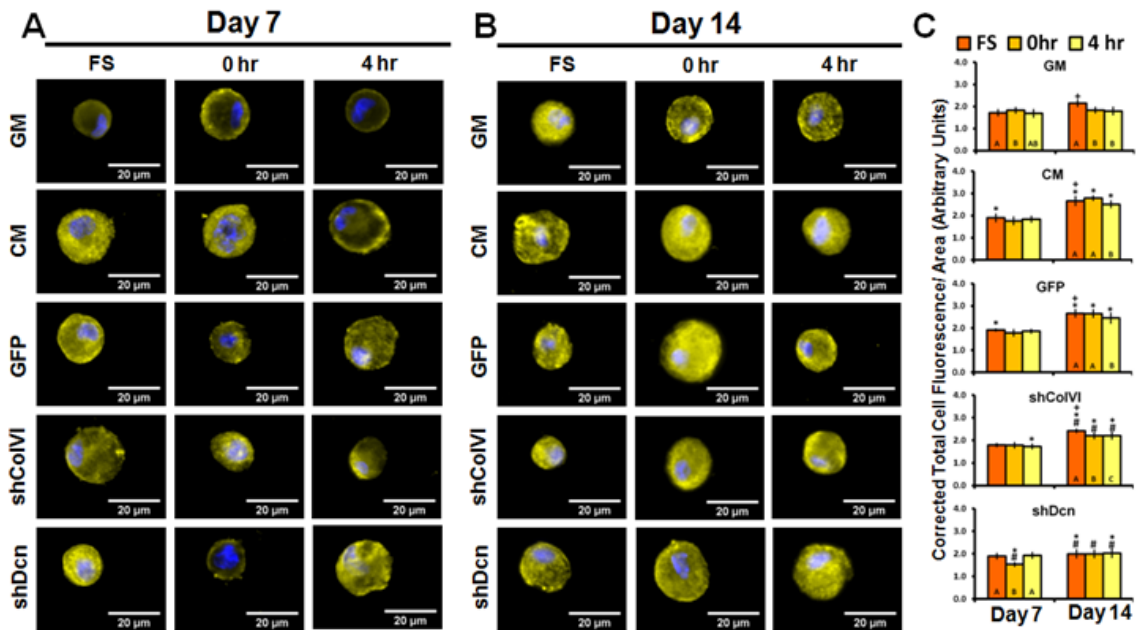


Fig. 5.7: Confocal fluorescence visualization of vinculin at (A) day 7 and (B) 14 in non-infected GM and CM hMSCs and GFP-, shColVI-, and shDcn-transduced cells in free-swelling (FS) conditions and immediately following (0 hr) and four hours post load (4 hrs). Scale bars = 20µm. C) Corrected total cell fluorescence per cellular area intensities for all samples at day 7 and day 14. *:p<0.05 from GM samples at each time point; #:p<0.05 from CM & GFP at each time point; +: p<0.05 from day 7 to day 14; A:B:C: p<0.05 between loading harvests.

5.3.4 Mechanosignaling cascades initiated by ColVI and DCN

Mechanical stimulation influences the metabolic activity of chondrocytes and chondrogenic hMSCs. Cells maintain their environment through this stimulation by

producing a balance of anabolic and catabolic proteins (106). We have previously seen that the altered matrix surrounding shColVI- and shDcn- transduced hMSCs causes varying levels of deformation under applied constant strain, which would affect the signaling cascade initiated following transient loading (113).

Mechanotransduction initiation was found to be directly controlled by amount of time in alginate culture which is directly related to PCM accumulation. Expression levels of *fgf2* and *bmp6* showed an increasing expression level post load at both time points in all samples cultured in chondrogenic media (fig. 5.8A and 5.8B). In growth controls, the expression levels of these genes were relatively unresponsive to load. The slow response of these two genes to be expressed, with a small level of increase until the four hour harvest shows that these genes are activated further down on the signaling cascade. At day 14, shColVI also showed a stronger response to the mechanical loading than at day 7, which wasn't seen in the other chondrogenic samples.

Comp expression showed no significant changes with loading in growth media or chondrogenic non-infected, GFP- and shColVI- transduced hMSCs, yet was responsive in shDcn samples at day 7. ShDcn cells exhibited a vast upregulation of *comp* expression in free-swelling samples compared to all other conditions and was unaffected by load until the 4 hour harvest point, where expression dropped to growth control levels. At day 14, this significantly higher expression was diminished in the free-swelling shDcn cells, and matched the chondrogenic non-infected and GFP-transduced cells, but still showed a difference in response to load. CM-hMSCs and GFP-hMSCs showed an increase immediately following load, which then dropped at 1 hour and then again increased by 4 hours post loading. The response was more robust in chondrogenic non-infected hMSCs,

than its GFP-transduced counterpart. ShColVI cells showed an upregulation of comp, which gradually increased following load, but not significantly.

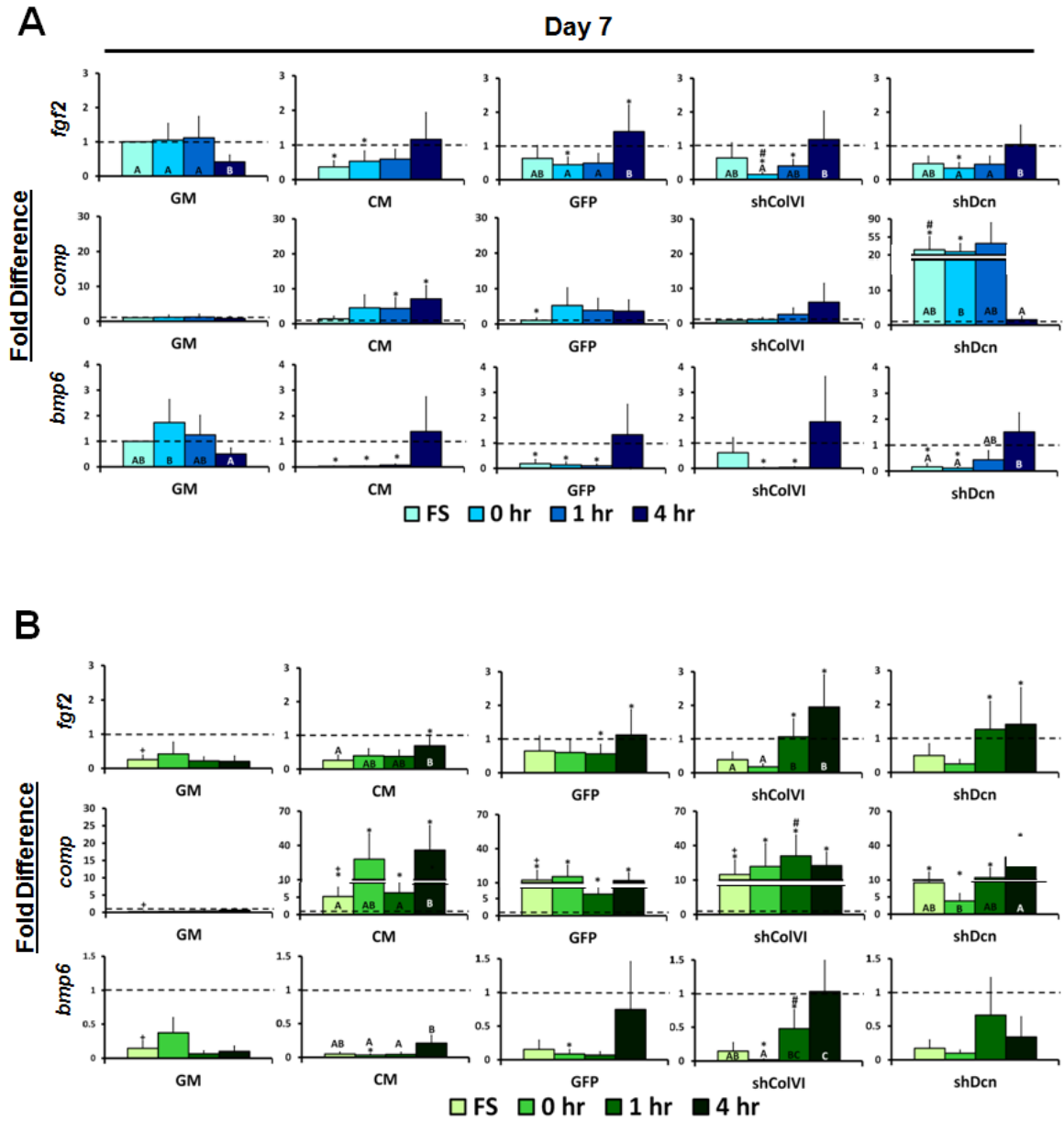


Fig. 5.8: Relative gene expression (fold difference) of day 7 (a) and day 14 (b) non-infected GM and CM cells and GFP-, shColVI-, and shDcn- transduced cells to free swelling GM-hMSCs at day 7. *:p<0.05 from GM samples at each time point; #:p<0.05 from CM & GFP at each time point; +: p<0.05 from day 7 to day 14; A:B:C: p<0.05 between loading harvests.

The chondrogenic and osteogenic markers of *sox9* and *runx2* were unaffected by mechanical loading at day 7 and showed a small response at day 14. The PCM proteins of *acan*, *bgn*, and *colla1*, showed significant increases in chondrogenic samples compared to growth, but showed no significant changes in expression levels following loading at either time point. *Rhoa1* expression was measured to compare against actin dynamics, and was seen to be unresponsive in all samples except chondrogenic non-infected and shColVI-transduced cells at both time points, but the gene expression trend was not reflected by the polymerization of g-actin staining (fig. 5.9A and 5.9B). *Vim* expression was also not significantly affected and did not match the cytoskeletal visualization (fig. 5.9A and 5.9B).

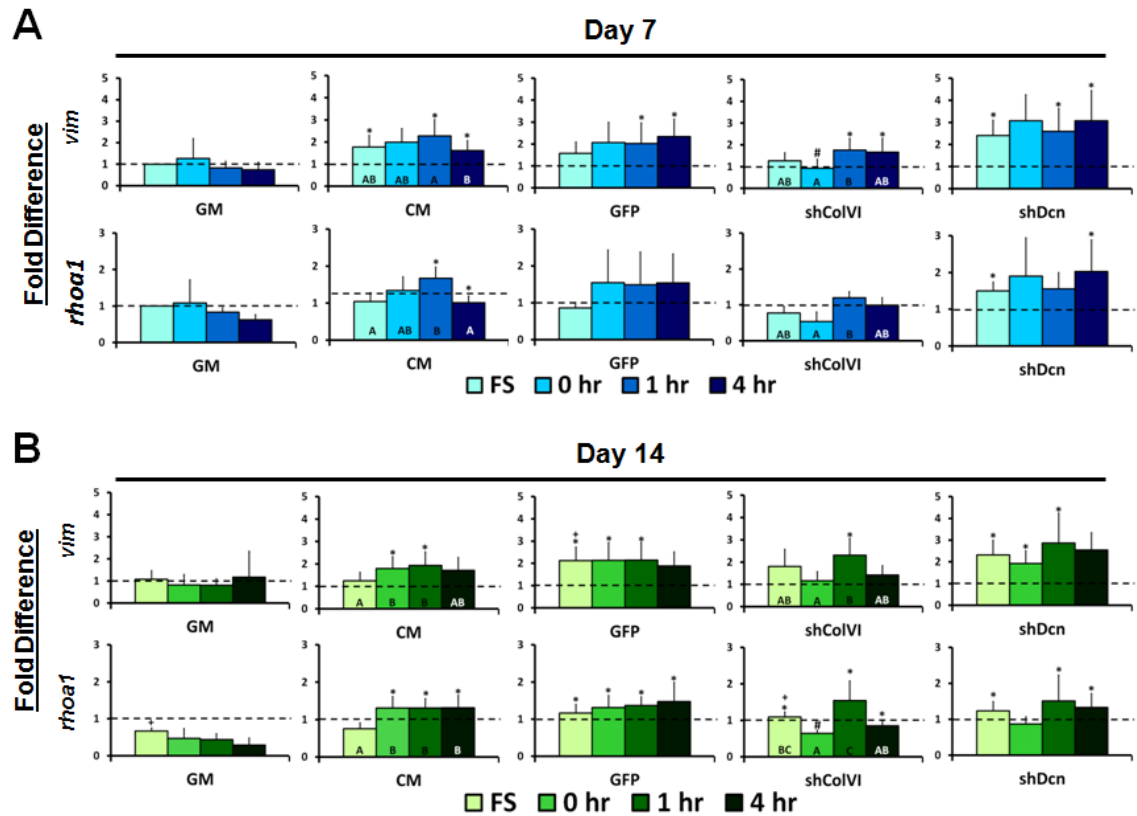


Fig. 5.9: Relative gene expression (fold difference) of day 7 (a) and day 14 (b) non-infected GM and CM cells and GFP-, shColVI-, and shDcn- transduced cells to free swelling GM-hMSCs at day 7. *:p<0.05 from GM samples at each time point; #:p<0.05 from CM & GFP at each time point; +: p<0.05 from day 7 to day 14; A:B:C: p<0.05 between loading harvests.

5.4 Discussion

Examining the relationship between mechanical stimulation and the cell's biological response during chondrogenic differentiation is necessary for construct design for articular cartilage tissue engineering. Current studies compare cartilage tissue explants (115,120), isolated chondrocytes (65,71,76,121,122), and differentiating stem cells (18,69,83) to examine how the mechanosignaling cascade changes during matrix development. Most frequently, agarose or alginate hydrogel constructs are used to identify these responses *in vitro* to allow the cells to maintain their round phenotype

within a homogenous environment (22,63,65,66,110). These studies apply physiologic loading at varying points during differentiation to analyze gene expression and matrix accumulation (53,55,67). Our study analyzed the contribution of ColVI and DCN to mechanosignaling through targeted mRNA knockdown prior to chondrogenic differentiation and studying gene expression and cytoskeletal changes following an applied load. Examining the shift in mechanotransduction events at varying points of PCM accumulation demonstrates the temporally specific control of cell-matrix dependent responses.

Mechanotransduction events are potentially controlled by cellular interactions with the developing matrix through $\alpha1\beta1$ (85,107), $\alpha2\beta1$, and $\alpha5\beta1$ integrins (67,123), annexin 5 (124), CD44 (98) and NG2. Integrins transmit forces from the matrix to the cell through focal adhesions where integrins link to the actin cortex via vinculin, activating GAG and collagen synthesis under dynamic compression (67). Specific integrin activation is dependent on the mode of physiologic loading (13,67). These actin-vinculin co-localizations are seen in cartilage explants (115) as well as during *in vitro* differentiation.

Vinculin staining was punctate in chondrogenic non-infected and GFP- and shDcn-transduced free-swelling samples. Following load, vinculin was spread through the cytoplasm in non-infected and GFP-transduced cells, mimicking g-actin distribution (72,115) but not in shDcn cells which remained fragmented. G-actin staining was consistent with literature, showing punctate and cortical localization, without stress fibers formation from cytoplasmic g-actin due to the round architecture of the cell from the alginate hydrogel (114). Punctate staining of vinculin and g-actin in growth media samples demonstrate that focal adhesions can be formed through mechanical stimulation

without a fully enveloping matrix. ShColVI samples showed a significantly higher intensity of the diffuse g-actin staining at day 14, which then lacked a dynamic response following load. These samples also showed a decrease in vinculin staining following load, with no concentrated aggregates. Focal adhesion creation is tied to a decrease in aggrecan, proteoglycan, and type II collagen synthesis (48). ShColVI samples have previously shown a lower expression of *acan* and *dcn* at day 14 than chondrogenic controls (113). The compositionally different PCM formed surrounding these cells may inhibit focal adhesion development through varied integrin expression, tying focal adhesion creation and proteoglycan gene expression into a more dependent relationship than previously examined, though this needs to be further explored.

Actin polymerization is tied with a stiffening ECM and hypertrophic differentiation (20,48,125), suppressing *sox9* transcription factor expression and varying chondrogenic markers through RhoA/ROCK signaling (72). *Rhoa1* was not seen to be consistent with actin polymerization, though transcription of this factor does not indicate the level of translated or activated RhoA (72). Chondrogenic non-infected and GFP-transduced cells decrease intensity of g-actin staining four hours post loading, potentially increasing the ability of the cell to deform under compression (114). Cyclic compressive loading upregulated cofilin in agarose-embedded chondrocytes, possibly explaining the decrease of cortical actin cortical staining following load. An upregulation of depolymerizing proteins and β -thymosins cause an inhibition of actin polymerization (120) instead of a direct mechanical breakdown (114).

Knockdown samples also demonstrated control over VIF organization, lacking the dynamically increasing response seen in non-infected growth and chondrogenic and GFP-

transduced cells. Growth samples at day 7 measured a significantly lower intensity and knockdown samples a higher intensity in free-swelling, which did not change intensity levels following mechanical compression. The dynamic response of these proteins is not necessarily dependent on the initial amount of protein available, but potentially more dependent on the deformability of the cell or the matrix-membrane interactions. Vimentin contributes to the integrity of the chondrocyte cytoskeleton, with a decrease in vimentin causing a decrease in the overall mechanical properties of the cell (116). Vimentin proteins increase during chondrogenesis (77) and are highly involved in chondrogenic marker expression possibly through PKA phosphorylation (77). VIFs and MTs demonstrate spatial similarity and increase directly related to the accumulation of PCM surrounding chondrocytes (122). A decrease in VIF content and organization is seen with osteoarthritis (116) and *in vitro* disruption of VIFs and MTs causes a decrease in sGAG and collagen synthesis and transcription (117,126). MT intensity was dynamic in all chondrogenic cells, with an overall decreasing intensity in knockdown samples following load. Both VIFs and MTs are involved in the synthesis and secretion of proteoglycans in response to mechanical stimulation (126). The stimulatory effect of MT dynamic turnover is also directly related to the stage of differentiation, with hypertrophic chondrocytes expressing a higher level of MTs than proliferative chondrocytes (118) which stimulate type X collagen synthesis and ALP activity. The higher intensity of MT staining and lack of dynamic response of AMF and VIF in shColVI samples could demonstrate an early shift towards hypertrophic differentiation which is unaffected by dynamic loading.

These cytoskeletal proteins directly transmit mechanical forces from the cell membrane, causing direct effects on chondrogenic gene expression following mechanical stimulation (13,115,127). Compression stimulates signaling pathways involving p38, mitogen-activated protein kinases (MAPK), cFos and cJun (63). These signaling cascades could be caused not only by a changing cytoskeleton, but by cell-membrane channels involved in ATP release (109) and changes in cellular volume and surface area (16,110).

Comp is mechanically activated in chondrocytes, having higher gene and protein expression levels in chondrocytes when dynamically cultured both in explants and when cultured in alginate in the presence of TGF- β for 14 days (107). COMP is both activated by TGF- β and causes TGF- β enhanced signaling (128). ShDcn samples showed a significantly higher expression of *comp* at day 7 in free-swelling and loaded samples, which decreased approximately four hours post loading. DCN sequesters TGF- β (3,21,62), controlling the growth factor presentation to the cell, and is stimulated directly through mechanical compression (65). Without DCN regulation, COMP protein could be continuously activating itself through this TGF- β signaling. COMP also enhances TGF- β efficiency through multiple binding sites of the growth factor increasing membrane presentation (128). This high upregulation in shDcn samples was decreased by day 14, matching the chondrogenic non-infected and GFP-transduced samples. With DCN knockdown samples at day 14, *comp* expression showed an initial decrease following loading, opposite to the chondrogenic controls. *Comp* upregulation has been tied to $\alpha 1$ integrin mechanotransduction (107), directly tying integrin-collagen interactions to the *comp* mechanotransduction regulation.

FGF2 has been seen to be important during dynamic loading, being released from its heparin sulfate GAG chains to stimulate the cell membrane (129,130) and has been seen to suppress aggrecanolysis by ADAMTS5 (131). The similar late onset following load for *fgf2* and *bmp6* could distinguish their expression as further down the mechanosignaling cascade and potentially competing for phenotype expression. FGF2 has inhibitory effects on BMP6 during chondrogenic culture (132). *Bmp6* is dynamically upregulated in pre-chondrogenic hMSCs (53) and is considered a potent inducer of osteogenic phenotype (133). *Bmp6* is activated through different SMAD receptors than TGF- β (134), with TGF- β inhibiting and BMP6 activating hypertrophic differentiation. When BMP6 is activated, there are significant increases in ColX and ALP expression. The more robust response of *bmp6* and *fgf2* at day 14 is potentially tied to the shift in AMF and MT dynamics in shColVI samples, demonstrating further acceleration towards a hypertrophic phenotype in ColVI knockdown samples. The same gene expression shift was unseen in shDcn cells, which actually shows an earlier peak response at 1 hour following load, though this is insignificant. Therefore the lack of VIF dynamics at day 14 in knockdown samples is not the direct influence on *fgf2* and *bmp6* signaling.

Stimulation of hMSCs during chondrogenesis is highly dependent on the duration (135), frequency (67,111), and amplitude of applied physiologic loading. Short term mechanical compression allows a narrower examination of activated cell signaling for understanding of longer duration matrix metabolic changes. Cells maintain their micromechanical environments through by balancing anabolic and catabolic responses to applied forces (106,135). The shift in matrix composition during osteoarthritis is considered to cause a change in the mechanical signaling cascade within chondrocytes,

causing the matrix to further degrade. We have demonstrated control over cytoskeletal dynamics and gene expression through targeted subtraction of PCM components. Intrinsically controlling mechanotransduction events using shRNA-mediated RNAi in differentiating hMSCs can aid regenerative therapies in overcoming the loss of structural integrity in degenerating load bearing tissues.

5.5 Conclusion

This study determined how ColVI and DCN directly affected cytoskeletal and mechanosignaling events during chondrogenic differentiation. ColVI and DCN knockdown arrested a dynamic response of cytoskeletal AMF and VIF reorganization following load. The higher fluorescence levels of AMF and VIF demonstrate a cellular stiffening to compensate for the altered micromechanical environment. These changes then cause a shift in mechanosignaling initiation. This study was the first to our knowledge to determine a relationship between ColVI and *fgf2* and *bmp6* mechanosignaling as well as the direct control of DCN over *comp* expression.

Understanding how these proteins are involved in mechanosignaling initiation advances the ability to control the gene expression cascade following load. Further examination of how these proteins are involved in long term mechanotransduction events is needed to understand their contribution in maintaining the structural environment under physiologic loading.

Chapter 6: ColVI and DCN's influence on cell-seeded alginate scaffold material properties and chondrogenic gene expression during long term dynamic compressive culture³

6.1 Introduction

Articular cartilage is composed of a complex network of collagens, specifically types I and II (21), proteoglycans (PGs), and non-collagenous proteins. These proteins are interwoven to withstand a complex combination of compression, tension and hydrostatic pressure during loading and transduce a safe level of mechanical stimulation to the cell to elicit a biochemical response. The cartilage extracellular matrix (ECM) is maintained through a balance of anabolic and catabolic effects caused by these environmental cues (106). The thin 2-6 μm pericellular matrix (PCM) developed during chondrogenesis enveloping the cell directly controls the metabolic activity of articular chondrocytes and chondrogenic human mesenchymal stem cells (hMSCs) in response to dynamic loading (13).

The PCM is composed of type VI collagen (ColVI) (17,22), hyaluronan (98), fibronectin, and PGs such as decorin (DCN), biglycan (BGN), perlecan (130) and aggrecan (17,123), which give the PCM biochemical and mechanical properties distinct from the surrounding extracellular matrix (ECM) (22,100). These proteins are accumulated in a temporally specific manner, with peaks of PGs and collagens and matrix organizing proteins, such as cartilage oligomeric matrix protein (COMP) (123), varying within

³I'd like to acknowledge the contribution of Ben A. Bulka to the design and implementation of the dynamic bioreactor culture system.

two weeks of chondrogenic induction (3,4,52,123). Exogenous addition of members of the transforming growth factor (TGF) family will cause hMSCs to commit to the chondrogenic lineage as well as simulated physiologic loading (55). Dynamic loading not only increases endogenous TGF- β release (97), directly improves matrix elaboration and GAG synthesis (30,39,44,52,54,97).

Mechanical stimulation in combination with growth factor chondrogenic induction has shown varying effects on chondrogenic phenotype with a complex pattern of gene expression (54,55). Dual stimulation causes more robust type II collagen synthesis (14,52,54), but does not show an additive effect on aggrecan expression (52). While chondrogenic markers are upregulated under dynamic stimulation, this may also increase the rate of terminal differentiation, increasing type X and type I collagen expression (54,97). Differentiation of hMSCs into physiologically functional chondrocyte like cells needs correct temporal applications of chemical and mechanical stimuli (45) and an understanding of how the cell responds to these specific stimulations.

We have previously shown that ColVI and DCN are highly involved in PCM expression and accumulation (113). ColVI knockdown decreased, while DCN knockdown accelerated PG and *comp* expression during the two week induction period. The change in proteoglycan content and knockdown proteins caused a higher cellular deformability under applied compression in shColVI samples and a highly irregular organized matrix in shDcn samples which act in a strain dependent manner (113). The shift in deformability altered the cytoskeletal mechanics and will change the transmission of forces to the nucleus (71).

Current studies have focused on understanding how mechanical load stimulates chondrogenesis, in the presence or absence of TGF- β (12,14,55) and in the presence or absence of an elaborated matrix (45,55). Whether the findings of improved chondrogenesis from initial matrix elaboration prior to dynamic stimulation are due to initial collagen or PG signaling or the changing mechanical properties has yet to be determined. This study analyzes the contribution of type VI collagen and decorin in chondrogenic gene expression, MSC proliferation, and the biomechanical composition of cell-seeded scaffolds during chondrogenic culture with the dual stimulation of TGF- β and dynamic compression. We believe that ColVI and DCN are highly involved in the matrix accumulation caused by dynamic compressive culture and that targeted knockdown of these proteins will significantly alter the biomechanical and biochemical composition of the developed matrix.

6.2 Materials and Methods

6.2.1 Cell culture and viral transduction

HMSCs were expanded in monolayer using a basal non-differentiation growth media (GM) containing high glucose DMEM (HG-DMEM) (Gibco/Invitrogen, Carlsbad, CA) supplemented with 10% fetal bovine serum (FBS) (Gibco), 100U/mL penicillin/streptomycin (Gibco), 1% MEM non-essential amino acids (Gibco), and 4mM L-Glutamine (Invitrogen) until passage 4. Cells were cultured at 37°C with 5% CO₂ with media changes three times per week.

HMSCs were separated into either non-infected or infected experimental samples. Infected experimental samples were treated with shRNA lentiviral vectors targeting either

human *col6a1* mRNA (shColVI) (Gen Bank: NM_001848), *dcn* mRNA (shDcn) (GenBank: NM_001920) (Table 6.1), or a GFP expression vector as previously described (113).

5'-'stem-loop-stem'-3' sense and 3'-'stem-loop-stem'-5' anti-sense sequences

shColVI	5'-CACCGCGGAGACGATAACAACGACATCGAAATGTCGTTGTTATCGTCTCCG-3' 3'-CGCCTCTGCTATTGTTGCTGTAGCTTTACAGCAACAATAGCAGAGGCAAAA-5'
shDcn	5'-CACCGCCGTTTCAACAGAGAGGCTTACGAATAAGCCTCTCTGTTGAAACGG-3' 3'-CGGCAAAGTTGTCTCTCCGAATGCTTATTCGGAGAGACAACCTTTGCCAAAA-5'

Table 6.1: Sense and anti-sense hairpin sequences for shColVI and shDcn.

All vectors included a blasticidin resistance gene with a U6 promoter and a PolIII termination sequence. Cells were infected at a multiplicity of infection (MOI) of 1 in the presence of 6µg/mL Polybrene (Sigma) to aid in transduction efficiency for 24 hours as previously described (113). MOI was determined for each lentiviral vector through a Quant-IT PicoGreen (Invitrogen) titer assay. 48 hours following viral removal, cells were incubated with GM containing 12 µg/mL of blasticidin to select for a pure population of transduced cells as previously described. After selection, non-infected and infected cells were lifted from monolayer using 0.25% trypsin-EDTA (Gibco), centrifuged at 600xg for 5 minutes before being re-suspended in a 2% (w/v) alginate solution (Research Products International, Mount Prospect, IL) at a concentration of 2.0×10^6 cells/mL. Alginate disks were formed as previously described by pipetting the cell-alginate solution into cylindrical disk-shaped molds (Ø 6mm x 3 mm in height) with a 5 µm porous membrane and Whatman filter paper attached to the top and bottom faces of the molds (92). Molds were immersed in a 102 mM CaCl₂ bath for 90 minutes to ensure complete alginate

crosslinking. To maintain position and unconfined conditions during loading, Ø8mm wells were punched out of a 1.5 mm thick layer of agarose pre-cast into Ø60 mm petri dishes(43,44), and alginate-cell disk constructs were each placed into a pre-formed well. Each petri dish was able to accommodate six constructs. All cell constructs were allowed to equilibrate in free-swelling conditions overnight prior to bioreactor culture. One non-infected cell group was cultured in GM. The remaining non-infected group and all transduced cell constructs were cultured in chondrogenic induction media (CM) containing HG-DMEM, ITS Universal Culture Supplement Premix (BD Biosciences, San Jose, CA), 10nM dexamethasone, 50µg/mL L-ascorbic acid (Sigma), 40 µg/mL L-Proline (Sigma), 100U/mL penicillin/streptomycin, 1mM sodium pyruvate, 0.584 g/mL L-glutamine, and 10ng/mL TGF-β3 (Lonza). All samples were cultured for 7 or 14 days at 37°C with 5% CO₂ with media changes three times per week. For qRT-PCR baseline controls, some disks were collected at day 1 of free-swelling GM culture prior to bioreactor loading.

6.2.2 Dynamic mechanical stimulation of cell-seeded alginate constructs

The Ø60 mm petri dishes containing the cell-seeded alginate disks and 1.5mm height agarose molds were placed into Ø 62 mm culture chambers of a custom designed polysulfone bioreactor. The bioreactor contains four culture chambers centered on a Zaber linear actuator (Zaber NA11B16, Zaber Technologies Inc., British Columbia, Canada) (fig. 6.1A). The polysulfone lid of the bioreactor consisted of four loading platens of Ø 50mm that would center above and be concentric with the culture chambers when attached to the motor (fig. 6.1 D and 6.1E). Assembled, the polysulfone lid

overlaps the base to ensure sterility within the bioreactor chambers and the entire assembly is maintained in a 37°C, 5% CO₂ incubator (fig. 6.1B).

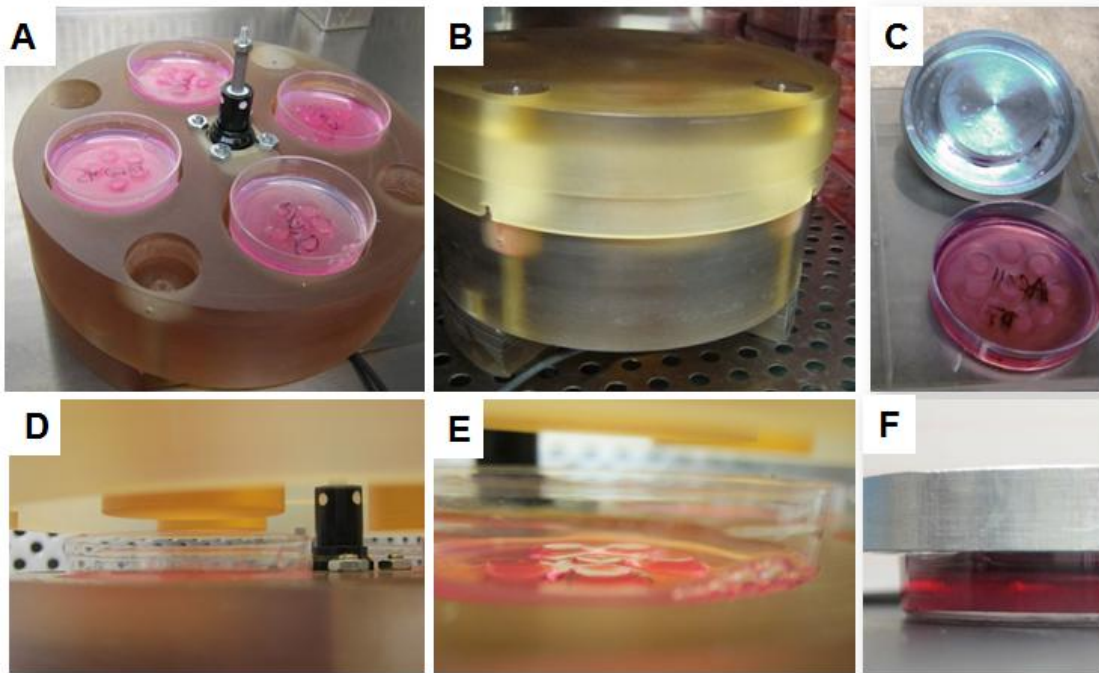


Fig. 6.1: Custom designed polysulfone bioreactor designed to apply displacement controlled sinusoidal unconfined compression. (A) The bioreactor has four culture wells centrally located around the Zaber linear actuator. Each well contains one Ø60 mm petri dishes with alginate disks (Ø6 mm x 3 mm in height) maintained in an agarose mold. (B) Once assembled, the polysulfone lid overlaps the base to ensure sterility while allowing free gas-exchange during loading while maintained in a temperature and gas controlled incubator. (D) The Ø50 mm loading platens are designed to concentrically locate above the individual wells to apply homogenous displacement controlled strain across all disks (E). Non-loaded (NL) static contact cultures incorporated an aluminum platen to maintain 0% strain for four hours per day (C,F) to mimic the nutrient diffusion limitations within the bioreactor.

Sinusoidal compression was applied at 0.1Hz from 2-12% strain for four hours per day for dynamically cultured samples. All compression was displacement controlled.

Following the loading duration, samples were removed from the bioreactor and returned to free-swelling conditions. Samples were cultured with alternating loading and free swell periods for 7 or 14 days, at which point disks were separated for viability, gene expression, mechanical property analysis, DNA quantification, histology, and immunofluorescence (fig. 6.2).

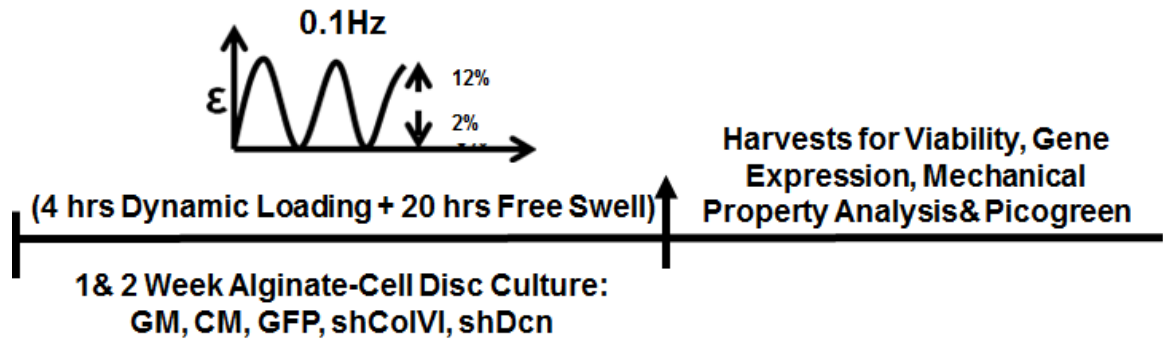


Fig. 6.2: Schematic of loading duration and harvest points.

Static non-loaded (NL) controls were cultured in parallel with platens placed on the alginate-cell scaffolds which maintained 0% strain, to prevent axial swelling and to mimic the diffusive qualities of the bioreactor platens (fig. 6.1C and 6.1F). These controls were subjected to the same daily alternating static contact condition for four hours and free-swelling condition for 20 hours.

6.2.3 Gene expression

Samples were collected from loaded and non-loaded cultures at day 7 and 14. Day 1 samples, prior to bioreactor culture were also harvested as a baseline control. Cells were recovered from cell-alginate constructs by immersion in a 100mM sodium citrate, 30mM EDTA solution as previously described. Cells were centrifuged at 600xg for five minutes and then resuspended in a buffer solution containing β -Mercaptoethanol (Fisher

Scientific, Pittsburgh, PA) before flash freezing. RNA was isolated (RNeasy Micro, Qiagen, CA) and total RNA was reverse transcribed. Gene expression was analyzed using qRT-PCR (MyiQ System, BioRad, CA) with primers designed for human genes (Table 6.2) using Primer3 software. Gene expression levels for *18s*, *acan*, *adamts4*, *bgn*, *colla1*, *col2a1*, *col6a1*, *comp*, *dcn*, *fgf2*, *runx2*, and *sox9* were quantitatively assessed as previously described (113,136). All primer amplification efficiencies were determined using linear regression efficiency methods and were determined to be between 89.4% and 117.7% efficient ($R^2 > 0.99$) (90). Expression levels were analyzed using the $\Delta\Delta Ct$ method. Cycle threshold (Ct) values were averaged and ΔCt was calculated by subtracting the average Ct values of the internal control gene *GAPDH* from that of the gene of interest ($\Delta Ct_{col6a1} = Ct_{col6a1} - Ct_{GAPDH}$) as previously described. $\Delta\Delta Ct$ for each gene of interest was determined by subtracting the ΔCt of day 1 samples from the experimental ΔCt at each time point (i.e. *col6a1* expression shColVI samples cultured in the bioreactor for 7 days: $\Delta\Delta Ct_{col6a1,shColVI, BR-D7} = (\Delta Ct_{col6a1,shColVI, BR-D7} - \Delta Ct_{col6a1,day 1})$). Relative gene expression levels (fold difference) were computed through the exponential relation $2^{-\Delta\Delta Ct}$ (91). Data are shown as average values of the range of calculated fold differences ($2^{\Delta\Delta Ct + SD}$ and $2^{-\Delta\Delta Ct - SD}$) \pm half the range.

Gene Name	Forward and Reverse primers	GenBank accession no.
<i>18s</i>	5'-AAACGGCTACCACATCCAAG-3' 5'-CCTCCAATGGATCCTCGTTA-3'	NR_003286
<i>acan</i>	5'-ACAGCTGGGGACATTAGTGG-3' 5'-GTGGAATGCAGAGGTGGTTT-3'	NM_001135
<i>adamts4</i>	5'-AGGCACTGGGCTACTAC-3' 5'-GGGATAGTGACCACATTGTT-3'	AY358886
<i>bgn</i>	5'-ACCTCCCTGAGACCCTGAAT-3' 5'-CTGGAGGAGCTTGAGGTCTG-3'	NM_001711
<i>colla1</i>	5'-GTGCTAAAGGTGCCAATGGT-3' 5'-CTCCTCGCTTTCCTTCCTCT-3'	NM_000088
<i>col2a1</i>	5'-TGGCCTGAGACAGCATGAC-3' 5'-AGTGTGGGAGCCAGATTGT-3'	NM_001844
<i>col6a1</i>	5'-CTACACCGACTGCGCTATCA-3' 5'-GCCACCGAGAAGACTTTGAC-3'	NM_001848
<i>comp</i>	5'-AGGACAACCTGCGTGACTGTG-3' 5'-GTTGTCCTTTTGGTCGTCGTT-3'	NM_000095
<i>den</i>	5'-AATTGAAAATGGGGCTTCC-3' 5'-GCCATTGTCAACAGCAGAGA-3'	NM_001920
<i>fgf2</i>	5'-TGCTGGTGATGGGAGTTGTA-3' 5'-CTGAGTATTCGGCAACAGCA-3'	NM_002006
<i>runx2</i>	5'-TTTGCACTGGGTCATGTGTT-3' 5'-TGGCTGCATTGAAAAGACTG-3'	NM_001015051
<i>sox9</i>	5'-AGTACCCGCACTTGCACAAC-3' 5'-CGTTCTTCACCGACTTCCTC-3'	NM_000346

Table 6.2: Sequences of Primers used for Aim 3 qRT-PCR.

6.2.4 Material Properties

To determine the changing micromechanical properties of the PCM within the alginate disks, unconfined stress-relaxation tests were performed using an Ø 7mm stainless steel chamber and a Ø6mm plunger attached in series with a 200g load cell. These components were attached to and controlled by a materials testing system (LM-1, Bose/Electroforce, Eden Prairie, MN). Disks were initially loaded with a 2g tare load and then maintained at

the achieved displacement for 5 minutes. Constructs underwent three rampings of displacement controlled 10% strain applied at 0.05%/second (55,137) followed by 1000 seconds of relaxation (55). Force and displacement measurements were collected during each mechanical test. From the individual rampings, viscosity (η), instantaneous (E_1+E_2) and steady state stiffnesses (E_1) were determined using the linear standard solid model for stress relaxation of: $\sigma = E_1 * \epsilon_0 * e^{-\frac{E_1}{\eta}t} + E_2 * \epsilon_0$ (fig. 6.3). E_1 and E_2 show the stiffness changes during the stress relaxation and η represents the viscous time-dependent behavior of the disk. Data were analyzed with the curve fitting toolbox using Matlab (Mathworks, Natick, MA).

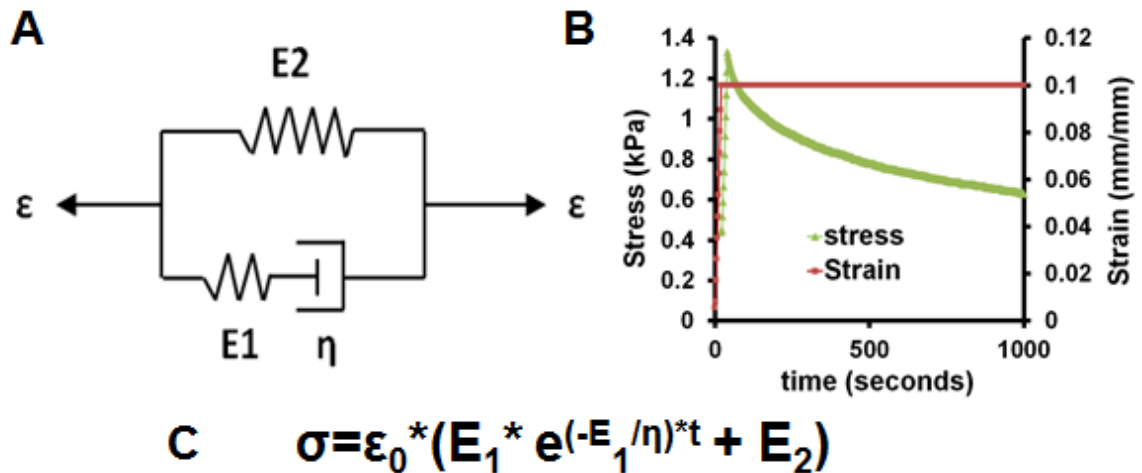


Fig. 6.3: Standard Linear Solid model was used to determine the mechanical properties of the stress-relaxation tests. (A) Representative spring-dashpot schematic of the standard linear solid model, where E_1 , E_2 , and η represent changing material properties under applied strain. $E_1 + E_2$ represents the instantaneous stiffness under an applied compression, E_1 represents the steady state stiffness of the construct, and η represents the viscosity of the changing disk under applied load. (B) Representative stress and strain curve vs. time for chondrogenic non-infected cells at day 14. (C) The standard linear solid model can determine the changing material properties from collected force and displacement data.

6.2.5 DNA quantitation

DNA was isolated from disks to determine effects of loaded and non-loaded culture on cellular proliferation. Cells were isolated from their alginate scaffolds using a 100mM sodium citrate, 30mM EDTA solution as previously described. Cells were separated from the alginate solution by spinning down at 600xg for five minutes before being resuspended in Tris-EDTA buffer and flash freezing. DNA was isolated using a DNeasy Tissue Kit (Qiagen, Valencia, CA), resulting in 400 μ L of DNA eluate. DNA was quantified using the Quant-iT PicoGreen kit according to manufacturer's instructions with a calibration curve generated from Lambda DNA. Fluorescence intensity was measured using a SpectraMax M5 plate reader (Molecular Devices, Sunnyvale, CA).

6.2.6 Statistical Analysis

Statistical analyses for gene expression, mechanical properties, and DNA quantitation were performed using one-way ANOVA. Tukey's HSD *post hoc* tests were performed for pairwise comparisons. All computations were performed using JMP7 (Cary, NC) with statistical significance set to $\alpha < 0.05$ as indicated in results.

6.3 Results

6.3.1 Targeted knockdown was unaffected by dynamic culture

Significant knockdown of *col6a1* and *dcn* was achieved over the 14 day experiment with lower expression levels in shColVI and shDcn-transduced cells in both non-loaded and bioreactor culture conditions. Expression of *col6a1* was reduced by 47-77% in the shColVI group compared to CM (fig. 6.4: *col6a1* gene expression: CM (D7-NL: 7.994 \pm 2.246; D7-BR: 8.180 \pm 2.242; D14-NL: 5.736 \pm 1.486; D14-BR: 4.442 \pm 1.422), GFP (D7-

NL: 7.521 ± 2.379 ; D7-BR: 5.838 ± 1.790 ; D14-NL: 5.204 ± 1.384 ; D14-BR: 3.340 ± 1.190), and shColVI: (D7-NL: 4.232 ± 1.215 ; D7-BR: 3.489 ± 1.331 ; D14-NL: 2.75 ± 0.698 ; D14-BR: 1.012 ± 0.348)). Expression of *dcn* decreased by 85-95% in the shDcn group compared to CM (*dcn* expression levels: CM (D7-NL: 2.661 ± 1.107 ; D7-BR: 4.34 ± 1.973 ; D14-NL: 1.349 ± 0.429 ; D14-BR: 1.831 ± 0.485), GFP (D7-NL: 3.301 ± 0.892 ; D7-BR: 2.412 ± 1.858 ; D14-NL: 0.306 ± 0.080 ; D14-BR: 0.540 ± 0.322), and shDcn (D7-NL: 0.412 ± 0.239 ; D7-BR: 0.619 ± 0.178 ; D14-NL: 0.093 ± 0.029 ; D14-BR: 0.088 ± 0.072)).

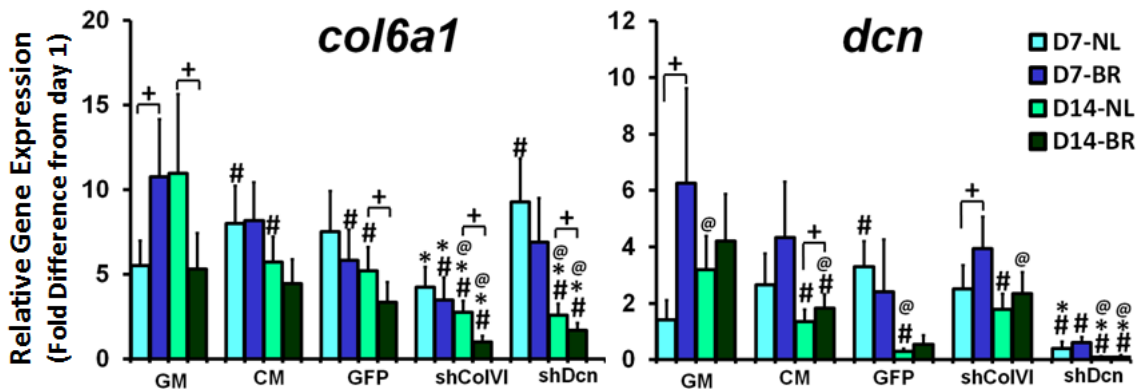


Fig. 6.4: Relative *col6a1* and *dcn* gene expression (fold difference) of day 7 and day 14 non-infected GM and CM cells and GFP-, shColVI-, and shDcn- transduced cells in non-loaded and bioreactor culture to day 1 cultures. (#: $p < 0.05$ from GM samples at each time point; *: $p < 0.05$ from CM & GFP at each time point; +: $p < 0.05$ between non-loaded and bioreactor cultured samples; @: $p < 0.05$ between day 7 to day 14 culture; $n \geq 3$).

6.3.2 Dynamic culture affected DNA quantity in non-infected samples

DNA content showed no significant differences between non-loaded and dynamically cultured samples at either time point in any of the chondrogenic conditions, but dynamic loading did affect GM samples at day 14 (fig. 6.5). GFP-, shColVI- and shDcn- transduced resulted in significantly lower DNA content than growth and chondrogenic

non-infected cells at both time points. Previous studies have not shown a significant difference in viability between non-infected and viral transduced cells (113). TGF- β culture has shown an increase in proliferative capacity initially in hMSCs (52), which could correspond to the increase in DNA content in non-infected CM samples between days 7 and 14.

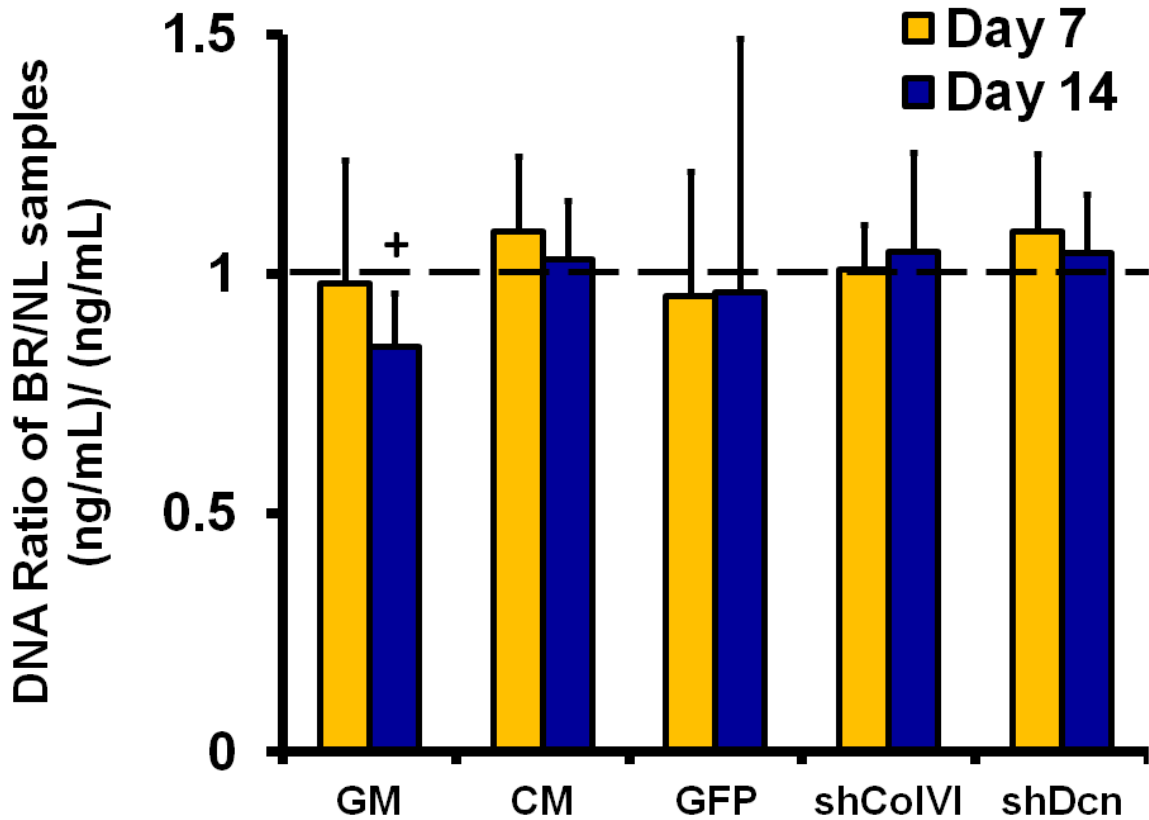


Fig. 6.5: Ratio of DNA content between bioreactor cultured and non-loaded disks in non-infected GM and CM and GFP-, shCoVI-, and shDcn-transduced cells disks at 7 or 14 days. DNA was quantified using Quant-iT Picogreen and a lambda DNA standard curve Data shown is the average DNA concentration (ng/mL) of bioreactor culture / average DNA concentration in non-loaded samples (ng/mL) + standard deviation. (+:p<0.05 between non loaded and bioreactor cultured samples; n \geq 5).

6.3.3 Dynamic culture affected material properties only after two weeks of culture

Mechanical properties of cell-seeded alginate scaffolds determined from stress-relaxation tests and the standard linear solid model were affected by both culture duration and dynamic loading. At day 7, mechanical characteristics were not significantly affected in chondrogenic medium cultured samples. CM and GFP samples had a slight decrease in their viscosity parameter under dynamic load, which was opposite in growth media conditions (fig. 6.6). The increase in GM viscosity was significantly higher than chondrogenic alginate disks. This trend was opposite at day 14, where dynamic load no longer affected the growth media samples, but increased the viscosity parameter in chondrogenic samples (fig. 6.7). The viscosity of the disk affects the rate of relaxation and stress dissipation under an applied compression, which will be indicative of the matrix elaborated and hydration levels. Growth media samples showed significantly higher viscosity, instantaneous and steady state stiffness parameters at day 14 in non-loaded cultures than chondrogenic samples. These properties all decreased with time from day 7 to day 14 in the chondrogenic cultures. By day 14 when cells will have developed a full PCM enveloping themselves (113), dynamic loading increased the viscosity and steady state stiffness of CM and GFP samples to match these growth media parameters at day 14. These increases in steady state stiffness in bioreactor culture could be potentially due to a stiffer matrix and higher synthesis and accumulation of proteins within the cell-alginate scaffolds. The instantaneous stiffness under applied compression at day 14 remained lower than growth media samples.

Mechanical Properties (Day 7)

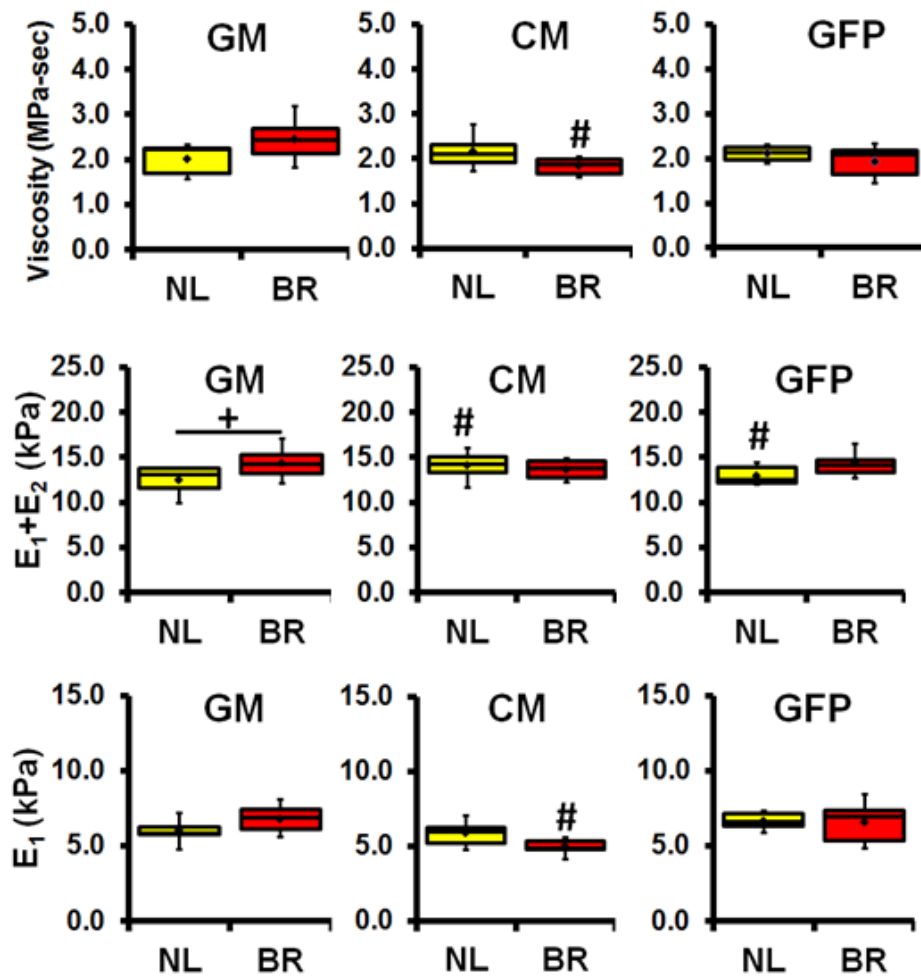


Fig. 6.6: Mechanical properties of non-infected GM and CM, and GFP-transduced cell alginate disks in either non-loaded (NL) or bioreactor (BR) culture for 7 days. Viscosity (η), instantaneous (E_1+E_2) stiffness, and steady-state (E_1) stiffness was unaffected at day 7. All properties were determined using displacement controlled stress-relaxation tests with 10% strain applied at 0.05%/second, which was maintained for 1000 seconds. Stress and strain calculations were determined from the force and displacement data collected. Mechanical properties were determined from standard linear solid model: $\sigma = E_1 * \varepsilon_0 * e^{-\frac{E_1 t}{\eta}} + E_2 * \varepsilon_0$. (#:p<0.05 from GM samples at each time point; *:p<0.05 from CM & GFP at each time point; +:p<0.05 between non-loaded to bioreactor cultured samples; n≥5 disks per sample).

Mechanical Properties (Day 14)

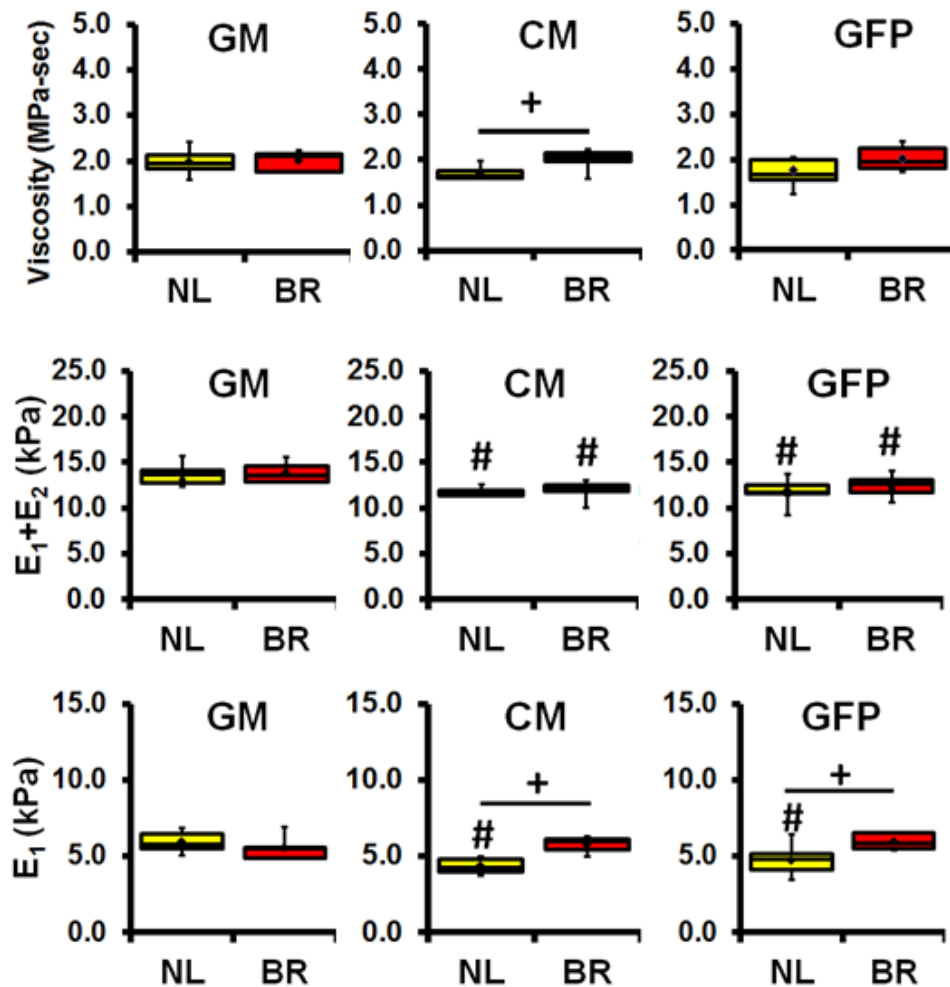


Fig. 6.7: Mechanical properties of non-infected GM, CM, and GFP-transduced cell alginate disks in either non-loaded (NL) or bioreactor (BR) culture for 14 days. Steady-state (E_1) stiffness significantly increased with dynamic culture. All properties were determined using displacement controlled stress-relaxation tests with 10% strain applied at 0.05%/second, which was maintained for 1000 seconds. Stress and strain calculations were determined from the force and displacement data collected. Mechanical properties were determined from standard linear solid model: $\sigma = E_1 * \varepsilon_0 * e^{-\frac{E_1 t}{\eta}} + E_2 * \varepsilon_0$. (#: $p < 0.05$ from GM samples at each time point; *: $p < 0.05$ from CM & GFP at each time point; +: $p < 0.05$ between non-loaded to bioreactor cultured samples; $n \geq 5$ disks per sample).

6.3.4 *Dynamic stimulation does not enhance gene expression in conjunction with TGF- β culture*

Mechanical stimulation demonstrated a strong control over chondrogenic gene expression, upregulating *bgn*, *acan*, *coll1a1*, and *fgf2* in GM samples to similar levels of chondrogenic non-infected and GFP-transduced cells (fig. 6.8). These samples resulted in a much higher response to loading than chondrogenic samples, demonstrating the competing mechanical and biochemical induction of the TGF- β pathway. Similar levels of chondrogenic gene expression was seen between loaded and non-loaded samples in CM and GFP samples.

Dynamic stimulation affected some chondrogenic markers, with *fgf2* remaining highly responsive, *col2a1*, *runx2*, and *sox9* expression levels were minimally different between time points and with dynamic loading. Hypertrophic gene expression was inhibited when dynamically loaded (fig. 6.8). While mechanical and biochemical induction of chondrogenesis may compete and decrease chondrogenic marker expression compared to each method by itself, the combined stimulation inhibited terminal differentiation of hMSCs.

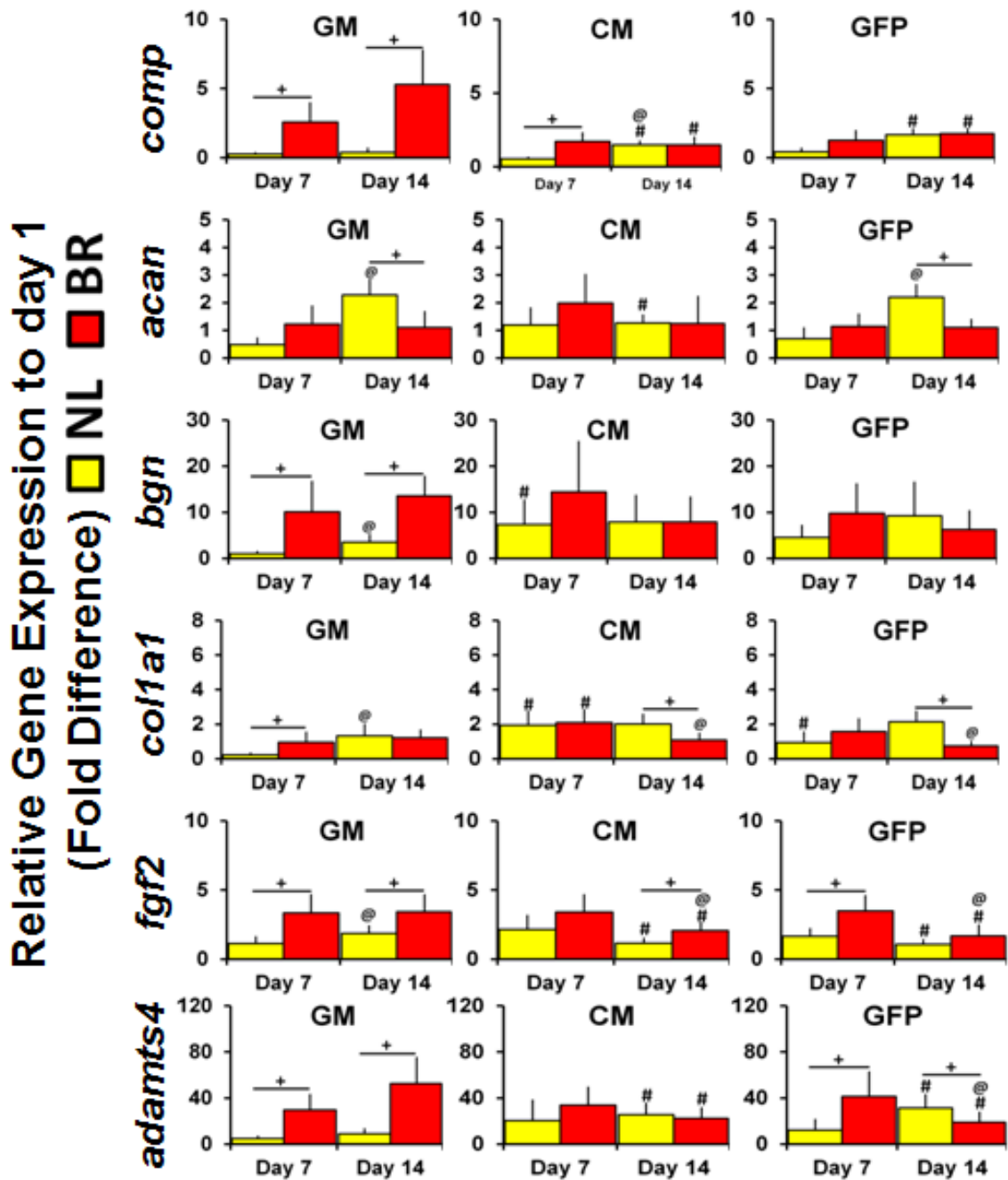


Fig. 6.8: Relative *comp*, *acan*, *bgn*, *col1a1*, *fgf2*, and *adamts4* gene expression (fold difference) of day 7 and day 14 non-infected GM and CM cells and GFP- transduced cells in non-loaded (yellow) and bioreactor (red) culture to day 1 cultures. (#:p<0.05 from GM samples at each time point; *:p<0.05 from CM & GFP at each time point; +:p<0.05 between non-loaded and bioreactor cultured samples; @: p<0.05 between day 7 to day 14 culture; n≥3).

6.3.5 ColVI and DCN knockdown caused varying material changes to dynamic culture

The contribution of ColVI and DCN were more drastic at day 14 than day 7 in alginate scaffold material properties (fig. 6.9). DCN knockdown caused an increase in the instantaneous stiffness at day 7, which wasn't seen at day 14. Dynamic culture did not affect any other properties in other conditions at day 7.

Bioreactor cultured shColVI samples showed a significant increase in instantaneous and long term stiffness. Dynamic culture potentially affected the matrix elaboration therefore changing the viscosity and instantaneous stiffness of the whole scaffold. ShDcn samples were the only chondrogenic condition at day 14 in which long term stiffness was unchanged by bioreactor culture. ShDcn samples that underwent unloaded culture had significantly higher viscosity and stiffness parameters at day 14, of which only the viscosity and instantaneous stiffness were affected under dynamic culture. ColVI knockdown samples may cause significant changes when dynamically cultured, but shDcn knockdown affected the material properties in the absence of mechanical stimulation.

shColVI Mechanical Properties shDcn Mechanical Properties

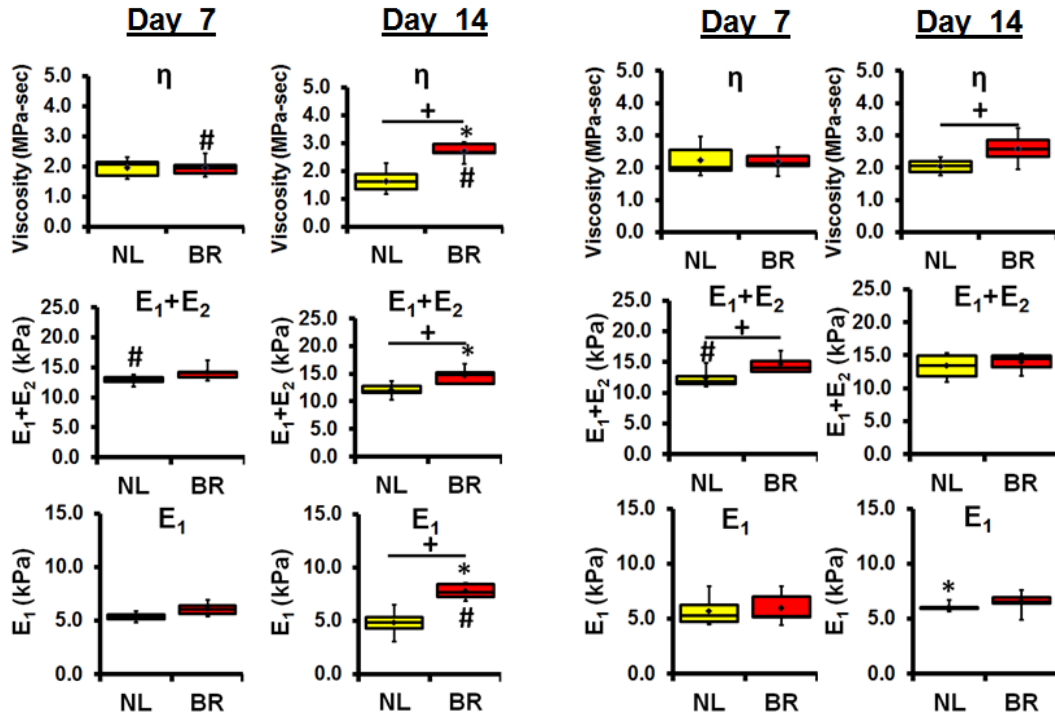


Fig. 6.9: Mechanical properties of shColVI-, and shDcn- transduced cell alginate disks in either static (NL) or bioreactor (BR) culture for 7 or 14 days. Viscosity (η), instantaneous (E_1+E_2) stiffness, and steady-state (E_1) stiffness were affected in all shColVI samples at day 14. Viscosity was affected in shDcn samples at day 14. All properties were determined using displacement controlled stress-relaxation tests with 10% strain applied at 0.05%/second, which was maintained for 1000 seconds. Stress and strain calculations were determined from the force and displacement data collected. Mechanical properties were determined from standard linear solid model: $\sigma = E_1 * \varepsilon_0 * e^{-\frac{E_1 t}{\eta}} + E_2 * \varepsilon_0$. (#:p<0.05 from GM samples at each time point; *:p<0.05 from CM & GFP at each time point; +:p<0.05 between non-loaded to bioreactor cultured samples; n \geq 5 disks per sample).

6.3.6 Targeted PCM knockdown had a greater effect on gene expression than dynamic compressive culture

Knockdown samples showed varied regulation over gene expression under non-loaded and dynamic culture conditions. In both knockdown samples, *adamts4* expression was higher in knockdown samples than all other conditions and continuously decreased with culture and dynamic loading. This expression profile was only seen in knockdown samples. *Adamts4* and *fgf2* expression profiles were opposite and potentially antagonistic in shColVI samples. *Fgf2* expression was similar in non-loaded knockdown samples at day 7, but shColVI samples showed an increase in expression under dynamic culture, which then increased with time. This same expression profile was seen in the GM samples (fig. 6.8). ShDcn knockdown samples did not show an *fgf2* responsiveness to bioreactor culture (fig. 6.10), maintaining levels from day 7 to day 14 under dynamic loading, which decreased over time in non-loaded conditions.

Acan and *bgn* expression were both slightly increased under load in shColVI samples at day 7 and then significantly lower at day 14. *Acan* expression was lower at all time points in ColVI knockdown samples than all other conditions which continued to decrease expression at day 14, which wasn't recovered by dynamic stimulation. *Comp* levels were lower in ColVI than all other chondrogenic samples, and decreased over the 14 days resulting in significantly lower expression.

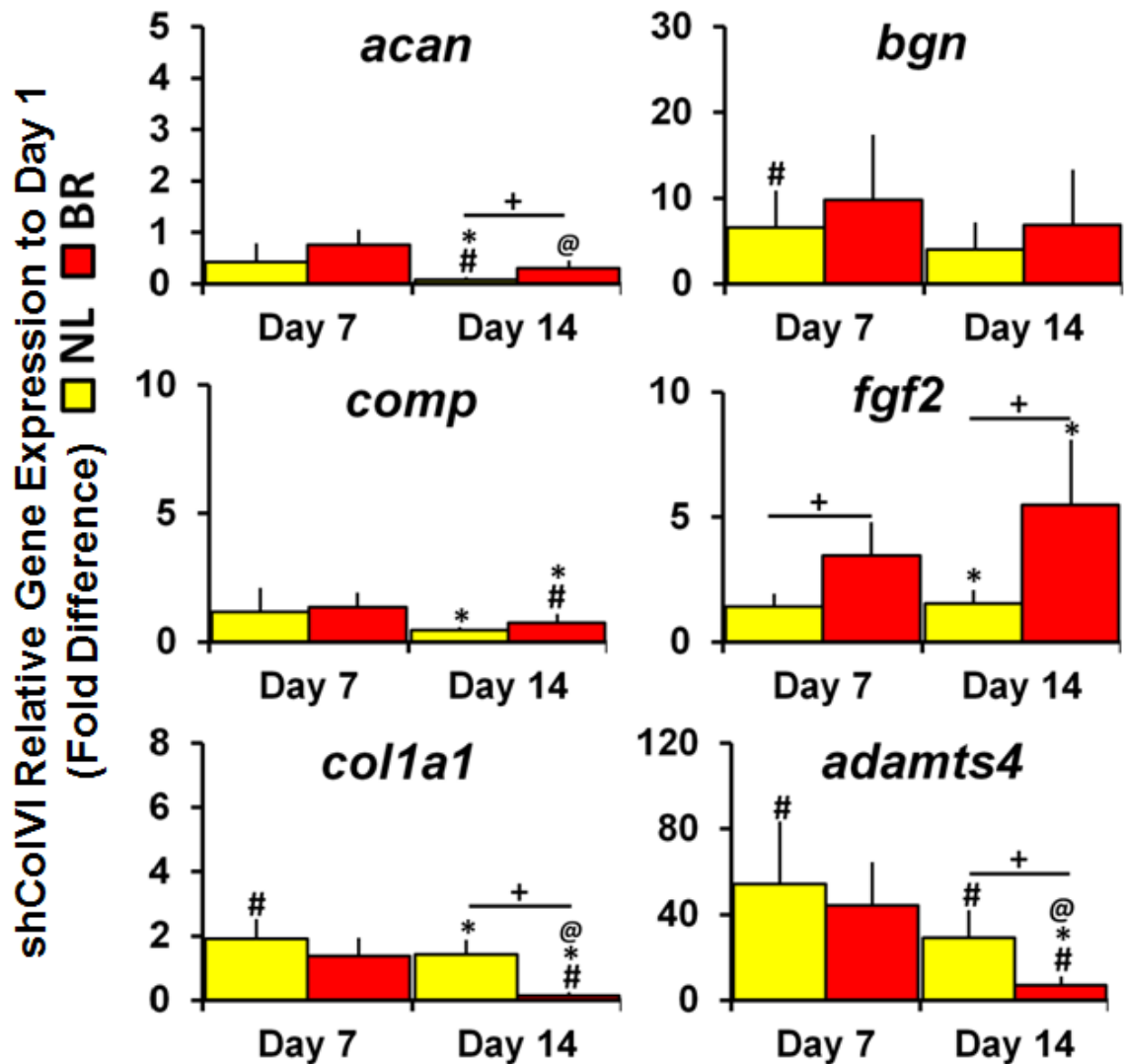


Fig. 6.10: Relative *comp*, *acan*, *bgn*, *col1a1*, *fgf2*, and *adamts4* gene expression (fold difference) of day 7 and day 14 shColVI- transduced cells in non-loaded (yellow) and bioreactor (red) culture to day 1 cultures. (#:p<0.05 from GM samples at each time point; *:p<0.05 from CM & GFP at each time point; +:p<0.05 between non-loaded to bioreactor cultured samples; @: p<0.05 between day 7 to day 14 culture; n≥3).

shDcn non-loaded samples showed a higher expression of *comp*, *acan*, *bgn*, and *col1a1* in non-loaded samples at day 7 that was returned to levels similar to chondrogenic non-infected and GFP-transduced cells. These levels were then significantly lower at day

14 than other samples, possibly due to the shift in peak levels during chondrogenic induction.

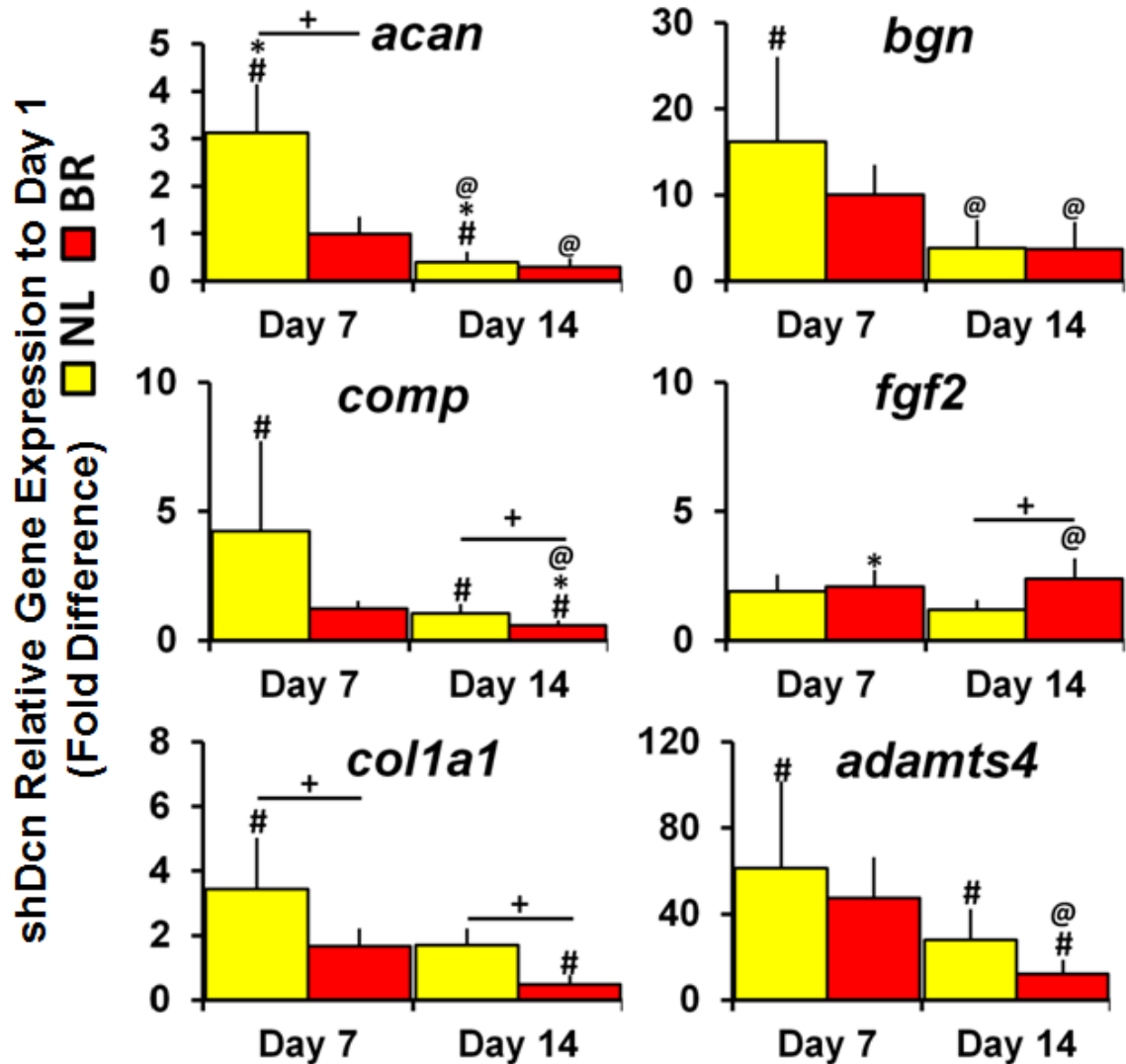


Fig. 6.11: Relative *comp*, *acan*, *bgn*, *col1a1*, *fgf2*, and *adamts4* gene expression (fold difference) of day 7 and day 14 shDcn- transduced cells in non-loaded (yellow) and bioreactor (red) culture to day 1 cultures. (#:p<0.05 from GM samples at each time point; *:p<0.05 from CM & GFP at each time point; +:p<0.05 between non-loaded to bioreactor cultured samples; @: p<0.05 between day 7 to day 14 culture; n≥3).

6.4 Discussion

Dynamic compression and chemical induction of chondrogenesis has shown complex regulation over gene expression, with combined stimulation inhibiting the rate of differentiation and the accumulation of GAG and collagens (14,54,55) compared to growth factor or compressive culture alone. Matrix development will shift the deformability of chondrogenic hMSCs, changing the means through which cells perceive mechanical stress. Regenerative therapies seek to include dynamic culture to improve material properties (44), increase matrix homogeneity, activate endogenous TGF release (65,138), and collagen synthesis (14,44,52) caused not only by direct mechanical compression, but increased fluid shear and nutrient delivery (13,138,139).

We have previously seen that altering individual proteins within the PCM has implications on the accumulation and organization of elaborated matrix during chondrogenesis (113). ColVI and DCN knockdown causes a change in proteoglycan expression, deformability under applied compression (113), and cytoskeletal responses to loading. In the present study, we examined the contribution of type VI collagen and decorin in gene expression and scaffold mechanical properties under dynamic culture. Changing the elaboration of the matrix will cause a shift in macroscopic scaffold properties as well as the micromechanical properties of the PCM. This study demonstrates a means to engineer a scaffold's material properties through control over individual proteins as well as elucidating the relationship between ColVI and DCN and cellular responses to dynamic stimulation.

One of the major findings of this study was the competing expression levels between non-loaded and dynamic culture in shDcn knockdown samples. DCN knockdown caused

a large upregulation of chondrogenic markers at day 7 which was inhibited under bioreactor culture. This stimulation of chondrogenic markers was only specific to proteoglycan and *comp*, unaffected *col2a1* expression. DCN is known to sequester TGF- β (3,21,62), controlling the growth factor availability to the differentiating cell. Lack of regulation and the self-promoting activation of COMP will increase chondrogenic markers directly stimulated by TGF- β 3 (107). COMP is activated by TGF- β and is self stimulated through binding and presenting the growth factor back to the cell membrane (4,128). *Comp* is also upregulated in mechanically loaded chondrocytes when in the presence of TGF- β (107,128). *Comp* over expression in DCN knockdown samples has previously shown inhibition by transient loading during the matrix organization phase of chondrogenesis. The direct control that DCN has over *comp* expression is either inhibited by the changing environment during mechanical stimulation or by a competing pathway during the first 7 days of chondrogenesis.

The mechanical stimulation of certain genes was shown to be dependent on chondrogenic induction or PCM development (55). Growth media samples showed drastic upregulations of *adamts4*, *fgf2*, *bgn*, and *comp* expression at both time points under dynamic culture, which was only seen in shColVI samples for *bgn* and *fgf2*. GM and shColVI samples both lack the ability to maintain a round cell shape under applied compression which directly impacted actin microfilament dynamics and organization in response to load (113). *Fgf2* expression therefore may be directly dependent on cell shape changes during loading. FGF-2 has conflicting results during chondrogenic culture, showing an inhibitive (132) or enhanced (3,131,140) affect on chondrogenesis (130), which is not currently linked directly to ColVI accumulation. FGF-2 is released from the

heparin sulfate GAG chains of perlecan during dynamic loading, directly stimulating the cell membrane (129,130), and has been shown to suppress enzymatic activity of A Disintegrin And Metalloproteinase with Thrombospondin Motifs-5 (ADAMT5) (131). The potential relationship between FGF2 and ADAMTS4 has not been explored. Altering the components of the PCM showed an increase in *adamts4* expression in non-loaded knockdown samples, which was then decreased with loading. Balancing anabolic and catabolic reactions in response to dynamic loading is imperative in maintaining a healthy PCM and ECM during chondrogenesis and scaffold maturation. When this balance is shifted catabolically, as seen in osteoarthritic or hypertrophic chondrocytes, with increases in metalloproteinase-2 (MMP-2) (30), tissue inhibitors of metalloproteinases-2 (TIMP-2) (30,31), MMP-7 (31), MMP-13, ADAMTS-4, and ADAMTS5, there will be a biochemical and biomechanical breakdown of the matrix (27,28,123).

Matrix elaboration within the hydrogel will directly shift the scaffold's bulk material properties, with increases in stiffness directly corresponding to increases in GAG (66,141) and collagen (142) synthesis. Material properties were determined to be directly related to matrix synthesis due to GM samples remaining unchanged with respect to duration and compressive culture. Chondrogenic culture maintained a steady level of *acan*, *bgn*, and *coll1a1* expression over the 14 days of chondrogenic culture in non-loaded samples, during which matrix elaboration caused a decrease in overall mechanical properties, contrary to what we expected. The bulk viscosity of the disc decreased with chondrogenic culture, resulting in lower material property levels than GM samples. Matrix synthesis and aggregation will also increase enzymatic activity, possibly expediting the breakdown of the scaffold. Steady state stiffness increased with dynamic

loading possibly due to a more homogenous matrix distribution and higher collagen content throughout the disk, which was also seen in shColVI samples (55). Instantaneous stiffness and viscosity parameters were similar in loaded and non-loaded samples, due to similar matrix expression levels. Fluid pressure within hydrogels are a large contributor to the instantaneous stiffness (44). Previous studies examining scaffold properties during chondrocyte culture has shown peak equilibrium moduli (44) and GAG content (44) after 2 weeks of culture.

PCM development in cartilage demonstrates an increase in elastic behavior (5), with alterations in ColVI content significantly decreasing these material properties. The alteration of the PCM by targeted protein knockdown will directly affect the biphasic viscoelastic behavior of the PCM (5,19), with the lack of organization affecting the compaction and release of the matrix following load. ColVI knockdown causes a decrease in proteoglycan content (113), together altering the overall biophysical microenvironment surrounding chondrogenic hMSCs. Knockdown effects on mechanical behavior disparities between loaded and non-loaded culture of the cell-seeded alginate discs were only observed after 14 days. ColVI knockdown in conjunction with dynamic stimulation increased all material properties under bioreactor culture, contrary to expected results. While the transcriptional regulation of *coll1a1* was not increased in shColVI samples, the knockdown could also be causing a more osteoarthritic matrix development (5). The increase in viscosity was increased potentially due to the looser matrix and higher catabolic reactions. Osteoarthritic breakdown of proteoglycans causes a decrease in matrix organization and an increase in overall PCM and cell volume, with type VI collagen lacking organization and increasing radial distance from the cell (1).

Dynamic stimulation has improved GAG synthesis, but may not improve GAG retention within the scaffold (97) depending on the initial elaboration of the matrix. The change in material property in knockdown samples may be due to an elevated enzymatic activity of ADAMTS4, which was highly expressed in knockdown samples relative to CM and GFP. ShDcn samples resulted in higher instantaneous and steady state stiffness parameters in non-loaded samples compared to CM, GFP, and shColVI samples. The increase in matrix properties will correspond to the higher COMP levels (143), which increases cross-linking of PCM proteins.

The inhomogeneous material properties in hydrogel scaffolds during dynamic loading may be enhanced in knockdown samples causing the shift in mechanical composition (142). Dynamic loading has a much more significant effect on the bulk material properties of the scaffolds following two weeks of culture, therefore a longer culture duration may reveal a greater disparity in the material property differences caused by these two proteins (142). These measurements were determined to be an order of magnitude lower than observed elastic moduli of the pericellular matrix surrounding chondrocytes (81,144). Cell-seeding density directly relates to matrix elaboration and mechanical property improvements (43), therefore a more accurate determination of matrix properties should be determined through a higher cell-seeding density.

Altering the composition of the PCM increases the compressive strains applied to the cell (113). The shifting mechanotransduction events due to this change in deformability caused significant changes in gene expression in knockdown samples, with a direct relationship determined between ColVI and *fgf2* expression. To form a functional tissue engineering construct for articular cartilage repair, a more thorough understanding of the

relationship between scaffold material properties, biochemical composition, and the effects of dynamic stimulation is needed. The PCM demonstrates very specific mechanical properties that are frequency dependent (42), due to fluid flow within the PCM or to its biphasic behavior (19). The exact mechanism through which these proteins are affecting the overall scaffold material properties needs to be further explored through immunohistochemical analysis.

Dynamic stimulation has been seen to improve matrix elaboration (55), sGAG synthesis (44), and collagen production (14,52), to closer mimic native cartilage properties. Development of a full PCM enhances the chondrogenic phenotype when dynamically stimulated (39,55,145), but this is highly dependent on cell-seeding density(142), application of TGF- β 3(45), and method of loading (13,14,51,52,97,108,138,142). These parameters determine the maintenance of a chondrogenic phenotype, with synthesis of type II collagen and sGAG production, versus a more hypertrophic phenotype, increasing type I and X collagen expression (54,55,138). Exploring the roles of biochemical and biomechanical induction of chondrogenesis is important and determining the exact role of PCM proteins in these two mechanisms could further regenerative medicine for articular cartilage. Studies have demonstrated that a fully elaborated matrix prior to dynamic loading will enhance chondrogenic markers and matrix elaboration(55) within hydrogel culture. To determine the contribution of type VI collagen and decorin in mechanotransduction events following matrix elaboration, future experiments are planned to pre-culture samples for two weeks to allow a PCM to form before dynamic mechanical culture.

6.5 Conclusions

Type VI collagen and decorin are highly involved in pericellular matrix elaboration and directly control mechanotransduction events. ColVI demonstrated a direct relationship to *fgf2* expression, which has not been previously seen, and DCN control over *comp* expression was further revealed through the direct overexpression mechanism seen in unloaded samples. The shifts in gene expression caused a surprising effect on the overall biomechanical properties of the cell-seeded alginate scaffolds. This study not only demonstrates the ability to control the cell's biological response to dynamic stimulation through targeted knockdown, but the ability to engineer the overall bulk material properties through direct control over individual PCM proteins. Further studies are needed to thoroughly examine the mechanism through which ColVI and DCN knockdown are causing these disparities in material properties in long term dynamic compressive culture.

Chapter 7: Conclusions and Future Work

The overall aim of this work was to determine the method through which differentiating human mesenchymal stem cells sense their microenvironment to potentially control chondrogenic mechanotransduction events. The exact method through which mechanical stimulation is perceived is difficult to determine due to the temporally changing micromechanical environment. We sought to elucidate the contribution of type VI collagen and decorin in cellular biophysics, cytoskeletal dynamics, and mechanotransduction events (fig. 7.1). Understanding the relationship between pericellular matrix proteins and the cell's gene expression response to mechanical stress is necessary for advancing tissue engineering and regenerative strategies for articular cartilage repair.

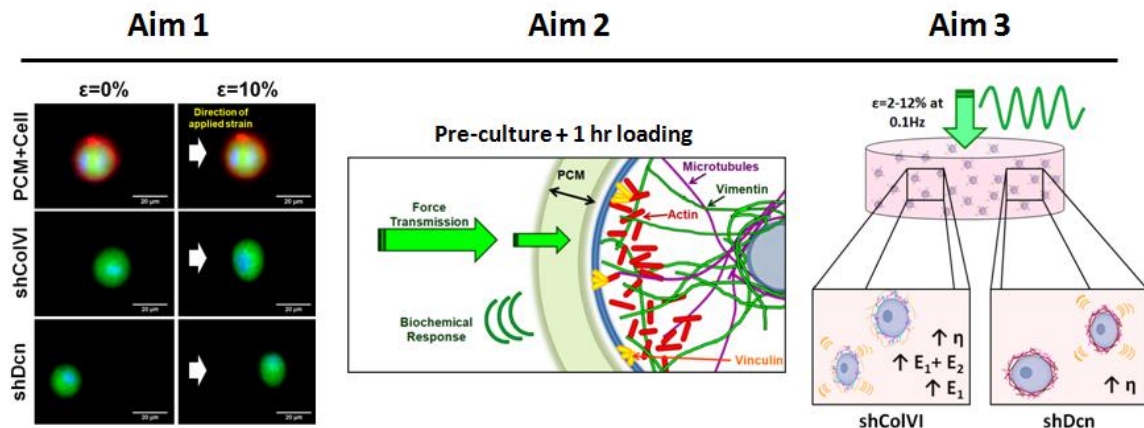


Fig. 7.1: Schematic outlining the overall goals of the three aims within this dissertation work. Aim 1 analyzed the biophysical contribution of ColVI and DCN, Aim 2 analyzed mechanosignaling gene expression and cytoskeletal kinetics following applied load, and Aim 3 analyzed mechanical property and gene expression differences between knockdown and control samples under long term sinusoidal unconfined compression.

Type VI collagen and decorin are necessary to maintain healthy cartilage (5,76,146) and a chondrogenic phenotype. ColVI knockout mice have shown increased OA

phenotype (5), more likely through control over the anabolic and catabolic biological responses of chondrocytes to mechanical stress than a breakdown of the tissue mechanical properties. ColVI knockout models showed an increase in articular cartilage fibrillation and a reduction in PCM strength. We wanted to analyze how ColVI was involved in maintaining the chondrocyte-like phenotype during chondrogenesis and *in vitro* culture to understand how this protein could be involved in OA development. Decorin is known to control ColVI microfibrillar organization (17,59,62,147) and growth factor sequestration within the PCM (62,87,105), assembling the PCM to maintain the chondrocyte-phenotype. Currently knockout models for decorin do not analyze the contribution of this proteoglycan in cartilage OA development or cartilage degradation. This thesis wanted to further explore how DCN is involved in the chondrogenic phenotype, not only to analyze how DCN is involved in cartilage maintenance, but how this protein could be used in therapeutic therapies.

We first examined the effects of targeted knockdown of ColVI and DCN on chondrogenic differentiation of hMSCs, PCM gene expression, and the biophysical response to applied strain. These were determined using gene expression analysis through qRT-PCR, immunofluorescence microscopy, western blotting, and cellular deformation analysis under uniaxial unconfined static application of strain. Targeted knockdown was optimized and achieved as verified by a significant reduction in mRNA and protein expression of ColVI and DCN. Knockdown samples still successfully differentiated, with chondrogenic marker upregulation, but knockdown of ColVI and DCN caused a varying expression level from chondrogenic controls. Knockdown of ColVI caused a downregulation while knockdown of DCN caused an upregulation of *acan* and *bgn*. This

downregulation of proteoglycan gene expression within ColVI knockdown samples could lead to the hypertrophic phenotype seen within OA knockout models (5,19,81). Aggrecan and biglycan are vital proteoglycans within PCM assembly. These alterations of the PCM composition caused a shift in the biophysical response, with ColVI deficient PCMs completely lacking the structural integrity to resist applied strain. DCN knockdown samples produced a strain dependent deformability under load potentially due to the increased GAG content or decreased collagen organization. **The PCM with ColVI and DCN knockdown differ in their ability to resist applied deformation, demonstrating the difference in their contribution to the biophysical environment.**

Knowing that ColVI and DCN directly changed the deformability of the cell, mechanosignaling changes were determined. ColVI and DCN knockdown directly inhibited a dynamic response of α -actin and vimentin intermediate filaments following load. The cytoskeleton of chondrogenic hMSCs is highly reactive to mechanical stimulation transducing mechanical signals from the cell membrane to the nucleus. ColVI and DCN knockdown arrested this response by activating a higher AMF and VIF concentration in free-swelling conditions. The cytoskeleton will protect the cell from destructive loading, causing cellular stiffening to prevent injurious deformation. ColVI knockdown also demonstrated a direct relationship to *fgf2* expression, which has not been previously seen. We propose *fgf2* expression is stimulated through cellular deformability. DCN knockdown also demonstrated a lack of TGF- β regulation, which caused the increased chondrogenic markers from aim 1, but also significant overexpression of *comp*. The TGF signaling pathway is activated through both biochemical and biomechanical means, which were shown to antagonistically compete in

shDcn samples. Currently the direct relationship between decorin and endogenous TGF- β secretion is unknown and being examined, but my work demonstrates the potential for decorin regulation over the TGF signaling pathway. **The direct of *fgf2* expression in ColVI knockdown samples and of *comp* expression in DCN knockdown samples demonstrate the ability to control downstream gene expression by altering the PCM.**

To fully determine the relationship between these PCM proteins and their effects on cellular metabolic maintenance of the structural environment during load, gene expression and scaffold material properties of cells undergoing chondrogenic induction and long term mechanical culture were determined. Targeted knockdown of ColVI and DCN further enhanced the previously seen relationships between ColVI and *fgf2* and DCN and *comp* expression. FGF2 could provide an additional pathway of chondrogenic stimulation, through increased cellular deformation. FGF2 is a highly studied protein (94,131), whose exact role in mechanotransduction has yet to be determined. ColVI knockdown also increased *adamts4* expression. OA rat models display an increase in proteoglycan fragments throughout articular cartilage, with an increase in enzymatic activity (106,148). The fibrillation and OA progression in ColVI knockout models (5) maybe due to the increased enzymatic gene expression seen in this study. The overstimulation of TGF- β in non-loaded shDcn samples caused significant upregulation of chondrogenic and hypertrophic genes, demonstrating an increased terminal differentiation. This advancement towards hypertrophy may be inhibited under dynamic stimulation, with dynamic loading reducing the over expression of chondrogenic markers. Decorin is known to sequester TGF- β through its CS/DS side chain, which also organizes

and binds collagen molecules together (62), but the effect of decorin knockdown hasn't been examined on TGF signaling.

The effect of targeted knockdown on the material properties of cell-seeded alginate scaffolds was contrary to what I expected, with knockdown and dynamic stimulation significantly increasing the bulk viscosity parameter. Decorin controls the fibrillogenesis of collagens, therefore controlling the mechanical properties of the PCM (149). The PCM with DCN knockdown will accumulate more CS/DS and increase the binding capabilities of biglycan, which requires two GAG side chains. The increased GAG side chains within the PCM will cause an increase in spacing and water content, causing this increase in mechanical properties, as opposed to the lack of core protein which hasn't shown an impact on the mechanical properties of cartilage (149). The exact means through which ColVI and DCN are affecting the material properties needs to be further examined, to understand how the proteins are affecting the matrix elaboration and homogeneity throughout the scaffold. While, the means through which these material properties were created need to be determined, **we demonstrated that the overall scaffold biomechanical composition can be specifically engineered through targeted subtraction of PCM proteins.**

The exact decoupling of the roles of these proteins in mechanotransduction events is difficult to determine due to the constantly changing physicochemical environment during differentiation. These studies taken together, demonstrate the affect of individual proteins on the overall accumulation and organization of matrix directly impacting cellular mechanoresponsiveness. We have also demonstrated the ability to determine the

functional roles of specific proteins at varying points of chondrogenesis and mechanosensing capabilities using RNAi.

Further work is needed to further clarify the mechanisms through which mechanotransduction events are activated. To isolate the means through which ColVI and DCN are involved in the mechanosignaling cascade, comparison studies should be developed to determine the roles of these proteins in cellular mechanosensing in an unaltered pericellular matrix. Comparing the shift in gene expression will determine whether the alteration in proteoglycan and organizing protein expression is due to the direct contribution of these proteins or a compensatory developed PCM. Determination of the composition in an altered PCM is needed to fully explain the changing biomechanical properties. After examining the altered PCM in non-loaded and loaded samples, further analysis of the effect of dynamic compressive culture following the two week chondrogenic induction period should be examined. The involvement of DCN in TGF sequestration should be further studied. Hypertrophic differentiation of chondrogenic hMSCs is potentially due to overstimulation from growth factors, creating a difficult means to maintain a chondrocyte-like phenotype *in vitro*. Using sLRPs to control growth factor stimulation of the cell could potentially help maintain phenotype within tissue engineered scaffolds for articular cartilage.

Establishing the ability to specifically engineer the micromechanical and therefore the macroscale cell-scaffold biomechanical properties through intrinsic cellular engineering provides the capabilities to engineer a stratified construct for articular cartilage tissue engineering. Articular cartilage demonstrates varying zones of extracellular matrix composition and mechanical characteristics, which are hard to mimic in tissue

engineering. Engineering the environment through cellular control and controlling the biological response to mechanical stimulation can potentially improve regenerative therapies for articular cartilage repair.

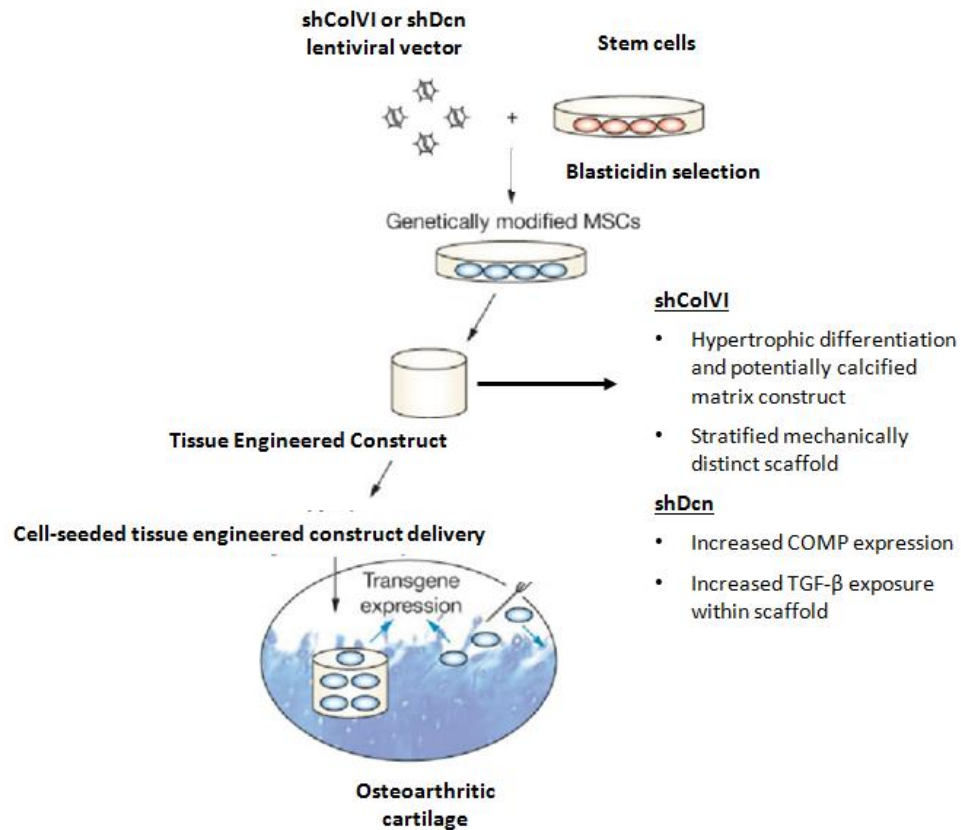


Fig. 7.2: Schematic of shRNA modified stem cells for tissue engineering. ShColVI and shDcn knockdown can be used for increased hypertrophic differentiation and TGF- β exposure.(As adapted from Noth, U, 2008 (2)).

The overall goal of tissue engineering for articular cartilage repair aims to maintain chondrogenic phenotype within the TEC and to mimic the physiologic environment at the implantation site. Continuous exposure to TGF- β improves chondrogenic phenotype stability and has been achieved through both cell viral transduction with TGF expression vectors (150), pharmacologically active microcarriers (151), or scaffolds embedded with TGF- β release mechanisms (152). These methods have improved chondrogenic marker

expression to maintain chondrogenic phenotype. Our research offers a different approach to controlling TGF- β exposure by adjusting the microenvironment around the cell to allow a higher concentration of TGF- β to reach the cell. DCN knockdown can be used to improve scaffold maturation of TEC by increased PG and collagen synthesis prior to implantation (fig. 7.2) . The increase in growth factor stimulation and improved matrix synthesis will aid in scaffold incorporation into focal defect sites during osteoarthritis.

Scaffold incorporation also should mimic the physiological mechanical characteristics of the tissue, with scaffold stratification improving the mechanical force transmission to each of the layers (fig. 7.2 and fig. 7.3). Stratification procedures currently adjust the TEC to mimic the different mechanical characteristics of the cartilage (153), but using shRNA lentiviral vectors can adjust the microenvironment in layers through cellular engineering (fig. 7.3). Cartilage displays depth dependent increases in tissue stiffness and zonal specificity for collagen and proteoglycan composition (40). The work presented in this thesis provides analysis at the functional roles of type VI collagen and decorin during chondrogenesis and mechanotransduction as well as the ability to engineer scaffold zonal properties of articular cartilage.

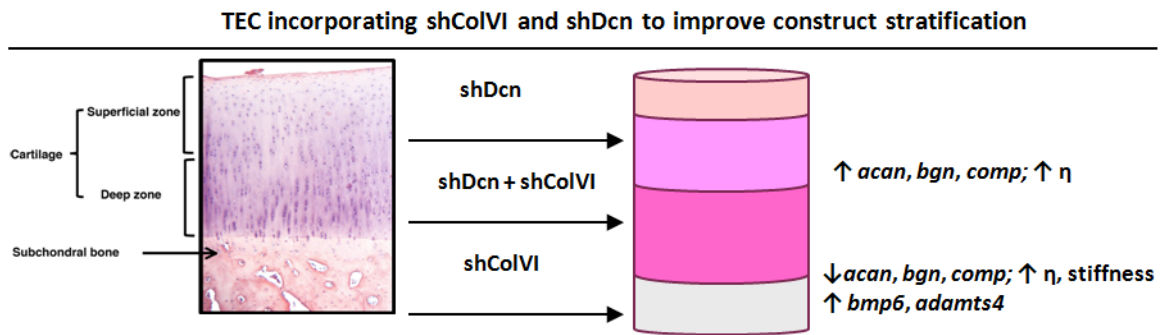


Fig. 7.3: Stratification strategy using shColVI and shDcn knockdown chondrocyte-like cells. Different composition and mechanical properties can be achieved through layering different knockdown populations within a TEC. (As adapted from Tat, SK, 2009 (9)).

Chapter 8: List of Abbreviations

ACAN- Aggrecan

AC-Articular cartilage

ADAMTS- A Disintegrin And Metalloproteinase with Thrombospondin Motifs

AMFs- Actin microfilaments

ANOVA- Analysis of variance

AR- Aspect ratio

BGN- Biglycan

BMP- Bone morphogenic protein

CM- Chondrogenic media

CMFDA- 5-chloromethylfluorescein diacetate

ColVI- Type VI collagen

COMP- Cartilage oligomeric matrix protein

CS/ DS- Chondroitin sulfate/ dermatan sulfate

CTCF- Corrected total cell fluorescence

DAPI- 4',6-diamidino-2-phenylindole

DCN- Decorin

DMEM- Dulbecco's modified eagle's medium

dsRNA- Double stranded RNA

ECM- Extracellular matrix

EthD-1- Ethidium homodimer

FBS- Fetal bovine serum

FGF- Fibroblast growth factor

FS- Free swelling

GAG- Glycosaminoglycan

GFP- Green fluorescent protein

GM- Growth media

HA- Hyaluronic acid

hMSCs- Human mesenchymal stem cells

IGF- Insulin growth factor

IL- Interleukin

MAPK- Mitogen-activated protein kinases

MMP- Matrix metalloproteinase

MOI- Multiplicity of infection

MT- Microtubules

NAR- Normalized aspect ratio

NT- Nucleotide

OA- Osteoarthritis

PCM- Pericellular matrix

PDGF- Platelet derived growth factor

PGs- Proteoglycans

qRT-PCR- Quantitative reverse-transcriptase polymerase chain reaction

RISC- RNA induced silencing complex

RNAi- RNA interference

SEM- Standard error of the mean

shColVI- shRNA virus targeting *col6a1*

shDCN-shRNA virus targeting *dcn*

shRNA- Short hairpin RNA

siRNA- Small interfering RNAs

sLRPG- Small leucine rich proteoglycan

TEC- Tissue engineered construct

TGF- Transforming growth factor

TNF- Tumor necrosis factor

TU- Titering units

VEGF- Vascular endothelial growth factor

VIFs- Vimentin intermediate filaments

Appendix A: PCR Amplification efficiencies of qRT-PCR primers created

gene	PCR Amplification Efficiency (%)	R ²
<i>18s</i>	111.391	R ² = 0.9901
<i>acan</i>	94.443	R ² = 0.998
<i>adamts4</i>	117.701	R ² = 0.9922
<i>adamts5</i>	102.704	R ² = 0.9588
<i>bgn</i>	95.952	R ² = 0.9925
<i>bmp6</i>	132.320	R ² = 0.9999
<i>colla1</i>	89.766	R ² = 0.9983
<i>col6a1</i>	99.260	R ² = 0.9949
<i>col6a2</i>	95.695	R ² = 0.9981
<i>col6a3</i>	91.209	R ² = 0.9945
<i>col9a2</i>	101.487	R ² = 0.9991
<i>comp</i>	89.429	R ² = 0.9951
<i>dcn</i>	108.157	R ² = 0.9948
<i>fgf2</i>	102.704	R ² = 0.9715
<i>gapdh</i>	98.363	R ² = 0.9966
<i>mmp13</i>	86.513	R ² = 0.978
<i>rhoa1</i>	114.497	R ² = 0.9911
<i>runx2</i>	104.487	R ² = 0.9983
<i>sox9</i>	106.101	R ² = 0.994
<i>vim</i>	91.951	R ² = 0.9964

Table A.1: qRT-PCR amplification efficiencies determined through serial cDNA compared to relative threshold count.

Efficiency is determined from the slope of the log(cDNA concentration) versus the Ct value achieved by the MyIQ Biorad qRT-PCR reaction. From the linear regression line, the efficiency of each primer is determined using: $E=(10^{(-1/\text{slope})}-1)*100\%$. Primers are considered to be efficient if they fall within the range of 89.5%-110.1%.

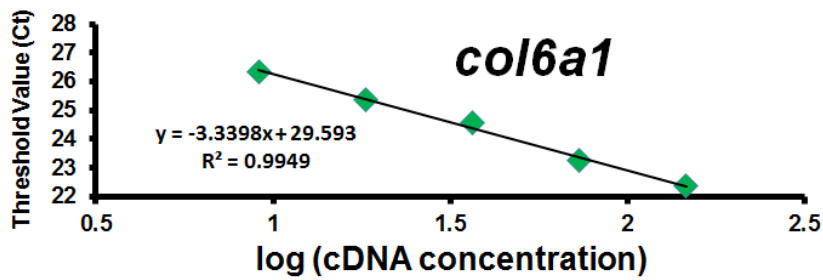


Fig. A-1: Representative figure determining primer efficiency of *col6a1*. The log of the concentration is plotted against the threshold value achieved at each concentration.

Appendix B: Compiled Computer Aided Design of custom designed unconfined compression bioreactor

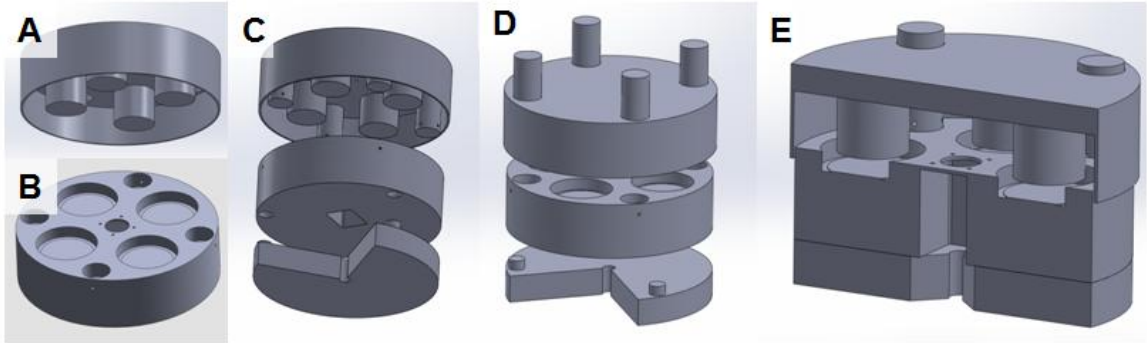


Fig. A-2: (A) Lid and (B) base of custom designed unconfined compressive bioreactor. Individual petri dishes are placed within each culture well of the bioreactor. The base and lid are concentrically placed on top of each other (C), with the Zaber linear actuator attached through the middle of the bioreactor. The lid's position is maintained by posts (D) to maintain the concentric position of the plungers above each culture well. A side view of the plungers located above the culture wells are seen in (E).

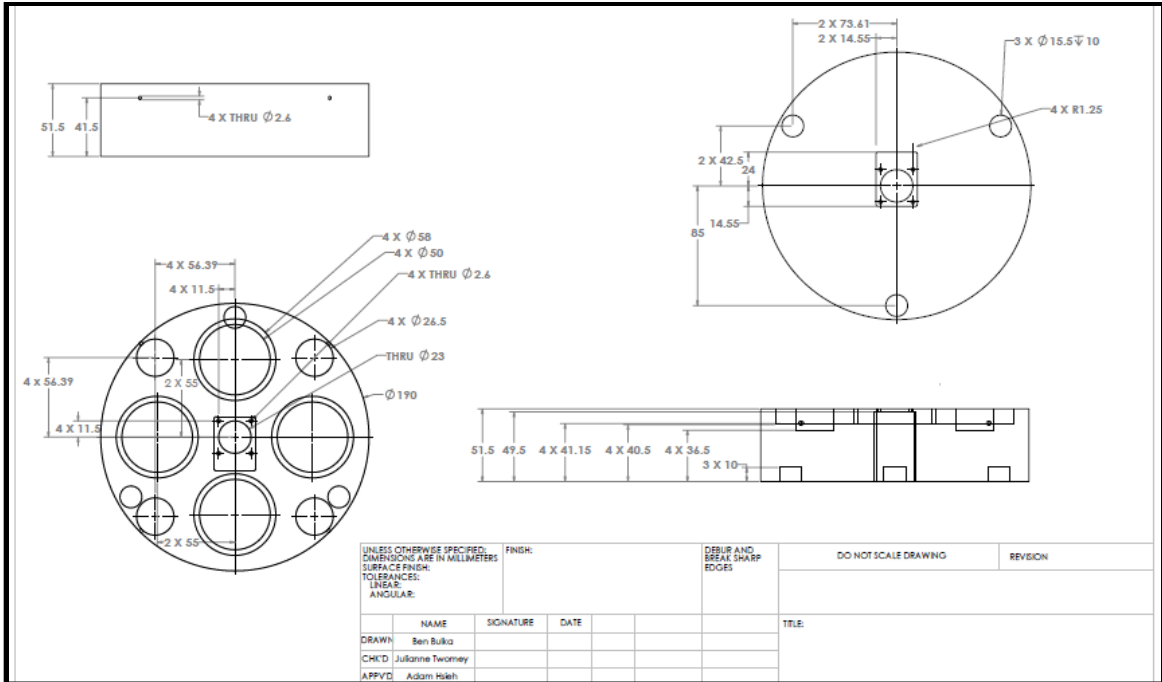


Fig. A-3: Engineering drawing of bioreactor base. Drawings shown are the top, bottom, and side views. Dimensions are in millimeters. All drawings were created using SolidWorks (created by Ben A. Bulka).

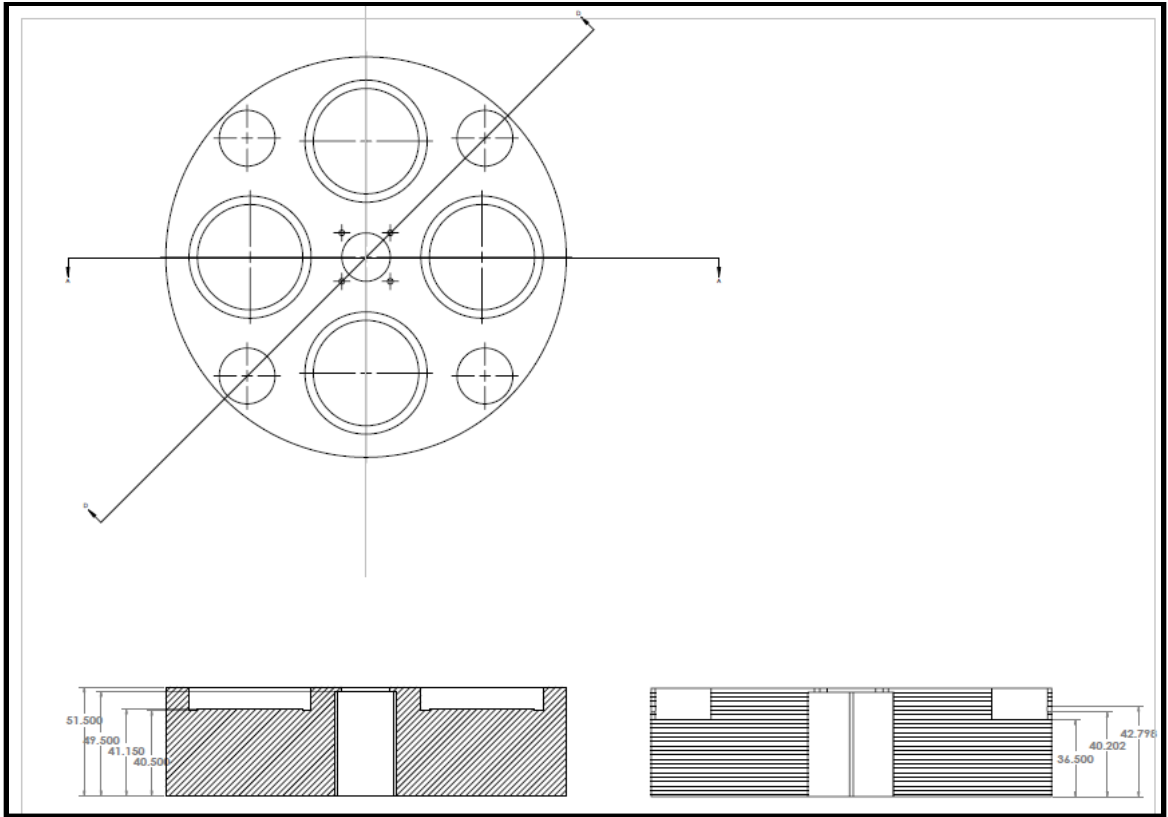


Fig. A-4: Engineering drawing of bioreactor base. Views shown are the top and cross-sectional as noted. Dimensions are in millimeters. All drawings were created using SolidWorks (created by Ben A. Bulka).

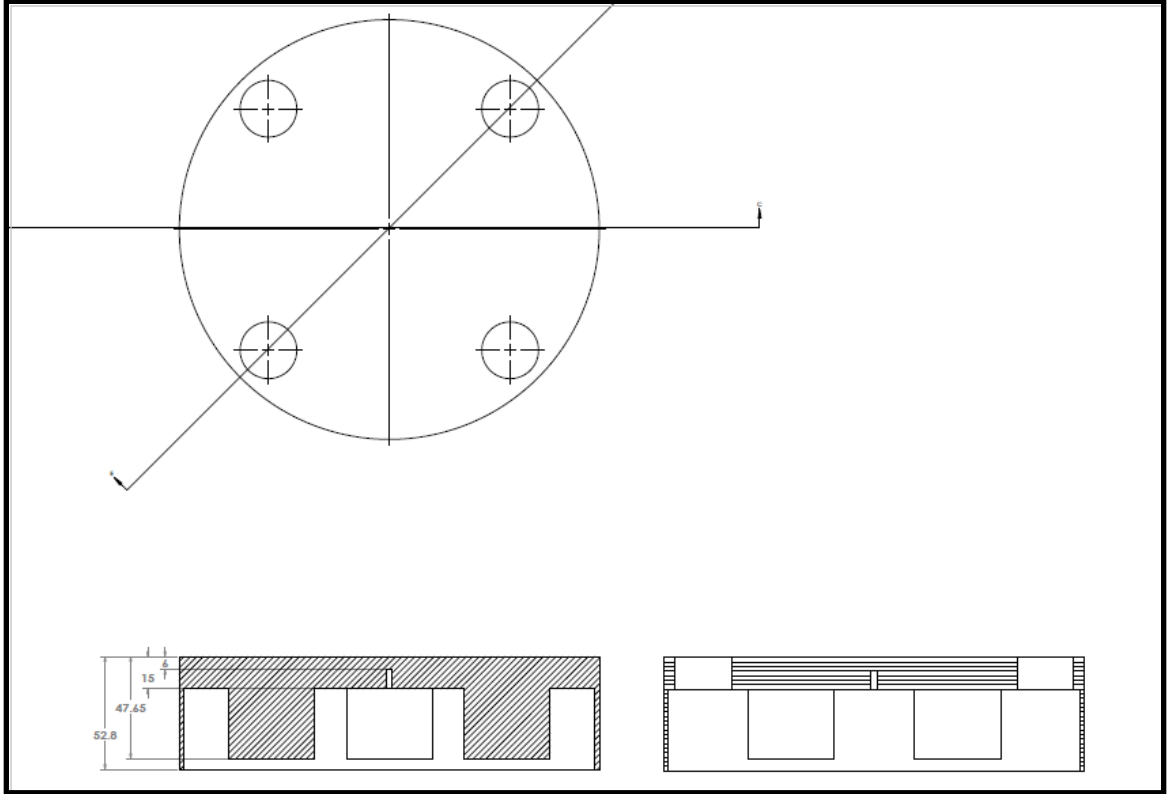


Fig. A-5: Engineering drawing of bioreactor lid. Views shown are top and cross-sectional cut as noted. Dimensions are in millimeters. All drawings were created using SolidWorks (created by Ben A. Bulka).

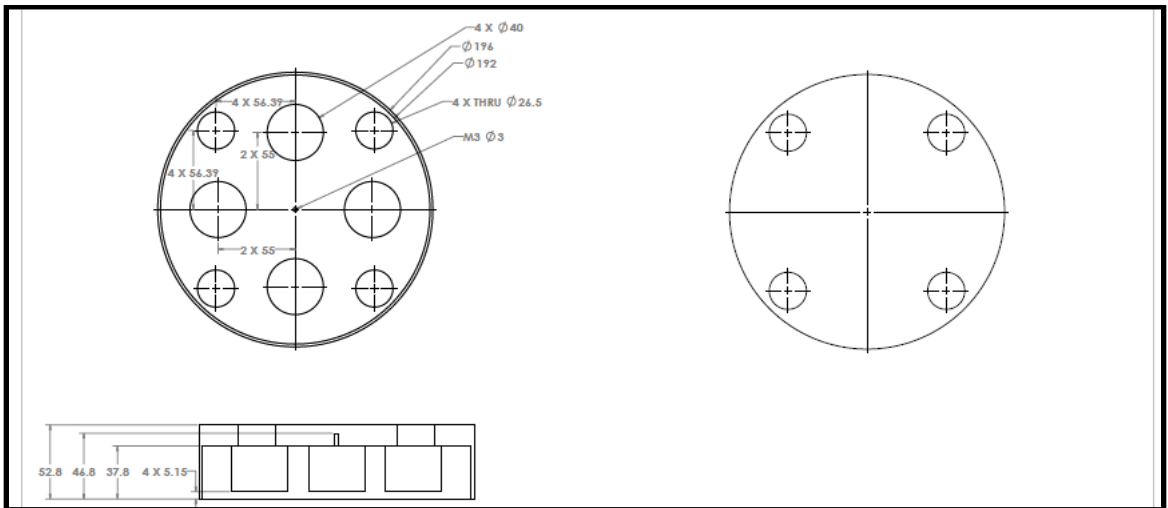


Fig. A-6: Engineering drawing of bioreactor lid. Views shown are bottom, top, and cross-sectional cut as noted. Dimensions are in millimeters. All drawings were created using SolidWorks (created by Ben A. Bulka).

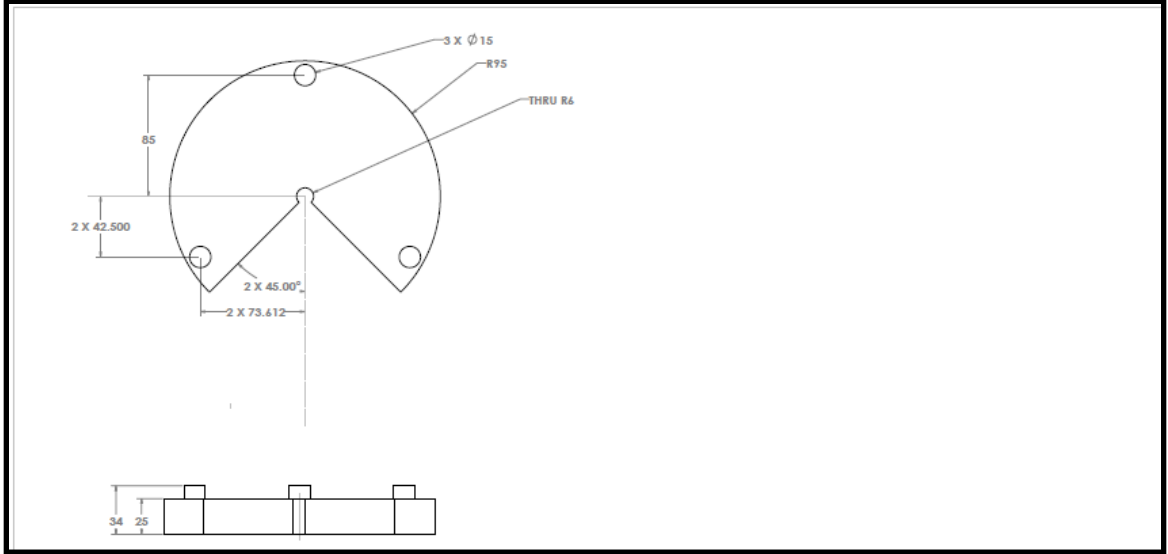


Fig. A-7: Engineering drawing of bioreactor base bottom. Views shown are top and side. Dimensions are in millimeters. All drawings were created using SolidWorks (created by Ben A. Bulka).

References

1. Wilusz, R. E., Zauscher, S., and Guilak, F. (2013) *Osteoarthritis Cartilage* **21**, 1895-1903
2. Noth, U., Steinert, A. F., and Tuan, R. S. (2008) *Nat. Clin. Pract. Rheumatol.* **4**, 371-380
3. Chen, W. H., Lai, M. T., Wu, A. T. H., Wu, C. C., Gelovani, J. G., Lin, C. T., Hung, S. C., Chiu, W. T., and Deng, W. P. (2009) *Arthritis Rheum.* **60**, 450-459
4. Xu, J. P., Wang, W., Ludeman, M., Cheng, K. V., Hayami, T., Lotz, J. C., and Kapila, S. (2008) *Tissue Eng. Part A* **14**, 667-680
5. Alexopoulos, L. G., Youn, I., Bonaldo, P., and Guilak, F. (2009) *Arthritis Rheum.* **60**, 771-779
6. Keene, D. R., Engvall, E., and Glanville, R. W. (1988) *J. Cell Biol.* **107**, 1995-2006
7. Hsieh, A. H., and Twomey, J. D. (2010) *J. Biomech.* **43**, 137-145
8. Rutz, S., and Scheffold, A. (2004) *Arthritis Research & Therapy* **6**, 78-85
9. Tat, S. K., Pelletier, J. P., Amiable, N., Boileau, C., Lavigne, M., and Martel-Pelletier, J. (2009) *Arthritis Research & Therapy* **11**
10. Brittberg, M., Lindahl, A., Nilsson, A., Ohlsson, C., Isaksson, O., and Peterson, L. (1994) *New England Journal of Medicine* **331**, 889-895
11. Mehlhorn, A. T., Schmal, H., Kaiser, S., Lepski, G., Finkenzeller, G., Stark, G. B., and Suekamp, N. P. (2006) *Tissue Eng.* **12**, 1393-1403
12. Kisiday, J. D., Frisbie, D. D., McIlwraith, C. W., and Grodzinsky, A. J. (2009) *Tissue Eng. Part A* **15**, 2817-2824
13. Steward, A. J., Wagner, D. R., and Kelly, D. J. (2013) *European Cells & Materials* **25**, 167-178
14. Angele, P., Schumann, D., Angele, M., Kinner, B., Englert, C., Hente, R., Fuchtmeier, B., Nerlich, M., Neumann, C., and Kujat, R. (2004) *Biorheology* **41**, 335-346

15. Wang, Z. H., Yang, Z. Q., He, X. J., Kamal, B. E., and Xing, Z. (2010) *Biotechnology and Bioengineering* **107**, 730-736
16. Choi, J. B., Youn, I., Cao, L., Leddy, H. A., Gilchrist, C. L., Setton, L. A., and Guilak, F. (2007) *J. Biomech.* **40**, 2596-2603
17. Connelly, J. T., Wilson, C. G., and Levenston, M. E. (2008) *Osteoarthritis Cartilage* **16**, 1092-1100
18. Vonk, L. A., Doulabi, B. Z., Huang, C. L., Helder, M. N., Everts, V., and Bank, R. A. (2010) *J. Cell. Biochem.* **110**, 260-271
19. Alexopoulos, L. G., Williams, G. M., Upton, M. L., Setton, L. A., and Guilak, F. (2005) *J. Biomech.* **38**, 509-517
20. DiMicco, M. A., Kisiday, J. D., Gong, H., and Grodzinsky, A. J. (2007) *Osteoarthritis Cartilage* **15**, 1207-1216
21. Zhang, Z. J., Jin, W., Beckett, J., Otto, T., and Moed, B. (2011) *Histochem. Cell Biol.* **136**, 153-162
22. Vigfusdottir, A. T., Pasrija, C., Thakore, P. I., Schmidt, R. B., and Hsieh, A. H. (2010) *Cell. Mol. Bioeng.* **3**, 387-397
23. Bollet, A. J., and Nance, J. L. (1966) *The Journal of Clinical Investigation* **45**, 1170-1177
24. Mankin, H. J. (1974) *New England Journal of Medicine* **291**, 1335-1340
25. Buckwalter, J. A., Mankin, H. J., and Grodzinsky, A. J. (2005) *Instructional course lectures* **54**, 465-480
26. Kleemann, R. U., Krockner, D., Cedraro, A., Tuischer, J., and Duda, G. N. (2005) *Osteoarthritis Cartilage* **13**, 958-963
27. Roach, H. I., Aigner, T., Soder, S., Haag, J., and Welkerling, H. (2007) *Current Drug Targets* **8**, 271-282
28. Lewis, J. L., Krawczak, D. A., Oegema, T. R., and Westendorf, J. J. (2010) *Connect. Tissue Res.* **51**, 159-170

29. Pritzker, K. P. H., Gay, S., Jimenez, S. A., Ostergaard, K., Pelletier, J. P., Revell, P. A., Salter, D., and van den Berg, W. B. (2006) *Osteoarthritis Cartilage* **14**, 13-29
30. Alam, M. R., Ji, J. R., Kim, M. S., and Kim, N. S. (2011) *Journal of Veterinary Science* **12**, 273-280
31. Ling, S. M., Patel, D. D., Garner, P., Zhan, M., Vaduganathan, M., Muller, D., Taub, D., Bathon, J. M., Hochberg, M., Abernethy, D. R., Metter, E. J., and Ferrucci, L. (2009) *Osteoarthritis Cartilage* **17**, 43-48
32. Kamm, J. L., Nixon, A. J., and Witte, T. H. (2010) *Equine Veterinary Journal* **42**, 693-699
33. Segal, N. A., Buckwalter, J. A., and Amendola, A. (2006) *Best Practice & Research in Clinical Rheumatology* **20**, 155-176
34. Steadman, J. R., Ramappa, A. J., Maxwell, R. B., and Briggs, K. K. (2007) *Arthroscopy-the Journal of Arthroscopic and Related Surgery* **23**, 948-955
35. Minas, T., and Peterson, L. (2000) *Operative Techniques in Sports Medicine* **8**, 144-157
36. Bartlett, W., Skinner, J. A., Gooding, C. R., Carrington, R. W. J., Flanagan, A. M., Briggs, T. W. R., and Bentley, G. (2005) *Journal of Bone and Joint Surgery-British Volume* **87B**, 640-645
37. Tallheden, T., Bengtsson, C., Brantsing, C., Sjogren-Jansson, E., Carlsson, L., Peterson, L., Brittberg, M., and Lindahl, A. (2005) *Arthritis Research & Therapy* **7**, R560-R568
38. Karlsson, C., Brantsing, C., Svensson, T., Brisby, H., Asp, J., Tallheden, T., and Lindahl, A. (2007) *J. Orthop. Res.* **25**, 152-163
39. Demarteau, O., Wendt, D., Braccini, A., Jakob, M., Schafer, D., Heberer, M., and Martin, I. (2003) *Biochemical and Biophysical Research Communications* **310**, 580-588
40. Coates, E. E., Riggin, C. N., and Fisher, J. P. (2012) *J. Orthop. Res.* **30**, 1886-1897
41. Bian, L., Zhai, D. Y., Mauck, R. L., and Burdick, J. A. (2011) *Tissue Eng. Part A* **17**, 1137-1145

42. Lee, B., Han, L., Frank, E. H., Chubinskaya, S., Ortiz, C., and Grodzinsky, A. J. (2010) *J. Biomech.* **43**, 469-476
43. Mauck, R. L., Seyhan, S. L., Ateshian, G. A., and Hung, C. T. (2002) *Ann. Biomed. Eng.* **30**, 1046-1056
44. Mauck, R. L., Soltz, M. A., Wang, C. C. B., Wong, D. D., Chao, P. H. G., Valhmu, W. B., Hung, C. T., and Ateshian, G. A. (2000) *J. Biomech. Eng.-Trans. ASME* **122**, 252-260
45. Lima, E. G., Bian, L., Ng, K. W., Mauck, R. L., Byers, B. A., Tuan, R. S., Ateshian, G. A., and Hung, C. T. (2007) *Osteoarthritis Cartilage* **15**, 1025-1033
46. Jung, H., Park, J. S., Yeom, J., Selvapalam, N., Park, K. M., Oh, K., Yang, J. A., Park, K. H., Hahn, S. K., and Kim, K. (2014) *Biomacromolecules* **15**, 707-714
47. Rosenzweig, D. H., Chicatun, F., Nazhat, S. N., and Quinn, T. M. (2013) *Acta biomaterialia* **9**, 9360-9369
48. Schuh, E., Kramer, J., Rohwedel, J., Notbohm, H., Muller, R., Gutschmann, T., and Rotter, N. (2010) *Tissue Eng. Part A* **16**, 1281-1290
49. Johnstone, B., Hering, T. M., Caplan, A. I., Goldberg, V. M., and Yoo, J. U. (1998) *Exp. Cell Res.* **238**, 265-272
50. Nelson, L., Fairclough, J., and Archer, C. W. (2010) *Expert Opinion on Biological Therapy* **10**, 43-55
51. Angele, P., Yoo, J. U., Smith, C., Mansour, J., Jepsen, K. J., Nerlich, M., and Johnstone, B. (2003) *J. Orthop. Res.* **21**, 451-457
52. Huang, C. Y. C., Hagar, K. L., Frost, L. E., Sun, Y. B., and Cheung, H. S. (2004) *Stem Cells* **22**, 313-323
53. Haudenschild, A. K., Hsieh, A. H., Kapila, S., and Lotz, J. C. (2009) *Ann. Biomed. Eng.* **37**, 492-502
54. Campbell, J. J., Lee, D. A., and Bader, D. L. (2006) *Biorheology* **43**, 455-470

55. Huang, A. H., Farrell, M. J., Kim, M., and Mauck, R. L. (2010) *European Cells & Materials* **19**, 72-85
56. Bruns, R. R., Press, W., Engvall, E., Timpl, R., and Gross, J. (1986) *J. Cell Biol.* **103**, 393-404
57. Guilak, F., Alexopoulos, L. G., Upton, M. L., Youn, I., Choi, J. B., Cao, L., Setton, L. A., and Haider, M. A. (2006) *Skeletal Development and Remodeling in Health, Disease, and Aging* **1068**, 498-512
58. Engvall, E., Hessel, H., and Klier, G. (1986) *J. Cell Biol.* **102**, 703-710
59. Bidanset, D. J., Guidry, C., Rosenberg, L. C., Choi, H. U., Timpl, R., and Hook, M. (1992) *J. Biol. Chem.* **267**, 5250-5256
60. Poole, C. A., Ayad, S., and Gilbert, R. T. (1992) *J. Cell Sci.* **103**, 1101-1110
61. Chen, S. J., and Birk, D. E. (2011) *Exp. Eye Res.* **92**, 444-445
62. Ferdous, Z., Wei, V. M., Iozzo, R., Hook, M., and Grande-Allen, K. J. (2007) *J. Biol. Chem.* **282**, 35887-35898
63. Bougault, C., Paumier, A., Aubert-Foucher, E., and Mallein-Gerin, F. (2008) *BMC Biotechnol.* **8**
64. Bougault, C., Paumier, A., Aubert-Foucher, E., and Mallein-Gerin, F. (2009) *Nat. Protoc.* **4**, 928-938
65. Bougault, C., Aubert-Foucher, E., Paumier, A., Perrier-Groult, E., Huot, L., Hot, D., Duterque-Coquillaud, M., and Mallein-Gerin, F. (2012) *PLoS One* **7**
66. Mauck, R. L., Yuan, X., and Tuan, R. S. (2006) *Osteoarthritis Cartilage* **14**, 179-189
67. Chai, D. H., Arner, E. C., Griggs, D. W., and Grodzinsky, A. J. (2010) *Osteoarthritis Cartilage* **18**, 249-256
68. Vincent, T. L., McLean, C. J., Full, L. E., Peston, D., and Saklatvala, J. (2007) *Osteoarthritis Cartilage* **15**, 752-763

69. Knight, M. M., Ross, J. M., Sherwin, A. F., Lee, D. A., Bader, D. L., and Poole, C. A. (2001) *Biochim. Biophys. Acta-Gen. Subj.* **1526**, 141-146
70. Lee, D. A., Knight, M. M., Bolton, J. F., Idowu, B. D., Kayser, M. V., and Bader, D. L. (2000) *J. Biomech.* **33**, 81-95
71. Guilak, F. (1995) *J. Biomech.* **28**, 1529-&
72. Kumar, D., and Lassar, A. B. (2009) *Mol. Cell. Biol.* **29**, 4262-4273
73. Dykxhoorn, D. M., and Lieberman, J. (2005) The silent revolution: RNA interference as basic biology, research tool, and therapeutic. in *Annual Review of Medicine*, Annual Reviews, Palo Alto. pp 401-423
74. Dykxhoorn, D. M., Novina, C. D., and Sharp, P. A. (2003) *Nat. Rev. Mol. Cell Biol.* **4**, 457-467
75. Stewart, S. A., Dykxhoorn, D. M., Palliser, D., Mizuno, H., Yu, E. Y., An, D. S., Sabatini, D. M., Chen, I. S. Y., Hahn, W. C., Sharp, P. A., Weinberg, R. A., and Novina, C. D. (2003) *RNA-Publ. RNA Soc.* **9**, 493-501
76. Wang, Q. G., Nguyen, B., Thomas, C. R., Zhang, Z. B., El Haj, A. J., and Kuiper, N. J. (2010) *Biomaterials* **31**, 1619-1625
77. Bobick, B. E., Tuan, R. S., and Chen, F. H. (2010) *J. Cell. Biochem.* **109**, 265-276
78. Pagnotto, M. R., Wang, Z., Karpie, J. C., Ferretti, M., Xiao, X., and Chu, C. R. (2007) *Gene Therapy* **14**, 804-813
79. Gersch, R. P., and Hadjiargyrou, M. (2009) *Bone* **45**, 330-338
80. Frka, K., Facchinello, N., Del Vecchio, C., Carpi, A., Curtarello, M., Venerando, R., Angelin, A., Parolin, C., Bernardi, P., Bonaldo, P., Volpin, D., Braghetta, P., and Bressan, G. M. (2009) *J. Biotechnol.* **141**, 8-17
81. Alexopoulos, L. G., Haider, M. A., Vail, T. P., and Guilak, F. (2003) *Journal of biomechanical engineering* **125**, 323-333

82. Wiberg, C., Klatt, A. R., Wagener, R., Paulsson, M., Bateman, J. F., Heinegard, D., and Morgelin, M. (2003) *J. Biol. Chem.* **278**, 37698-37704
83. DiMicco, M. A., Kisiday, J. D., Gong, H., and Grodzinsky, A. J. (2007) *Osteoarthritis Cartilage* **15**, 1207-1216
84. Knight, M. M., Lee, D. A., and Bader, D. L. (1998) *Biochimica et Biophysica Acta* **14**, 67-77
85. Loeser, R. F., Sadiev, S., Tan, L., and Goldring, M. B. (2000) *Osteoarthritis Cartilage* **8**, 96-105
86. Doane, K. J., Howell, S. J., and Birk, D. E. (1998) *Invest. Ophthalmol. Vis. Sci.* **39**, 263-275
87. Nareyeck, G., Seidler, D. G., Troyer, D., Rauterberg, J., Kresse, H., and Schonherr, E. (2004) *Eur. J. Biochem.* **271**, 3389-3398
88. Guilak, F., Jones, W. R., Ting-Beall, H. P., and Lee, G. M. (1999) *Osteoarthritis Cartilage* **7**, 59-70
89. Rastogi, A., Thakore, P., Leung, A., Benavides, M., Machado, M., Morschauer, M. A., and Hsieh, A. H. (2009) *J. Cell. Physiol.* **220**, 698-705
90. Rutledge, R. G., and Cote, C. (2003) *Nucleic Acids Research* **31**
91. Livak, K. J., and Schmittgen, T. D. (2001) *Methods* **25**, 402-408
92. Wang, P., Yang, L., and Hsieh, A. H. (2011) *Ann. Biomed. Eng.* **39**, 1101-1111
93. Villanueva, I., Weigel, C. A., and Bryant, S. J. (2009) *Acta biomaterialia* **5**, 2832-2846
94. Vincent, T. L. (2013) *Current opinion in pharmacology* **13**, 449-454
95. Quinn, T. M., Schmid, P., Hunziker, E. B., and Grodzinsky, A. J. (2002) *Biorheology* **39**, 27-37
96. Lee, V., Cao, L., Zhang, Y., Kiani, C., Adams, M. E., and Yang, B. B. (2000) *J. Cell. Biochem.* **79**, 322-333

97. Li, Z., Kupcsik, L., Yao, S. J., Alini, M., and Stoddart, M. J. (2010) *J. Cell. Mol. Med.* **14**, 1338-1346
98. Knudson, W., Aguiar, D. J., Hua, Q., and Knudson, C. B. (1996) *Exp. Cell Res.* **228**, 216-228
99. Appelman, T. P., Mizrahi, J., and Seliktar, D. (2011) *Journal of biomechanical engineering* **133**, 041010
100. Knight, M. M., Bravenboer, J., Lee, D. A., van Osch, G., Weinans, H., and Bader, D. L. (2002) *Biochim. Biophys. Acta-Gen. Subj.* **1570**, 1-8
101. McLane, L. T., Chang, P., Granqvist, A., Boehm, H., Kramer, A., Scrimgeour, J., and Curtis, J. E. (2013) *Biophysical journal* **104**, 986-996
102. Fisher, L. W., Termine, J. D., and Young, M. F. (1989) *The Journal of biological chemistry* **264**, 4571-4576
103. Neame, P. J., Choi, H. U., and Rosenberg, L. C. (1989) *The Journal of biological chemistry* **264**, 8653-8661
104. Krishnan, P., Hocking, A. M., Scholtz, J. M., Pace, C. N., Holik, K. K., and McQuillan, D. J. (1999) *The Journal of biological chemistry* **274**, 10945-10950
105. Wiberg, C., Hedbom, E., Khairullina, A., Lamande, S. R., Oldberg, A., Timpl, R., Morgelin, M., and Heinegard, D. (2001) *J. Biol. Chem.* **276**, 18947-18952
106. Blain, E. J., Gilbert, S. J., Wardale, R. J., Capper, S. J., Mason, D. J., and Duance, V. C. (2001) *Archives of Biochemistry and Biophysics* **396**, 49-55
107. Giannoni, P., Siegrist, M., Hunziker, E. B., and Wong, M. (2003) *Biorheology* **40**, 101-109
108. Elder, S. H., Shim, J. W., Borazjani, A., Robertson, H. M., Smith, K. E., and Warnock, J. N. (2008) *Biorheology* **45**, 479-486
109. Garcia, M., and Knight, M. M. (2010) *J. Orthop. Res.* **28**, 510-515

110. Freeman, P. M., Natarajan, R. N., Kimura, J. H., and Andriacchi, T. P. (1994) *J. Orthop. Res.* **12**, 311-320
111. Elder, S. H., Goldstein, S. A., Kimura, J. H., Soslowky, L. J., and Spengler, D. M. (2001) *Ann. Biomed. Eng.* **29**, 476-482
112. Langelier, E., Suetterlin, R., Hoemann, C. D., Aebi, U., and Buschmann, M. D. (2000) *Journal of Histochemistry & Cytochemistry* **48**, 1307-1320
113. Twomey, J. D., Thakore, P. I., Hartman, D. A., Myers, E. G. H., and Hsieh, A. H. (2014) *European Cells & Materials (Accepted for publication)*
114. Campbell, J. J., Blain, E. J., Chowdhury, T. T., and Knight, M. M. (2007) *Biochemical and Biophysical Research Communications* **361**, 329-334
115. Durrant, L. A., Archer, C. W., Benjamin, M., and Ralphs, J. R. (1999) *Journal of Anatomy* **194**, 343-353
116. Haudenschild, D. R., Chen, J. F., Pang, N. N., Steklov, N., Grogan, S. P., Lotz, M. K., and D'Lima, D. D. (2011) *J. Orthop. Res.* **29**, 20-25
117. Blain, E. J., Gilbert, S. J., Hayes, A. J., and Duance, V. C. (2006) *Matrix Biology* **25**, 398-408
118. Farquharson, C., Lester, D., Seawright, E., Jefferies, D., and Houston, B. (1999) *Bone* **25**, 405-412
119. Parry, W. L., and Hemstreet, G. P. (1988) *J. Urol.* **139**, 270-274
120. Blain, E. J., Mason, D. J., and Duance, V. C. (2003) *Biorheology* **40**, 111-117
121. Haudenschild, D. R., D'Lima, D. D., and Lotz, M. K. (2008) *Biorheology* **45**, 219-228
122. Idowu, B. D., Knight, M. M., Bader, D. L., and Lee, D. A. (2000) *Histochem.J.* **32**, 165-174
123. Djouad, F., Delorme, B., Maurice, M., Bony, C., Apparailly, F., Louis-Pence, P., Canovas, F., Charbord, P., Noel, D., and Jorgensen, C. (2007) *Arthritis Research & Therapy* **9**

124. McGlashan, S. R., Jensen, C. G., and Poole, C. A. (2006) *Journal of Histochemistry & Cytochemistry* **54**, 1005-1014
125. Wang, G. Y., Woods, A., Sabari, S., Pagnotta, L., Stanton, L. A., and Beier, F. (2004) *J. Biol. Chem.* **279**, 13205-13214
126. Jortikka, M. O., Parkkinen, J. J., Inkinen, R. I., Karner, J., Jarvelainen, H. T., Nelimarkka, L. O., Tammi, M. I., and Lammi, M. J. (2000) *Archives of Biochemistry and Biophysics* **374**, 172-180
127. Guilak, F., Ratcliffe, A., and Mow, V. C. (1995) *J. Orthop. Res.* **13**, 410-421
128. Haudenschild, D. R., Hong, E., Yik, J. H. N., Chromy, B., Morgelin, M., Snow, K. D., Acharya, C., Takada, Y., and Di Cesare, P. E. (2011) *J. Biol. Chem.* **286**, 43250-43258
129. Vincent, T., and Saklatvala, J. (2006) *Biochem. Soc. Trans.* **34**, 456-457
130. Vincent, T. L. (2011) *Arthritis Research & Therapy* **13**
131. Chia, S. L., Sawaji, Y., Burleigh, A., McLean, C., Inglis, J., Saklatvala, J., and Vincent, T. (2009) *Arthritis Rheum.* **60**, 2019-2027
132. Hildner, F., Peterbauer, A., Wolbank, S., Nurnberger, S., Marlovits, S., Redl, H., van Griensven, M., and Gabriel, C. (2010) *J. Biomed. Mater. Res. Part A* **94A**, 978-987
133. Friedman, M. S., Long, M. W., and Hankenson, K. D. (2006) *J. Cell. Biochem.* **98**, 538-554
134. Li, T. F., Darowish, M., Zuscik, M. J., Chen, D., Schwarz, E. M., Rosier, R. N., Drissi, H., and O'Keefe, R. J. (2006) *J. Bone Miner. Res.* **21**, 4-16
135. Fehrenbacher, A., Steck, E., Rickert, M., Roth, W., and Richter, W. (2003) *Archives of Biochemistry and Biophysics* **410**, 39-47
136. Rastogi, A., Kim, H., Twomey, J. D., and Hsieh, A. H. (2013) *Arthritis Research & Therapy* **15**
137. Hung, C. T., Mauck, R. L., Wang, C. C. B., Lima, E. G., and Ateshian, G. A. (2004) *Ann. Biomed. Eng.* **32**, 35-49

138. Henrionnet, C., Wang, Y., Roeder, E., Gambier, N., Galois, L., Mainard, D., Bensoussan, D., Gillet, P., and Pinzano, A. (2012) *Bio-Med. Mater. Eng.* **22**, 209-218
139. Chahine, N. O., Albro, M. B., Lima, E. G., Wei, V. I., Dubois, C. R., Hung, C. T., and Ateshian, G. A. (2009) *Biophysical journal* **97**, 968-975
140. Handorf, A. M., and Li, W. J. (2011) *PLoS One* **6**
141. Buschmann, M. D., Gluzband, Y. A., Grodzinsky, A. J., and Hunziker, E. B. (1995) *J. Cell Sci.* **108**, 1497-1508
142. Kelly, T. A. N., Wang, C. C. B., Mauck, L., Ateshian, G. A., and Hung, C. T. (2004) *Biorheology* **41**, 223-237
143. Haleem-Smith, H., Calderon, R., Song, Y. J., Tuan, R. S., and Chen, F. H. (2012) *J. Cell. Biochem.* **113**, 1245-1252
144. Wilusz, R. E., DeFrate, L. E., and Guilak, F. (2012) *Matrix Biology* **31**, 320-327
145. Nicodemus, G. D., and Bryant, S. J. (2008) *J. Biomech.* **41**, 1528-1536
146. Gronau, T., Hansen, U., Seidler, D., Iozzo, R., Aszodi, A., Prein, C., Clausen-Schaumann, H., Kruger, K., Mooren, F., Pap, J. B. T., Pap, T., Bruckner, P., and Dreier, R. (2013) *Arthritis Rheum.* **65**, S29-S29
147. Danielson, K. G., Baribault, H., Holmes, D. F., Graham, H., Kadler, K. E., and Iozzo, R. V. (1997) *J. Cell Biol.* **136**, 729-743
148. Melrose, J., Fuller, E. S., Roughley, P. J., Smith, M. M., Kerr, B., Hughes, C. E., Caterson, B., and Little, C. B. (2008) *Arthritis Research & Therapy* **10**
149. Reese, S. P., Underwood, C. J., and Weiss, J. A. (2013) *Matrix Biology* **32**, 414-423
150. Lu, C. H., Yeh, T. S., Yeh, C. L., Fang, Y. H. D., Sung, L. Y., Lin, S. Y., Yen, T. C., Chang, Y. H., and Hu, Y. C. (2014) *Mol. Ther.* **22**, 186-195
151. Morille, M., Tran, V. T., Garric, X., Cayon, J., Coudane, J., Noel, D., Venier-Julienne, M. C., and Montero-Menei, C. N. (2013) *Journal of Controlled Release* **170**, 99-110

152. Lu, H. D., Lv, L. L., Dai, Y. H., Wu, G., Zhao, H. Q., and Zhang, F. C. (2013) *PLoS One* **8**
153. Liu, M., Yu, X., Huang, F. G., Cen, S. Q., Zhong, G., and Xiang, Z. (2013) *Orthopedics* **36**, 868-873

Web References

Web Ref. 1) <<http://cancan.cshl.edu/cgi-bin/Codex/Codex.cgi>> [10-06-2009]

Web Ref. 2) <<http://frodo.wi.mit.edu>> [01-07-2009]